LARGE DEFLECTION ELASTIC-PLASTIC ANALYSIS OF PLATE STRUCTURES BY THE FINITE STRIP METHOD

by

SARATH BANDARA SAMARASINGHE ABAYAKOON

B.Sc.Eng.(Hons), University of Peradeniya, Sri Lanka, 1979
M.A.Sc., The University of British Columbia, 1983

A THESIS SUBMITTED IN PARTIAL FULFILMENT OF

THE REQUIREMENTS FOR THE DEGREE OF

DOCTOR OF PHILOSOPHY

in

THE FACULTY OF GRADUATE STUDIES

(Department of Civil Engineering)

We accept this thesis as conforming

to the required standard

THE UNIVERSITY OF BRITISH COLUMBIA

September 1987

In presenting this thesis in partial fulfilment of the requirements for an advanced degree at the University of British Columbia, I agree that the Library shall make it freely available for reference and study. I further agree that permission for extensive copying of this thesis for scholarly purposes may be granted by the head of my department or by his or her representatives. It is understood that copying or publication of this thesis for financial gain shall not be allowed without my written permission.

Department of CIVIL ENGINEERING

The University of British Columbia
1956 Main Mall
Vancouver, Canada
V6T 1Y3

Date 28th SEP 1987

ABSTRACT

A solution procedure based on the finite strip method is presented herein, for the analysis of plate systems exhibiting geometric and material non-linearities. Special emphasis is given to the particular problem of rectangular plates with stiffeners running in a direction parallel to one side of the plate. The finite strip method is selected for the analysis as the geometry of the problem is well suited for the application of this method and also as the problem is too complicated to solve analytically.

Large deflection effects are included in the present study, by taking first order non-linearities in strain-displacement relations into account. Material non-linearities are handled by following von-Mises yield criterion and associated flow rule. A bi-linear stress-strain relationship is assumed for the plate material, if tested under uniaxial conditions. Numerical integration of virtual work equations is performed by employing Gauss quadrature. The number of integration points required in a given direction is determined either by observing the individual terms to be integrated or by previous experience. The final set of non-linear equations is solved via a Newton-Raphson iterative scheme, starting with the linear solution.

Numerical investigations are carried out by applying the finite strip computer programme to analyse uniformly loaded rectangular and I beams with both simply supported and clamped ends. Displacements, stresses and moments along the beam are compared with analytical solutions in linear analyses and with finite element solutions in non-linear analyses. Investigations are also extended to determine the response of laterally loaded square plates with simply supported and clamped boundaries. Finally, a uniformly loaded stiffened panel is analysed and the results are compared with finite element results. It was revealed that a single mode in the strip direction was sufficient to yield engineering accuracy for design purposes, with most problems.

TABLE OF CONTENTS

		Page
	Abstract	ii
	Table of Contents	iii
	List of Tables	vi
	List of Figures	vii
	Dedication	xi
	Acknowledgement	xii
Chapter I	**INTRODUCTION**	**1**
Chapter II	**METHODS OF ANALYSIS AND PREVIOUS WORK**	**4**
2.1	The General Plate Problem	4
2.2	Elastic Methods of Analysis	5
2.2.1	Unstiffened plates	5
2.2.2	Stiffened plates	8
2.3	Plastic Methods of Analysis	10
2.4	Numerical Methods	12
2.4.1	Introduction	12
2.4.2	The finite element method	13
2.5	The Finite Strip Method	14
Chapter III	**MATHEMATICAL FORMULATION**	**18**
3.1	Introduction	18
3.2	Finite Strip Discretisation	20
3.3	Displacement Functions	22
3.3.1	General	22
3.3.2	Plate strips	23
3.3.3	Stiffener strips	24
3.3.4	I beam analysis	24

Page

3.4	Strain-Displacement Relations		26
3.5	Constitutive Relations		27
3.6	Stiffness Formulation		33
	3.6.1	Shape functions	33
	3.6.2	Virtual work principle	35
3.7	Newton-Raphson Iterative Procedure		37
3.8	Numerical Integration		39
3.9	Computer Implementation		40

Chapter IV NUMERICAL INVESTIGATIONS **42**

4.1	Introduction		42
4.2	Numerical Integration		44
4.3	Analysis of a Rectangular Beam		47
	4.3.1	Simply supported ends	47
	4.3.2	Clamped ends	55
4.4	Analysis of an I Beam		64
	4.4.1	Simply supported ends	64
	4.4.2	Clamped ends	71
4.5	Analysis of Unstiffened Plates		83
	4.5.1	Square plate with all four edges simply supported	83
	4.5.2	Square plate with all four edges clamped	97
4.6	Analysis of a Stiffened Panel		109
4.7	Convergence of the Newton-Raphson Iterative Scheme		131

Page

Chapter V SUMMARY, CONCLUSIONS AND SUGGESTIONS FOR FUTURE RESEARCH 132

5.1 Summary 132
5.2 Conclusions 134
5.2.1 Rectangular beam 134
5.2.2 I beam 134
5.2.3 Square plate 135
5.2.4 Stiffened panel 136
5.2.5 Numerical integration 136
5.3 Suggestions for Future Research 137

References 138
Appendix A 142
Appendix B 143
Appendix C 145

LIST OF TABLES

Table No.	Title	Page
4.1	Numerical integration of circular and hyperbolic functions	45
4.2	Abscissae and weight coefficients of Gaussian quadrature formula	47
4.3	Linear elastic response of a simply supported rectangular beam	49
4.4	Linear elastic response of a clamped rectangular beam	56
4.5	Linear elastic response of a simply supported I beam	66
4.6	Linear elastic response of a clamped I beam	73
4.7	Linear elastic response of a simply supported plate	85
4.8	Linear elastic response of a built-in plate	99
4.9	Central deflections of a built-in plate	103
4.10	Linear elastic response of a stiffened panel	114

LIST OF FIGURES

Figure No.	Title	Page
3.1	Schematic diagram of a stiffened plate	19
3.2	Finite strip modelling of a plate	21
3.3	Plate-stiffener assemblage	25
3.4	Modelling of an I beam	25
3.5	Stress-strain relationship	28
3.6	Hardening models	30
3.7	Stress-plastic strain relationship	32
4.1	Deflected shape of the simply supported rectangular beam	50
4.2	Bending moment distribution of the simply supported rectangular beam	50
4.3	Central deflection of the simply supported rectangular beam	52
4.4	Strain energy comparison in the simply supported rectangular beam	53
4.5	Deflection response of the simply supported rectangular beam with varying numerical integrations	53
4.6	Deflected shape of the clamped rectangular beam	58
4.7	Bending moment distribution of the clamped rectangular beam	58
4.8	Central deflection of the clamped rectangular beam	59
4.9	u displacement along the clamped rectangular beam for q = 2.5N/mm^2	61
4.10	Strain energy comparison in the clamped rectangular beam	61
4.11	Central deflection of the clamped beam in a large deflection, elastic-perfectly plastic analysis	62
4.12	Central deflection of the clamped beam with varying numerical integrations	62
4.13	Symmetric I beam example	65
4.14	Central deflection of the simply supported I beam in an elastic analysis	69
4.15	Central deflection of the simply supported I beam in an elastic-perfectly plastic analysis	69

Page

4.16	Central deflection of the simply supported I beam with varying support points	70
4.17	Varying support points	72
4.18	Central deflection of the clamped I beam in an elastic analysis	74
4.19	Central deflection of the clamped I beam in an elastic perfectly-plastic analysis	76
4.20	Parametric study on the clamped I beam	78
4.21	Central deflection of the clamped I beam with varying displacement modes	79
4.22	Strain energy variation in the clamped I beam	81
4.23	Spread of plastic zones in the clamped I beam	82
4.24	Rectangular plate configuration	84
4.25	Bending moment distribution along AB, in the simply supported square plate - M_x	87
4.26	Bending moment distribution along CD, in the simply supported square plate - M_x	87
4.27	Bending moment distribution along AB, in the simply supported square plate - M_y	88
4.28	Bending moment distribution along CD, in the simply supported square plate - M_y	88
4.29	Variation of central deflection response of the simply supported square plate with different discretizations	90
4.30	Central deflection response of the simply supported square plate with in one and two mode analyses	90
4.31	Deflected shape of the simply supported square plate along a centre line in the direction of the strips at 0.2 N/mm^2	91
4.32	Strain energy variation of the simply supported square plate	91
4.33	Comparison of central deflection of the simply supported square plate with ADINA	93
4.34	Comparison of central deflection of the simply supported square plate with another finite strip solution	93

Page

4.35	Central deflection of a simply supported square plate in an elastic plastic analysis	95
4.36	Spread of plastic zones in a simply supported square plate	96
4.37	Comparison of central deflections of a simply supported square plate with the yield line solution	98
4.38	Comparison of central deflections of a simply supported square plate with plastic membrane solution	98
4.39	Bending moment distribution along AB, in the clamped square plate - M_x	101
4.40	Bending moment distribution along CD, in the clamped square plate - M_x	101
4.41	Bending moment distribution along AB, in the clamped square plate - M_y	102
4.42	Bending moment distribution along CD, in the clamped square plate - M_y	102
4.43	Central deflection of the clamped square plate by different discretizations	104
4.44	Central deflection of the clamped square plate by one and two modes	104
4.45	Strain energy variation in the clamped square plate	105
4.46	Central deflection of the clamped square plate in a small deflection, elastic-plastic analysis	105
4.47	Spread of plastic zones in the clamped square plate	107
4.48	Comparison of central deflections of a clamped square plate with the yield line solution	109
4.49	Comparison of central deflections of a clamped square plate with plastic membrane solution	109
4.50	Stiffened panel configuration	110
4.51	Finite element grid	112
4.52	Finite strip models	113
4.53	Panel centre deflections with DRES and DRES1 models	116
4.54	Panel centre deflections with ADINA, DRES1 and DRES2 models	117

Page

4.55	Deflections at mid-span of the stiffener	118
4.56(a)	Displacement shapes of DRES test panel along BF	120
4.56(b)	Displacement shapes of DRES test panel along EG	121
4.56(c)	Displacement shapes of DRES test panel along GF	122
4.57(a)	Normal stress perpendicular to the stiffener at 0.5 psi	124
4.57(b)	Normal stress perpendicular to the stiffener at 20 psi	125
4.57(c)	Normal stress perpendicular to the stiffener at 50 psi	126
4.58(a)	Normal stress parallel to the stiffener at 0.5 psi	127
4.58(b)	Normal stress parallel to the stiffener at 20 psi	128
4.58(c)	Normal stress parallel to the stiffener at 50 psi	129

To my mother
and to the memory of my father

ACKNOWLEDGEMENT

The author wishes to express his appreciation and gratitude to his supervisors, Drs. M. D. Olson and D. L. Anderson for their advice and guidance in the preparation of this thesis. He would also like to thank Dr. R. Khalil for his continued interest and many valuble sugesstions throughout this research. Thanks are also extended to all my friends in Vancouver, for their companionship and encouragement.

Financial support of Natural Sciences and Engineering Research Council of Canada in forms of UBC Graduate Fellowships and Research Assistantships is gratefully acknowledged.

CHAPTER I

INTRODUCTION

In the early stages of development, the existence of stiffened structural forms was probably learned from the great book of nature. Sea shells, leaves and trees can be considered as some examples of the vast group of naturally stiffened structures. It has long been realised, by a scientific study of living things that strength and rigidity of a structure depend not only on the material, but also upon its form. It is known that the Egyptians, at least 5000 years ago, developed a craft made of planks fastened around a wooden framework using much the same principle as is employed today.

The development of structurally stiffened elements was restricted, due to limited materials and limited knowledge of materials, until the start of the nineteenth century. Invention of materials such as steel, concrete and aluminium has brought about a revolution in structural design, and their full possibilities are still being explored. The wide use of stiffened structural elements began mainly with the application of steel plates for hulls of ships and with the development of steel bridges and aircraft structures. In addition to these applications, stiffened plates are also widely used in other areas of structural engineering. Stiffened plates in the shape of ribbed and waffle type slabs are used for floor and roof construction in buildings. Composite concrete-steel beams have also found wide applications in floor construction. Retaining walls, storage tanks, railway cars, large transportation carrier panels

and steel lock gates are some other structural applications of stiffened panels.

Bending is one of the most important engineering problems associated with the stiffened plates, stability and vibration being the others. When a plate, stiffened or unstiffened, is loaded laterally, the deflections are considered small, if they are less than about 20% of the plate thickness. However, by increasing the magnitude of the maximum deflection beyond a certain level, say 30% of the plate thickness, the deflections are accompanied by stretching of the middle surface, provided that the edges of the plate are restricted against in-plane motion. Large deflections can also stress the plate material over the elastic limit, thus causing significant plastic deformations in the structure. These plastic deformations are acceptable to the structural engineer as long as they do not violate serviceability requirements of the structure. Nevertheless, the design engineer is faced with the challenge of accurately predicting the deformation profile and the stress pattern throughout the structure, in order to carry out a safe design. One of the objectives of the present study is to provide a numerical tool which accommodates both geometric and material non-linearities for designing such structures.

Development of an analytical method for the present purpose is extremely difficult, if not impossible, due to the complexity of the problem. Looking at the arena of numerical procedures for solving structural engineering problems, the finite element method is noted above the other techniques, because of its versatility and flexibility. Several all purpose computer programmes based on the finite element method are presently in use, some with the capabilities of handling non-linear geometry and material problems. However, for the particular problem of large deflection elastic-plastic analysis of stiffened panels, the finite strip method is chosen in the present study because of the simple geometric pattern involved. The finite strip method has proven its cost efficiency and relative ease in data preparation over the finite element method in an extensive area of structural applications. In applying

the finite strip method, it is possible to obtain results within the engineering accuracy needed for design problems, even with a small number of modes. Although the use of the finite strip method has recently been extended to the domain of geometrically non-linear problems, it has yet to find applications in the important realm of materially non-linear problems. The second objective of this thesis is to study the applicability of the finite strip method in both geometric and material non-linear analyses.

The third and final objective of the present analysis is to open up a new dimension of research which can assist in solving the problems in the more demanding area of blast loading of structures.

Chapter 2 of this thesis presents a discussion of the general plate problem and the existing methods of solutions. Both analytical and numerical procedures are discussed with special reference to the finite strip method. Chapter 3 consists mainly of the mathematical derivations necessary for the computer implementation of the proposed numerical procedure. It also includes a description of the iterative scheme and the method of numerical integration included in the computer programme. The chapter concludes with a small discussion about the computer programme itself. In order to evaluate the ability of the present solution scheme to predict the response of beams, plates, and stiffened plates, numerical results have been generated for several example problems. Chapter 4 includes a detailed description of these examples and the comparisons of the results with either analytical, experimental, or other numerical procedures whenever possible. Chapter 5 contains a summary of the present work and a list of the conclusions drawn from the present study. It also includes some suggestions for extending the proposed numerical procedure into other areas of structural engineering.

CHAPTER II

METHODS OF ANALYSIS AND PREVIOUS WORK

2.1 The General Plate Problem

The theory of bending of plates can be started by dealing with the simplest possible problem, the bending of a long rectangular plate subjected to a transverse load that does not vary along the length of the plate. Boobnev[1] reduced this problem to the investigation of an elemental strip submitted to the action of a lateral load and also an axial force which depends on the deflection of the strip. The differential equation which relates this deflection to the applied load is similar to that for a bent beam, and thus can be easily integrated.

Elastic analysis of plates has since been developed to handle plates of various shapes, various loading and boundary conditions, and plates with different forms of stiffening. Analytical solution procedures have yielded differential equations, along with the pertinent boundary conditions, to be solved for deflections and/or stresses. Both isotropic and orthotropic material properties are considered in each of the solution schemes. The analytical solutions for the elastic analysis of plates are summarised in section 2.2

Plastic analysis of plates, though not as developed as elastic analysis, has made considerable progress in this century. Because of these developments, plastic methods now

cover a vast area of practical interest. Rigid plastic assumptions provide solutions of plate problems via the upper bound theorem and the yield line analysis. Section 2.3 deals with these aspects of the general plate problem.

The major difficulty in plate analysis lies in the integration of the resulting differential equations. These have led to the application of various numerical procedures in plate analysis. A description of these methods is included in section 2.4. Applications of the finite strip method are further discussed in section 2.5.

2.2 Elastic Methods of Analysis

2.2.1 Unstiffened plates

Small deflection elastic analysis of a laterally loaded unstiffened isotropic plate yields the following differential equation for the lateral displacements.

$$\nabla^4 w = q/D \tag{2.1}$$

where, w = lateral deflection,

∇^4 = biharmonic operator,

q = distributed load,

D = $Eh^3/12(1-\nu^2)$ = flexural rigidity of the plate,

h = thickness of the plate, and

E, ν = elastic constants of the plate material.

In deriving this equation, it was assumed that the effects of transverse shear can be neglected. At the boundary, the edges of the plate are assumed to be free to move in the

plane of the plate, thus restricting the end reactions to be normal to the plate surface.

Solution of the equation 2.1 requires two boundary conditions at each side of the plate if the plate is rectangular, or two boundary conditions at the outer boundary and an admissibility condition at the center of the plate if the plate is circular. However, analytical solutions of this differential equation can be found only for special sets of boundary conditions and also for some special types of loading conditions. Timoshenko and Woinowsky-Krieger[2] have provided solutions of this equation for some classical boundary conditions.

However, the structural theory of the first order is valid only if the basic requirements of the theory are satisfied; namely, that the deflections are small compared to the plate thickness. When the magnitude of the maximum deflection reaches the order of the plate thickness, the membrane action in carrying the applied load becomes comparable to that of bending. In 1910, Th.von Karman[3] derived the following two partial differential equations for the large deflection of isotropic plates.

$$\nabla^4 F = E\left[\left(\frac{\partial^2 w}{\partial x \partial y}\right)^2 - \frac{\partial^2 w}{\partial x^2}\frac{\partial^2 w}{\partial y^2}\right], \tag{2.2}$$

$$\nabla^4 w = \frac{h}{D}\left[\frac{q}{h} + \frac{\partial^2 F}{\partial y^2}\frac{\partial^2 w}{\partial x^2} + \frac{\partial^2 F}{\partial x^2}\frac{\partial^2 w}{\partial y^2} - 2\frac{\partial^2 F}{\partial x \partial y}\frac{\partial^2 w}{\partial x \partial y}\right], \tag{2.3}$$

where F is the airy stress function, which is related to the membrane stresses N_x, N_y and N_{xy} by,

$$N_x = h\frac{\partial^2 F}{\partial y^2}, \quad N_y = h\frac{\partial^2 F}{\partial x^2} \quad \text{and} \quad N_{xy} = -h\frac{\partial^2 F}{\partial x \partial y} \tag{2.4}$$

These equations are derived in reference to a two dimensional Cartesian coordinate system attached to the mid-surface of the plate. They are to be solved for the stress

function F and the lateral displacement w. The geometric non-linearities are caused either by higher order terms of derivatives or by their products. These equations can be solved analytically for the particular case of bending of a plate to a cylindrical surface, or for very thin plates which may have deflections many times higher than their thicknesses. In the latter case, bending can be neglected and the membrane solutions are sought if the plate is restricted against in-plane motion.

Apart from homogeneous and isotropic materials, modern construction also uses materials with definitely expressed differences in elastic properties in different directions. Such materials are called anisotropic. In the case where a body possesses different elastic properties in perpendicular or orthogonal directions, it is called orthotropic. There are two kinds of 'orthotropy' in structural elements. The first kind shows an orthotropy which is a result of the different physical properties in two mutually perpendicular directions of the material itself, and is therefore called "natural orthotropy". The second kind includes elements which are reinforced to ensure strength and stability, arranged in the proper geometrical configurations. This latter kind of orthotropy is called "structural orthotropy". An elastic small deflection analysis of a rectangular orthotropic plate yields the following differential equation to be solved for the lateral diaplacement w.

$$D_x\frac{\partial^4 w}{\partial x^4} + 2H\frac{\partial^4 w}{\partial x^2 \partial y^2} + D_y\frac{\partial^4 w}{\partial y^4} = q \tag{2.5}$$

where, D_x = flexural rigidity in the x direction $= E_x h^3/\big[12(1-\nu_x\nu_y)\big]$,

D_y = flexural rigidity in the y direction $= E_y h^3/\big[12(1-\nu_x\nu_y)\big]$,

D_{xy} = torsional rigidity $= G_{xy}h^3/12$

$2H$ = effective torsional rigidity $= D_x\nu_y + D_y\nu_x + 4D_{xy}$

E_x, E_y = elastic modulii in x and y directions respectively,

ν_x, ν_y = Poisson's ratios in x and y directions respectively, and

G_{xy} = shear modulus of the orthotropic material.

This equation was first deduced by Huber[4] and is hence known as "Huber's equation". It is clear that this equation reduces to equation 2.1 for $D_x = D_y$, $E_x = E_y$ and $\nu_x = \nu_y$.

Large deflections of orthotropic plates have been analysed by following von-Karman's theory for isotropic plates. This has resulted in a modified version of the equations 2.2 and 2.3, again in terms of the stress function F and the lateral displacement w[7].

$$\frac{1}{E_y}\frac{\partial^4 F}{\partial x^4} + \left(\frac{1}{G} - \frac{2\nu_x}{E_x}\right)\frac{\partial^4 F}{\partial x^2 \partial y^2} + \frac{1}{E_x}\frac{\partial^4 F}{\partial y^4} = \left(\frac{\partial^2 w}{\partial x \partial y}\right)^2 - \frac{\partial^2 w}{\partial x^2}\frac{\partial^2 w}{\partial y^2} \tag{2.7}$$

$$D_x\frac{\partial^4 w}{\partial x^4} + 2H\frac{\partial^4 w}{\partial x^2 \partial y^2} + D_y\frac{\partial^4 w}{\partial y^4} = q + h\left(\frac{\partial^2 F}{\partial y^2}\frac{\partial^2 w}{\partial x^2} - 2\frac{\partial^2 F}{\partial x \partial y}\frac{\partial^2 w}{\partial x \partial y} + \frac{\partial^2 F}{\partial x^2}\frac{\partial^2 w}{\partial y^2}\right) \tag{2.8}$$

Equations 2.7 and 2.8, together with the boundary conditions, determine the two functions F and w. Integration of these equations is accompanied by great difficulties as a result of the non-linear terms in the first equation. Therefore, the solution of these equations in the general case is unknown. Some approximate solutions of the problem are known for some special combinations of the orthotropic material properties.

2.2.2 Stiffened plates

Boobnev[1,5] was the first to apply stress analysis to steel plates stiffened by a system of interconnected longitudinal and transverse beams. He was also the first to apply the theory of bending of plates in the structural design of ships. In the initial analysis, he treated the stiffened panel problem as it were a beam on an elastic foundation. By following this

analysis, Boobnev was able to prepare a set of design charts for stiffened panel structures.

Stiffened plates can also be analysed by the use of the theory of orthotropic plates. As stated in the previous section, orthotropy due to physical structure of the material is called "natural orthotropy". On the other hand, orthotropy due to geometrical composition is called "structural" or "technical" orthotropy. Stiffened plates fall under the latter category, if the stiffeners run in mutually perpendicular directions.

Huber's equation (Eq.2.5), was first derived for naturally orthotropic plates. However, in the elastic domain structurally orthotropic plates may also be treated on the basis of the same theory with some modifications. Orthogonally stiffened plates may be substituted by an equivalent orthotropic plate of constant thickness when the ribs are disposed symmetrically with respect to the middle plane of the plate. It is also required that the ratios of stiffener spacing to plate boundary dimensions are small enough to ensure approximate homogenity of the problem. The expressions for D_x,D_y and H to be used in equation 2.5 for a plate reinforced by equidistant stiffeners in one direction are given by Timoshenko and Woinowsky-Krieger[2].

However, Huber's equation cannot be applied for most of the engineering plate structures, as the ribs are located on only one side of the plate, i.e. they are disposed asymmetrically with respect to the middle plane. In this case, the location of the neutral surfaces of the boundary stresses is unknown. Consequently, there is a drastic increase in the complexity of the determination of the orthotropic rigidity factors. The analysis of the problem should be extended to include the effect of strain in the middle plane of the plate, which produces additional shear stresses disregarded in Huber's method.

Pflüger recognized the above facts and formulated the force displacement relations for a typical plate element with ribs on one side of the plate. A system of three differential equations for such a plate element was developed in terms of the middle surface of the plate.

Forces and moments acting on the element were derived from the middle surface. Further, by expressing the displacements in an infinite series form, Pflüger obtained a set of eighth order partial differential equations, each involving one displacement component[6].

After Pflüger, several other investigators attacked the problem of stiffened panels, some considering special types of stiffeners. According to Troitsky[7], Trenks[8], Giencke[9], Wilde[10] and Ganowicz[11] each came up with different methods for analysing stiffened plates. Clifton et al.[12] presented a generalized exact theory in 1963, following Pflüger's analysis.

The theory of stiffened plates having large deflections presents a complex part of the general theory of stiffened plates. In 1961, Vogel[13] applied the large deflection theory of orthotropic plates to analyse two way stiffened plates. Steinhardt and Abdel-Sayed[14] also discussed the large deformation elastic analysis of such panels.

All the procedures described above are much too complicated computationally to be considered for practical applications in design. A major difficulty lies in the integration of the resulting partial differential equations. If the plate material possesses plastic and/or non-linear elastic stress-strain relationships, analysis will be still more complicated. Plastic analysis has been simplified to a great extent with the use of bound theorems and the yield line theory. These methods are described in the next section.

2.3 Plastic Methods of Analysis

Baker[15] reported the importance and economy in using plastic design methods over conventional elastic design procedures for beams and portal frames. These factors are equally valid in the design of stiffened or unstiffened plate structures. Although a structural analysis based on elastic theory yields good results for deformations and stresses produced by

working - service - loads, it fails to assess the real load carrying capacity of the structure. At failure, the fundamental assumptions of the theory of elasticity are no longer valid. In most cases, an elastic design is overly conservative. In some cases, such as aerospace applications, an overly conservative theory might give unsafe results. It is necessary, therefore, to investigate the plastic behaviour of plates.

The mathematical theory of plasticity of plates is much more complicated than its elastic counterpart. However, by introducing an idealized rigid plastic stress-strain relationship, the mathematics can be simplified by a great deal.

Plastic collapse analysis of a structure can be carried out by following the well known bound theorems. The upper bound theorem, which is analogous to the potential energy theorem, states that the external load that produces work at the same rate as the internal forces for a kinematically admissible field will be greater than or equal to the true collapse load of the structure. Yield line analysis of plates is simply the application of the upper bound theorem to a plate collapse mechanism. The method is similar to the plastic hinge analysis of beams. The critical load is obtained either from virtual work or equilibrium considerations. Although the yield line analysis is generally used and tested for the cases of concrete slabs, experimental verification for metallic plates has not been a popular area of research[16].

Once an upper bound solution for the plate collapse load is obtained via the yield line theory, the exact collapse load can be bracketed if a lower bound solution is available. A lower bound can be estimated by following the lower bound theorem, which states that the external load that produces a statically admissible stress field that nowhere exceeds the yield criteria will be lower than or equal to the true collapse load. For example, any elastic solution is a lower bound for the plastic collapse load.

Plastic analysis of unstiffened plates following yield line theory has limited applications.

Applicability of this theory depends on slenderness of the plate. Slenderness μ can be defined as,

$$\mu = S/h, \tag{2.9}$$

where S is some span of the plate with thickness h[17].

For a plate of a given material to carry transverse loads primarily by bending stresses, μ must be bounded both from above and below. Indeed if μ is unduly small, there no longer exists a thin plate but a body with comparable horizontal and vertical dimensions. On the other hand, if μ is unduly large, the plate acts like a membrane that carries transverse loads by direct stresses after undergoing deflections that are comparable to its thickness.

The limit load obtained from simple plastic theory based on the rigid perfectly plastic schemes will thus prove to have a real physical meaning only for a limited domain of values of μ. Even in this domain of μ, the limit load will not correspond to large plastic deformations under constant load, such as that usually occur in frame structures. In most cases, favorable geometry changes due to unrestricted plastic flow will cause membrane action that eventually enables the plate to carry a load in excess of the limit load.

A complete plastic analysis is extremely difficult, if not impossible, to carry out in the case of stiffened plates. One has to resort to numerical procedures, especially when large deflections are involved. Methods of numerical analysis are discussed in the next section.

2.4 Numerical Methods

2.4.1 Introduction

The well known numerical methods for solving engineering problems are finite difference and finite element methods, the latter being more popular in recent years. Both methods have similar accuracy. Computer cost is often less when finite differences are used, although the cost comparisons depend on the type of problem and the program organization as well as on the method of analysis[18]. However, the finite difference method is not suited to a structure that must be modelled by a mixture of materials or by different structural forms, such as a structure that combines bar, beam, plate and shell components. Finite elements appeal to the structural engineer because they resemble components of the actual structure. Improvements in finite element methods have come from both physical and mathematical insight. These improvements have led to the establishment of the finite element method as the most powerful and versatile tool of solution in structural analysis.

2.4.2 The finite element method

In the finite element method, the structure is divided into a finite number of elements. Stress and/or displacement variation inside an element is predetermined depending on the accuracy sought, and is a function of the nodal variables. These elements are then assembled back to form the original structure, thereby obtaining a set of simultaneous equations to be solved for the nodal variables.

Several plate elements are available at the present time and are in use for solving practical problems. Unlike the case of analytical solutions, extensions to stiffened plates can be made with very little additional effort, with finite elements. In small deflection

theory, in-plane and lateral deformations of the plate are uncoupled and hence can be treated separately. However, the coupling between these two deformations has to be taken into account if large deformation analysis is needed.

The finite element method has also been extended to include material non-linearities. If the stress-strain relations are linear, or non-linear but elastic, it is possible to write an expression relating stress to strain which is unique. If there are plastic strains, the stress-strain relation is path dependent. A given state of stress can be produced by many different straining procedures. In plastic analysis, increments of stresses are related to the increments of strains via an elastic-plastic matrix. This matrix takes the place of the elasticity matrix used in incremental analysis for elastic problems. Zienkiewicz[19] has discussed the development of the elastic-plastic matrix by following von-Mises yield criteria and an associated flow rule.

It is clear from the preceeding discussion that the finite element method is capable of handling a large class of engineering problems. However, for many structures having regular geometric plans and simple boundary conditions, a full finite element analysis is often both extravagant and unnecessary, and at times even impossible[20]. The cost of solutions can be very high, and usually increases by an order of magnitude when a more refined, higher dimensional analysis is required. For eigenvalue problems and vibration analysis, machine limitations force the user to be satisfied with a less accurate solution by using lower order elements. To overcome these drawbacks in analysing a certain class of problems, the finite strip method was developed in the late 1960's by Y. K. Cheung[21].

2.5 The Finite Strip Method

The finite strip method can be considered as a special form of the finite element procedure

using the displacement approach. In the finite strip method, the structure is divided into strips or prisms, in which one opposite pair of the sides or one or more opposite pairs of the faces respectively, are in coincidence with the boundaries of the structure. Unlike the standard finite element method which uses polynomial displacement functions in all directions, the finite strip method calls for use of simple polynomials in some directions and continuously differentiable smooth series in the other directions, with the stipulation that such series should satisfy *a priori* the boundary conditions at the ends of the strips or prisms. The general form of the displacement function is given as a product of polynomials and series. Thus for a strip, the lateral displacements are given by,

$$w = \sum_{m=1}^{r} f_m(x)\, Y_m(y) \tag{2.10}$$

In the above expression, the series has been truncated at the r^{th} term. $f_m(x)$ is a function which satisfies the end conditions in the x direction and also represents the deflected shapes in that direction and $Y_m(y)$ is a polynomial expression with undetermined constants for the m th term of the series.

Cheung's first paper[21] on the finite strip method dealt with the analysis of elastic plates with two opposite simply supported ends. Cheung analysed simply supported plates with variable thickness as well as with isotropic and orthotropic material properties. In all these cases, the finite strip results were in very good agreement with the theoretical predictions. Cheung[22] has also extended the analysis for finite strips to cases with both ends clamped, and one end clamped and the other end simply supported. These analyses also yielded very satisfactory results.

The finite strip method has since been extended to analyse folded plate structures [23], vibration of thin and thick plates [24,25], sectoral plates [26], and also for post buckling analysis of plates [27].

Mawenya and Davies [28] developed a finite strip computer programme to handle transverse shear deformation. They presented numerical examples which demonstrated the applicability of the formulation to the analysis of thin, thick and sandwich plates.

It appears that the first paper on application of the finite strip method in the more demanding realm of geometrically non-linear analysis of plate structures was published in 1981 by Hancock[29]. The displacement functions used by Hancock were slightly varied from those used by Graves Smith and Sridharan[27] in their post-buckling analyses. In 1984, Gierlinski and Graves Smith[30] have presented a geometrically non-linear analysis of prismatic thin-walled structures. In both these papers, the theory was based on the moderately large displacement assumptions, giving non-linear strain-displacement relations, but linear curvature-displacement relations. The corresponding non-linear equilibrium equations were produced by the principle of stationary potential energy, using finite strip discretisation. The equilibrium equations were solved using incremental and incremental- iterative numerical methods. Langyel and Cusens[31] have also developed a finite strip method which can carry out a geometrically non-linear analysis including the possibility of taking structural imperfections into account. Azizan and Dawe[32] presented a general finite strip method of analysis following Mindlin plate theory. Thus, this analysis includes geometric non-linearities as well as the effects of transverse shear deformations. The non-linearity was introduced via the strain displacement equations. Correspondingly, the analysis pertains to problems involving moderate displacements but small rotations. The principle of stationary potential energy was used in the development of stiffness equations for the strip and the complete plate stiffness. These equations were solved using the Newton-Raphson iterative scheme.

In order to overcome problems of the finite strip method associated with mixed boundary conditions, concentrated loads and continuous spans, the spline finite strip method was

developed by Cheung et al. in 1982 [33]. This method was originally introduced for the analysis of rectangular plates. In the spline finite strip method, each strip was divided into a number of subdomains. A set of spline functions was used to define the displacement variation inside a given subdomain. Li et al.[34], extended this method to the elastic analysis of general plates with the help of a coordinate transformation.

To analyse linear elastic flat plate systems that are continuous over deflecting supports, Puckett and Gutkowski[35] introduced what they termed as the "compound strip method". Their approach incorporates the effect of the support elements in a direct stiffness methodology. The stiffness contribution of the support elements was derived and added directly to the plate stiffness matrix at the element(strip) level. This summation of plate and support stiffness contribution constitutes a substructure which was termed a *compound strip* . Puckett and Lang [36], extended this method to cover continuous sector plates. Recently the compound strip method has also been used for free vibration analysis of continuous plates[37].

Application of the finite strip method for the analysis of plate systems with material non-linearity and/or plasticity is extremely limited. Mofflin[38] introduced the use of the finite strip method for the collapse analysis of compressed plates and plate assemblages. Mofflin et al.[39] presented a feasibility study of a finite strip analysis on beams and unstiffened plates under dynamic lateral loads. The predictions from the method seem to agree closely with known theoretical and experimental results. In the present work, a large deformation elastic plastic static analysis of stiffened and unstiffened plates has been conducted. The mathematical formulation of the problem is presented in the next chapter.

CHAPTER III

MATHEMATICAL FORMULATION

3.1 Introduction

The stiffened panel, essentially a two dimensional structure, is also rectangular (Fig. 3.1). Other than being a thin strip perpendicular to the plate surface, the stiffeners can also take the shape of an inverted T beam, L beam or a box section. In all these cases, stiffeners run in one direction, parallel to each other, separating the plate into strips, which may or may not be of the same thickness. Thus the geometry of this problem warrants the use of the finite strip method for the analysis in hand. This chapter presents the mathematical formulation necessary for the computer implementation of the finite strip method to analyse large deflection elastic-plastic behaviour of stiffened panels.

Section 3.2 introduces the finite strip discretisation and also the displacement components involved in the formulations that follow. Selection of the appropriate displacement functions according to the boundary conditions of the plate is discussed in section 3.3. Sections 3.4 and 3.5 deal with the strain displacement and the constitutive relations employed in the present analysis, respectively. Derivation of the equilibrium equations via a stiffness formulation is presented in section 3.6. As the resulting system of equations is non-linear,

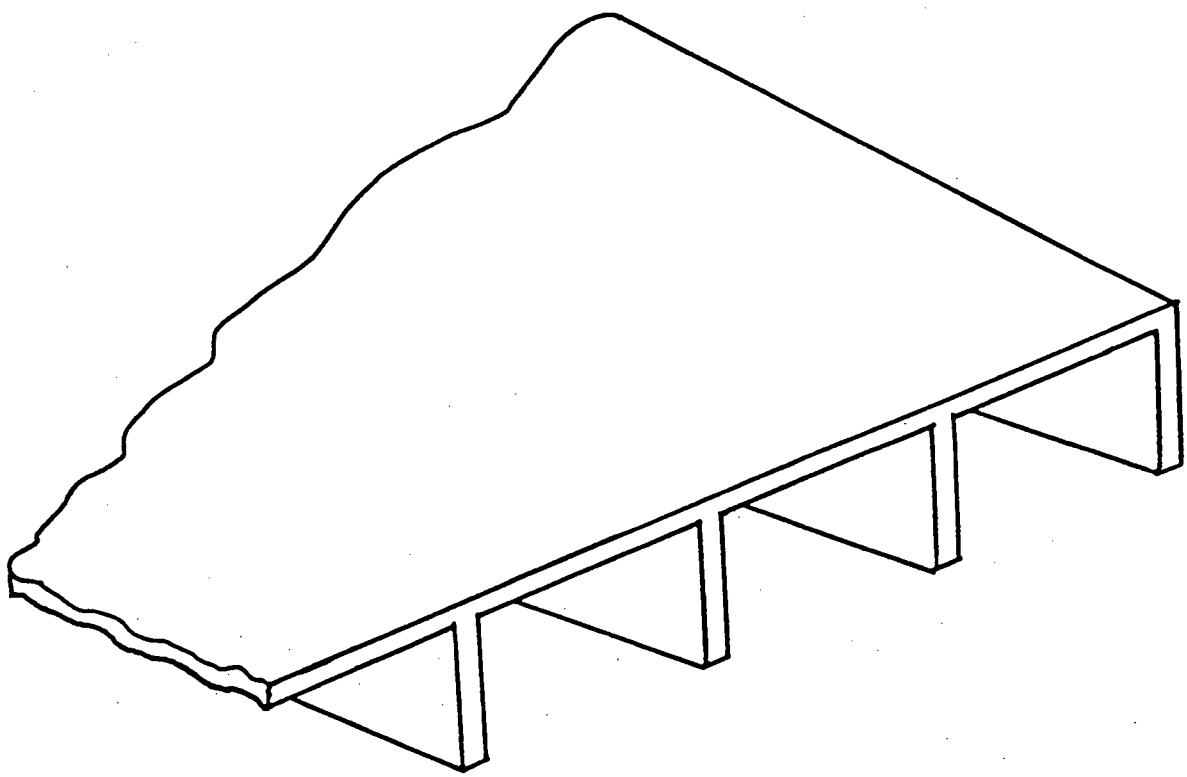

Figure 3.1 – Schematic diagram of a stiffened plate

the Newton-Raphson iterative scheme is chosen as the solution procedure. The necessary mathematical derivations for the implementation of this scheme are included in section 3.7. Section 3.8 describes the method of numerical integration adopted in the computer programme, and finally, section 3.9 highlights some of the important features of the computer programme itself.

3.2 Finite Strip Discretisation

Figure 3.2(a) shows a typical finite strip division of an unstiffened rectangular plate. The global rectangular co-ordinate system XYZ is attached to the mid surface of the plate. Boundary conditions at $X = 0$ and at $X = a$ are known *a priori* and will be considered in the choice of displacement functions in the X direction. The arrows in the Figure 3.2(a) indicate the possible in-plane and lateral loading conditions. Any two finite strips are connected along a nodal line. In the assembly process, the nodal variables are matched along such lines for compatibility. It is not necessary that the plate have constant thickness in each strip and conceivably the width and thickness could vary along the length. However, constant thickness and width will be assumed in this formulation.

In a displacement formulation, the nodal variables are the displacement components that will adequately represent the problem. As the analysis includes both bending and membrane effects, it is necessary to include both in plane and out-of plane displacements as nodal variables. Figure 3.2(b) shows an isolated strip with the local co-ordinate system xyz. Displacement nodes are placed at the middle of each side, marked 1 and 2 in Figure 3.2(b), with the three displacements and one rotation taken as the degrees of freedom. u and v are the in-plane displacements, w is the out-of plane displacement and $\theta = \partial w/\partial y$ is the rotation about the x axis.

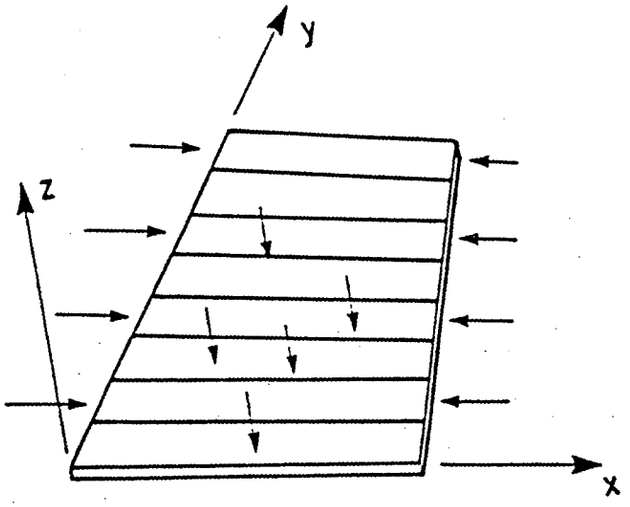

(a) Typical Strip Division for a Plate

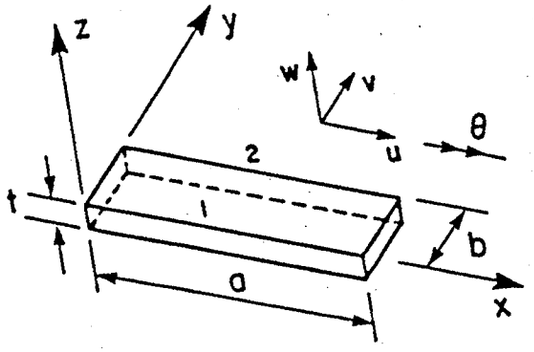

(b) Strip Parameters

Figure 3.2 – Finite strip modelling of a plate

3.3 Displacement Functions

3.3.1 General

The displacement functions in the x direction, i.e. the longitudinal direction, are chosen so as to satisfy the boundary conditions at the ends of the strip. One set of functions that can be used are the mode shapes of a vibrating beam. These are given by,

$$g_n(\xi) = C_1 \sin \beta_n \xi + C_2 \cos \beta_n \xi + C_3 \sinh \beta_n \xi + C_4 \cosh \beta_n \xi \tag{3.1}$$

where C_1, C_2, C_3, C_4 and β_n are constants and $\xi = x/a$, where a is the length of the strip. The variation of the displacements in the y direction, i.e. across the strip, will be taken as linear for the u and v displacements and cubic for the w displacement. These cubic shape functions for the w degree of freedom are the well known Hermitian polynomials used in the finite element analysis of beam bending, thus ensuring slope and displacement compatibility between adjacent strips.

The u, v and w displacement distributions of a single strip can be written in terms of the nodal displacements by combining the shape functions. These expressions for a strip of size $a \times b$ are given by,

$$\begin{aligned}
u &= \left[(1-\eta)u_{1m} + \eta\, u_{2m}\right] g_m^u(\xi), \\
v &= \left[(1-\eta)v_{1n} + \eta\, v_{2n}\right] g_n^v(\xi) \qquad \text{and} \\
w &= \left[\left(1 - 3\eta^2 + 2\eta^3\right) w_{1p} + \left(\eta - 2\eta^2 + \eta^3\right) b\theta_{1p} + \left(3\eta^2 - 2\eta^3\right) w_{2p} + \left(\eta^3 - \eta^2\right) b\theta_{2p}\right] g_p^w(\xi)
\end{aligned} \tag{3.2}$$

where, u_{1m},u_{2m} etc. are the nodal variables, $\eta = y/b$ and the summation convention is used

for repeated indices m, n and p. Along the length, the displacements vary according to the $g_m^u(\xi), g_n^v(\xi)$ and $g_p^w(\xi)$ functions. For different boundary conditions, these functions are given in next sub sections.

3.3.2 Plate strips

(a) Simply supported ends

1. constrained in the x direction

$$g_m^u(\xi) = \sin m\pi\xi \qquad ; m = 2, 4, 6, \ldots,$$

$$g_n^v(\xi) = \begin{cases} \sin n\pi\xi & ; n = 1, 3, 5, \ldots, \\ \cos n\pi\xi & ; n = 2, 4, 6, \ldots, \end{cases}$$

$$g_p^w(\xi) = \sin p\pi\xi \qquad ; p = 1, 3, 5, \ldots,$$

2. not constrained in the x direction

$$g_m^u(\xi) = \cos m\pi\xi \qquad ; m = 1, 3, 5, \ldots,$$

and the other functions are as above.

(b) Clamped ends

$g_m^u(\xi)$ and $g_n^v(\xi)$ are as above, and

$$g_p^w(\xi) = \phi_p(\xi) = \left[\alpha_p\left(\sinh\beta_p\xi - \sin\beta_p\xi\right) + \left(\cosh\beta_p\xi - \cos\beta_p\xi\right)\right]/A_p \qquad ; p = 1, 3, 5, \ldots,$$

where, $A_p = \alpha_p\left(\sinh 0.5\beta_p - \sin 0.5\beta_p\right) + \left(\cosh 0.5\beta_p - \cos 0.5\beta_p\right)$,

$$\alpha_p = \frac{\cos\beta_p - \cosh\beta_p}{\sinh\beta_p - \sin\beta_p}$$

and, β_p are the solutions of the transcendental equation, $\cosh \beta_p = \sec \beta_p$.

3.3.3 Stiffener strips

Figure 3.3 shows a single stiffener strip attached at right angles to two plate strips. The displacements shown are the local ones for each strip respectively. It is clear that there are no changes in u displacement pattern necessary for the stiffener strip from the plate strip. Nevertheless, the v displacement for the stiffener should be compatible with the w displacement of the plate to which it is attached. To preserve this compatibility along the length of the strip, $g_n^v(\xi)$ has to be restricted to be of the same shape as $g_p^w(\xi)$. If the bending boundary conditions of the stiffener and the plate are different, the compatibility will be very difficult to achieve. However, in these cases, the bending associated with the stiffener is much more important and thus some errors in the plate moments are unlikely to be of much importance.

3.3.4 I beam analysis

A rectangular beam can be analysed by considering it as a single finite strip. An I beam can be considered as an assemblage of several finite strips (Fig 3.4). In the latter case, each flange is discretised into two plate strips and the web is modelled by one stiffener strip. For linear analysis, the u displacement in the beam should be of the same shape as the slope of the w displacement in the x direction. Considering this restriction and the necessary compatibility between the v and w displacements for the stiffener strip, the shape functions for an I beam are,

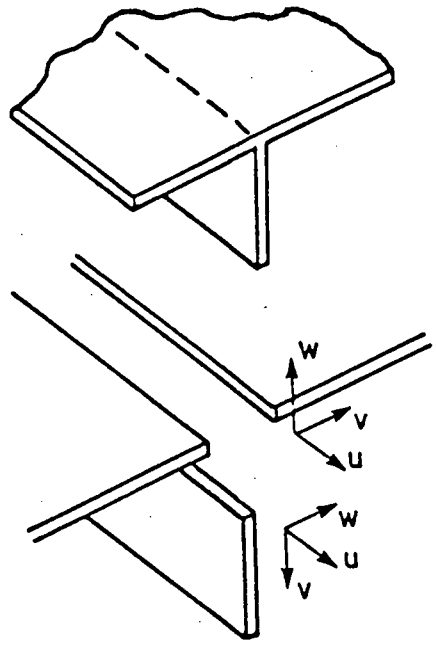

Figure 3.3 – Plate–stiffener assemblage

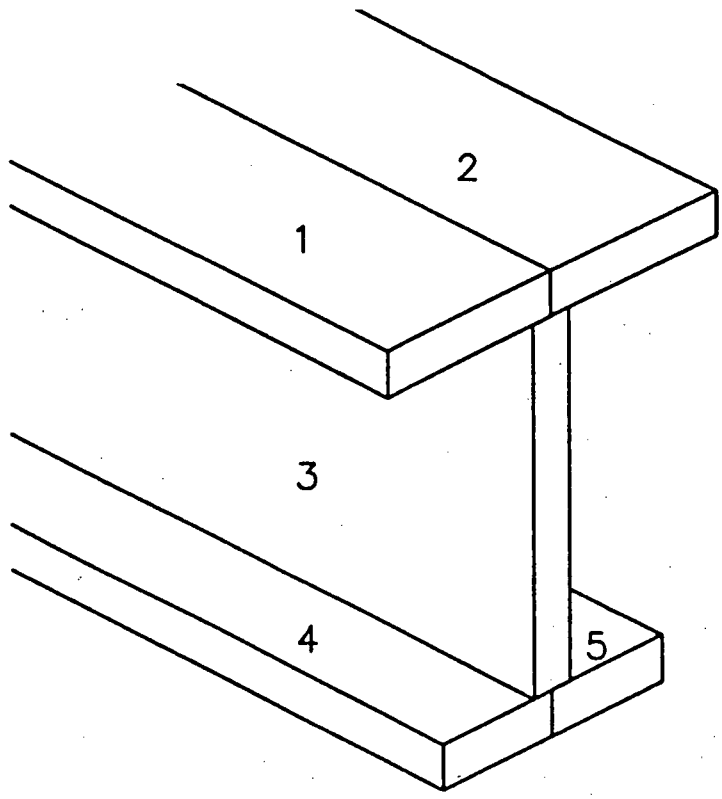

Figure 3.4 – Modelling of an I beam

(a) Simply supported ends

$$g_m^u(\xi) = \cos m\pi\xi \qquad ; m = 1,3,5,...$$

$$g_n^v(\xi) = \sin n\pi\xi \qquad ; n = 1,3,5,...$$

$$g_p^w(\xi) = \sin p\pi\xi \qquad ; p = 1,3,5,...$$

In performing a linear elastic analysis with these shape functions, the top and the bottom flanges will show equal and opposite u displacements at any given section if the I beam is symmetric. This results in a strain free axis at the middle of the web. Therefore, in order to solve large deflection problems an additional u mode, which varies as $\sin 4\pi\xi$ was used. This will be discussed in detail, in the next chapter.

(b) Clamped ends

$$g_m^u(\xi) = \frac{\partial \phi_m(\xi)}{\partial x} \qquad ; m = 1,3,5...$$

$$g_n^v(\xi) = \phi_n(\xi) \qquad ; n = 1,3,5...$$

$$g_p^w(\xi) = \phi_p(\xi) \qquad ; p = 1,3,5...$$

where the ϕ functions are the same as in the clamped plate strip. Even for the clamped I beam, it was necessary to include an additional u mode to obtain accurate results. Selection of this mode will also be discussed in Chapter 4.

3.4 Strain-Displacement Relations

The well known large deflection strain-displacement relations for plate bending are,

$$\epsilon_x = \frac{\partial u}{\partial x} - z\frac{\partial^2 w}{\partial x^2} + \frac{1}{2}\left(\frac{\partial w}{\partial x}\right)^2,$$
$$\epsilon_y = \frac{\partial v}{\partial y} - z\frac{\partial^2 w}{\partial y^2} + \frac{1}{2}\left(\frac{\partial w}{\partial y}\right)^2, \quad \text{and} \tag{3.3}$$
$$\gamma_{xy} = 2\epsilon_{xy} = \frac{\partial u}{\partial y} + \frac{\partial v}{\partial x} - 2z\frac{\partial^2 w}{\partial x \partial y} + \frac{\partial w}{\partial x}\frac{\partial w}{\partial y},$$

where ϵ_x, ϵ_y and ϵ_{xy} are the components of strain in two dimensions. γ_{xy} is the engineering shear strain. u, v and w are the displacements of the mid-surface of the plate, in the x, y and z directions respectively. The mid surface coincides with the xy plane and z is measured perpendicular to this surface.

The terms with a linear variation in z in these expressions represent the bending strain and the other terms represent the strain due to the stretching of the middle surface of the plate. It should be noted that the non-linear effect of u and v displacements on the mid surface stretching is neglected as they are small compared to the w displacement. However, when finite strips are used as stiffeners (Figs 3.3 and 3.4), the v displacement of the stiffener must be of the same magnitude as the w displacement of the plate. For these strips, mid surface stretching should include quadratic terms due to the v displacement. Accordingly, equations 3.3 will be modified for stiffener strips by adding $\frac{1}{2}\left(\frac{\partial v}{\partial x}\right)^2$, $\frac{1}{2}\left(\frac{\partial v}{\partial y}\right)^2$ and $\left(\frac{\partial v}{\partial x}\frac{\partial v}{\partial y}\right)$ to the three strains ϵ_x, ϵ_y and γ_{xy}, respectively.

3.5 Constitutive Relations

The assumed stress-strain diagram for the plate material under uniaxial loading is given in Figure 3.5. σ_0 and ϵ_0 are the uniaxial yield stress and the uniaxial yield strain respectively. E and E_T are the slopes of this bi-linear representation.

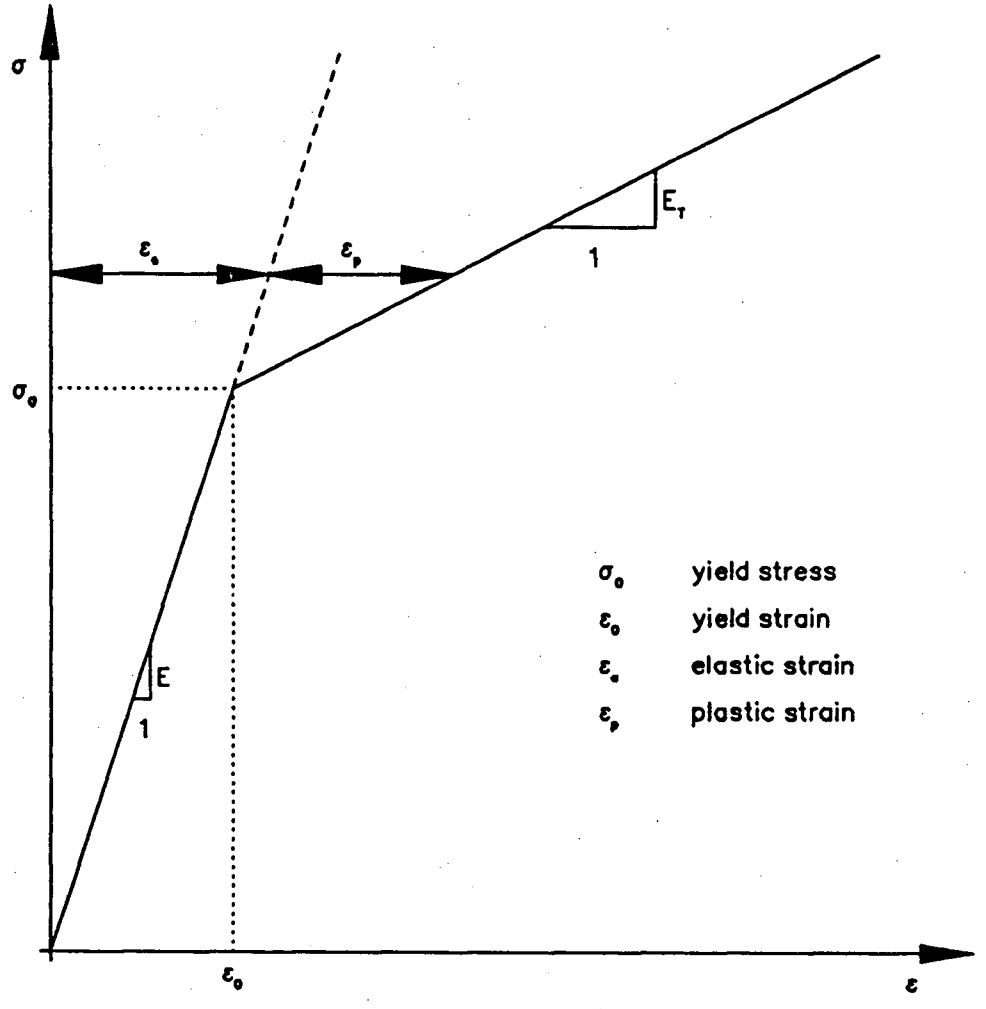

Figure 3.5 – Bi–linear stress–strain relationship

The first step in an elastic-plastic analysis is to decide upon a yield criterion. The yield criterion is used to find out which combination of multiaxial stresses will cause yielding.

The general form of the yield function can be expressed as,

$$F(\{\sigma\}, K) = 0 \tag{3.4}$$

where F is the yield function, $\{\sigma\}$ is a vector of the components of the two dimensional stress tensor, and K is a material parameter which represents the amount of work hardening.

In the present analysis, the von-Mises yield criterion will be followed as it is the closest available representation of the actual behaviour of metals.

The second step in a plastic analysis is to decide on how to describe the behaviour of the material after the yielding has taken place. This is governed by the so called flow rule. One has to decide upon the flow rule depending on the type of material under consideration. The flow rule is said to be *associated* if the incremental strain vector at a point on the yield surface is perpendicular to the yield surface at that point. If the strain vector takes any other direction, the flow rule will be *non-associated.* In the present analysis, an associated flow rule will be followed as it is generally accepted at the present time.

The final step in a plastic analysis is the selection of the hardening rule. After initial yielding, the stress level at which further yielding occurs may be dependent upon the current degree of plastic straining. Such a phenomenon is termed 'work' or 'strain' hardening. Thus the yield surface will vary at each stage of the plastic deformation, with the subsequent yield surfaces being dependent on the plastic strain in some way. Behaviour of most engineering materials follows a path between the two well known hardening models, *isotropic* hardening and *kinematic* hardening[40](Fig 3.6). In isotropic hardening, the yield surface will expand with stress and strain history, but will retain the same initial shape.

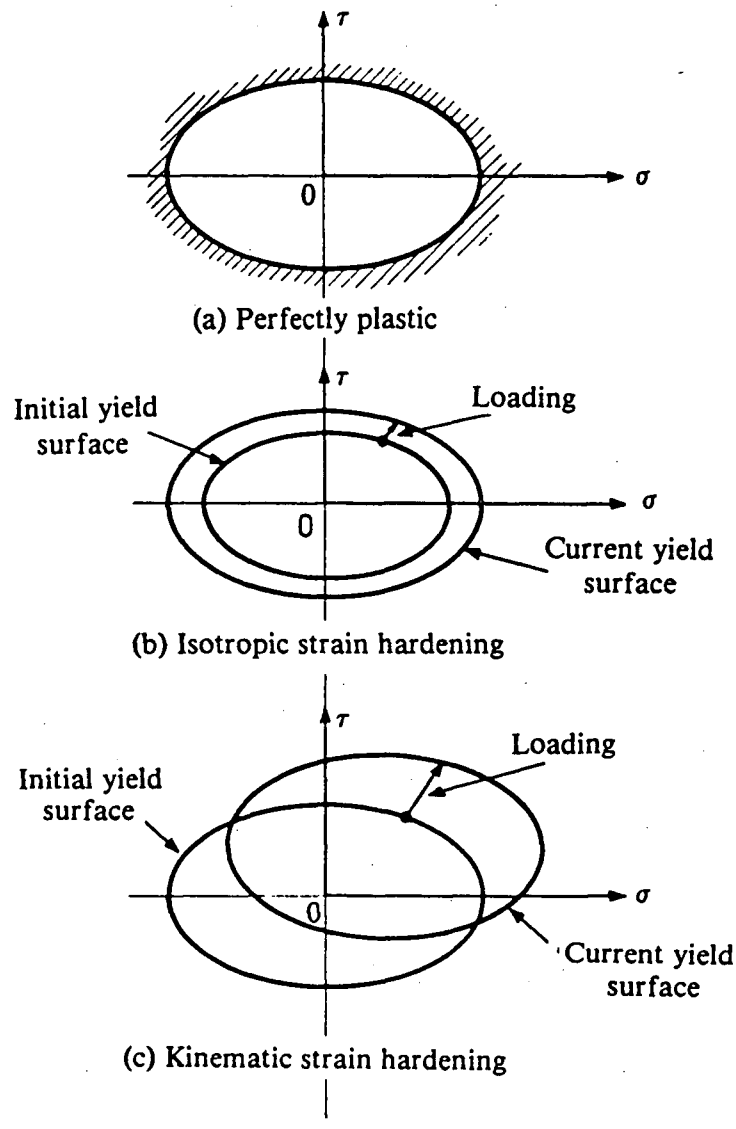

Figure 3.6 – Hardening models

Although the assumption of isotropic hardening is the simplest one mathematically to use, it does not take into account the Bauschinger effect. The Bauschinger effect would tend to reduce the size of the yield locus on one side as that on the other side is increased. To account for the Bauschinger effect, kinematic hardening model is introduced. In kinematic hardening the yield surface maintains the original size, but translates in space with the stress and strain history. However, as this model maintains the total elastic range constant (Fig. 3.6), it probably overcorrects somewhat for the Bauschinger effect[40]. In the analysis that follow, the isotropic hardening is included for mathematical simplicity.

The three steps discussed above can be combined to obtain plastic stress-strain relationship. This can be presented in matrix form as[19],

$$\{d\sigma\} = [D_T]\{d\epsilon\}, \tag{3.5}$$

where,

$$[D_T] = [D] - [D]\{V\}\{V\}^T[D]\left[A + \{V\}^T[D]\{V\}\right]^{-1}. \tag{3.6}$$

In equation 3.6, $[D]$ is the elasticity matrix, $\{V\}$ is a vector defined by $\{V\} = \partial F/\partial\{\sigma\}$ and A is the slope of stress-plastic strain relationship in a uniaxial test. For the assumed bi-linear stress-strain relationship (Fig.3.5), it can be shown that (Fig.3.7),

$$A = \frac{E_T}{1 - \frac{E_T}{E}}, \tag{3.7}$$

The elasto plastic matrix $[D_T]$ takes the place of the elasticity matrix $[D]$ in incremental analysis[19].

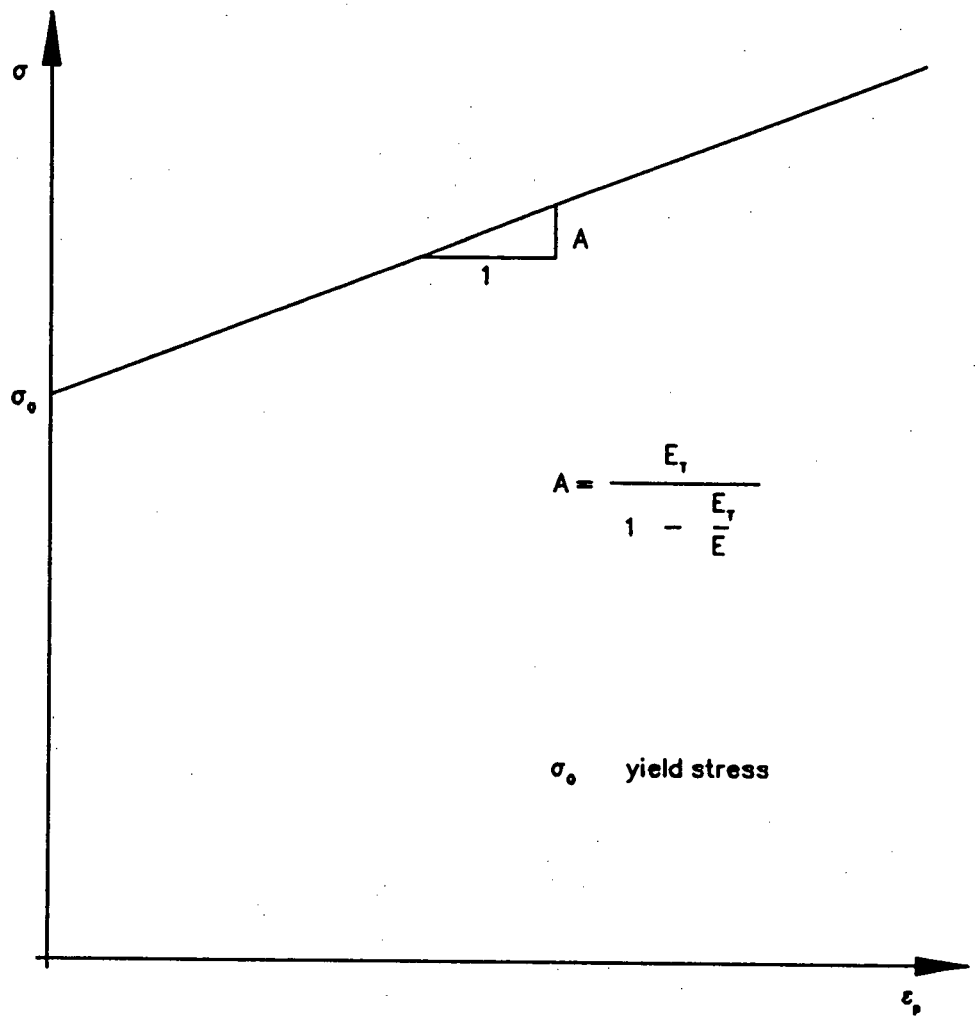

Figure 3.7 – Stress–plastic strain relationship

Equations 3.5 and 3.6 can now be used to get the stress increment for any given strain increment. The sum of the stress increment and stress from the previous iteration results in the stress vector $\{\sigma\}$ at the end of the present iteration. Once the stress vector is obtained, an equivalent effective stress σ_e is calculated by

$$\sigma_e^2 = \sigma_x^2 - \sigma_x\sigma_y + \sigma_y^2 + 3\tau_{xy}^2. \tag{3.8}$$

Initial yield takes place when σ_e exceeds σ_0 for the first time [40], where σ_0 is the yield stress in uniaxial loading. Within this iteration, stresses are scaled down to coincide with the yield surface and the plastic constitutive relations (Eq. 3.6) are used from that point. For subsequent iterations, the material is loaded or unloaded depending on whether σ_e has been increased or decreased. If loading had taken place while in the plastic region, the iterative process is repeated with plastic constitutive relations. If unloading had taken place, the iterative process is repeated with elastic constitutive relations until yielding occurs again.

3.6 Stiffness Formulation

3.6.1 Shape functions

Variation of the displacements u, v and w within a single finite strip was given by the equations 3.2. Considering only the first term in the x direction for simplicity, these equations can be written in index notation as follows.

$$\begin{aligned} u &= N_i^u u_i, \qquad i = 1,2 \\ v &= N_i^v v_i, \qquad i = 1,2 \qquad \text{and} \\ w &= N_i^w w_i, \qquad i = 1,2,3,4. \end{aligned} \tag{3.9}$$

where,

$$
\begin{aligned}
N_1^u &= (1-\eta)\, g_1^u(\xi) \\
N_2^u &= \eta\, g_1^u(\xi) \\
N_1^v &= (1-\eta)\, g_1^v(\xi) \\
N_2^v &= \eta\, g_1^v(\xi) \\
N_1^w &= \left(1-3\eta^2+2\eta^3\right) g_1^w(\xi) \\
N_2^w &= \left(\eta-2\eta^2+\eta^3\right) g_1^w(\xi) \\
N_3^w &= \left(3\eta^2-2\eta^3\right) g_1^w(\xi) \\
N_4^w &= \left(\eta^3-\eta^2\right) g_1^w(\xi)
\end{aligned}
\tag{3.10}
$$

and $u_{11}, u_{21}, v_{11}, v_{21}, w_{11}, b\theta_{11}, w_{21}$ and $b\theta_{21}$ in equation 3.2 are replaced by $u_1, u_2, v_1, v_2, w_1, w_2, w_3$ and w_4 respectively. Equation 3.9 can also be written collectively as,

$$
\begin{Bmatrix} u \\ v \\ w \end{Bmatrix} = [N]\,\{\delta_e\} \tag{3.11}
$$

where, $\{\delta_e\}$ is the nodal displacement vector given by,

$$
\{\delta_e\} = \begin{Bmatrix} u_1 \\ v_1 \\ w_1 \\ w_2 \\ u_2 \\ v_2 \\ w_3 \\ w_4 \end{Bmatrix} \tag{3.12}
$$

and $[N]$ is the matrix of shape functions given by,

$$[N] = \begin{bmatrix} N_1^u & 0 & 0 & 0 & N_2^u & 0 & 0 & 0 \\ 0 & N_1^v & 0 & 0 & 0 & N_2^v & 0 & 0 \\ 0 & 0 & N_1^w & N_2^w & 0 & 0 & N_3^w & N_4^w \end{bmatrix} \tag{3.13}$$

Substitution of the equation 3.11 into the strain displacement relations 3.3 results in the following relationship between the strains and the nodal line displacements.

$$\{\epsilon\} = \begin{Bmatrix} \epsilon_x \\ \epsilon_y \\ \gamma_{xy} \end{Bmatrix}$$

$$= \begin{bmatrix} \frac{\partial N_1^u}{\partial x} & 0 & -z\frac{\partial^2 N_1^w}{\partial x^2} & -z\frac{\partial^2 N_2^w}{\partial x^2} & \frac{\partial N_2^u}{\partial x} & 0 & -z\frac{\partial^2 N_3^w}{\partial x^2} & -z\frac{\partial^2 N_4^w}{\partial x^2} \\ 0 & \frac{\partial N_1^v}{\partial y} & -z\frac{\partial^2 N_1^w}{\partial y^2} & -z\frac{\partial^2 N_2^w}{\partial y^2} & 0 & \frac{\partial N_2^v}{\partial y} & -z\frac{\partial^2 N_3^w}{\partial y^2} & -z\frac{\partial^2 N_4^w}{\partial y^2} \\ \frac{\partial N_1^u}{\partial y} & \frac{\partial N_1^v}{\partial x} & -z\frac{\partial^2 N_1^w}{\partial x \partial y} & -z\frac{\partial^2 N_2^w}{\partial x \partial y} & \frac{\partial N_2^u}{\partial y} & \frac{\partial N_2^v}{\partial x} & -z\frac{\partial^2 N_3^w}{\partial x \partial y} & -z\frac{\partial^2 N_4^w}{\partial x \partial y} \end{bmatrix} \{\delta_e\} +$$

$$\begin{bmatrix} \frac{1}{2}\frac{\partial N_i^w}{\partial x}\frac{\partial N_j^w}{\partial x} w_i w_j \\ \frac{1}{2}\frac{\partial N_i^w}{\partial y}\frac{\partial N_j^w}{\partial y} w_i w_j \\ \frac{1}{2}\left(\frac{\partial N_i^w}{\partial x}\frac{\partial N_j^w}{\partial y} + \frac{\partial N_i^w}{\partial x}\frac{\partial N_j^w}{\partial y}\right) w_i w_j \end{bmatrix}, \qquad i,j = 1,2,3,4. \tag{3.14}$$

The strain displacement relations will be different for the stiffener strips because of the non-linear terms in v. The corresponding matrix forms are given in Appendix A.

3.6.2 Virtual work principle

The equilibrium equations are obtained via a virtual work principle. It can be seen from the equation 3.14 that the virtual strains are related to the virtual displacements by,

$$\{\tilde{\epsilon}\} = [[B] + [C]]\{\tilde{\delta}_e\} \tag{3.15}$$

where, $\{\tilde{\epsilon}\}$ is the virtual strain vector, $\{\tilde{\delta}_e\}$ is the virtual displacement vector,

$$[B] = \begin{bmatrix} \frac{\partial N_1^u}{\partial x} & 0 & -z\frac{\partial^2 N_1^w}{\partial x^2} & -z\frac{\partial^2 N_2^w}{\partial x^2} & \frac{\partial N_2^u}{\partial x} & 0 & -z\frac{\partial^2 N_3^w}{\partial x^2} & -z\frac{\partial^2 N_4^w}{\partial x^2} \\ 0 & \frac{\partial N_1^v}{\partial y} & -z\frac{\partial^2 N_1^w}{\partial y^2} & -z\frac{\partial^2 N_2^w}{\partial y^2} & 0 & \frac{\partial N_2^v}{\partial y} & -z\frac{\partial^2 N_3^w}{\partial y^2} & -z\frac{\partial^2 N_4^w}{\partial y^2} \\ \frac{\partial N_1^u}{\partial y} & \frac{\partial N_1^v}{\partial x} & -z\frac{\partial^2 N_1^w}{\partial x \partial y} & -z\frac{\partial^2 N_2^w}{\partial x \partial y} & \frac{\partial N_2^u}{\partial y} & \frac{\partial N_2^v}{\partial x} & -z\frac{\partial^2 N_3^w}{\partial x \partial y} & -z\frac{\partial^2 N_4^w}{\partial x \partial y} \end{bmatrix}, \tag{3.16}$$

and

$$[C] = \begin{bmatrix} 0 & 0 & \frac{\partial N_1^w}{\partial x}\frac{\partial N_j^w}{\partial x}w_j & \frac{\partial N_2^w}{\partial x}\frac{\partial N_j^w}{\partial x}w_j \\ 0 & 0 & \frac{\partial N_1^w}{\partial y}\frac{\partial N_j^w}{\partial y}w_j & \frac{\partial N_2^w}{\partial y}\frac{\partial N_j^w}{\partial y}w_j \\ 0 & 0 & (\frac{\partial N_1^w}{\partial x}\frac{\partial N_j^w}{\partial y} + \frac{\partial N_1^w}{\partial y}\frac{\partial N_j^w}{\partial x})w_j & (\frac{\partial N_2^w}{\partial x}\frac{\partial N_j^w}{\partial y} + \frac{\partial N_2^w}{\partial y}\frac{\partial N_j^w}{\partial x})w_j \\ 0 & 0 & \frac{\partial N_3^w}{\partial x}\frac{\partial N_j^w}{\partial x}w_j & \frac{\partial N_4^w}{\partial x}\frac{\partial N_j^w}{\partial x}w_j \\ 0 & 0 & \frac{\partial N_3^w}{\partial y}\frac{\partial N_j^w}{\partial y}w_j & \frac{\partial N_4^w}{\partial y}\frac{\partial N_j^w}{\partial y}w_j \\ 0 & 0 & (\frac{\partial N_3^w}{\partial x}\frac{\partial N_j^w}{\partial y} + \frac{\partial N_3^w}{\partial y}\frac{\partial N_j^w}{\partial x})w_j & (\frac{\partial N_4^w}{\partial x}\frac{\partial N_j^w}{\partial y} + \frac{\partial N_4^w}{\partial y}\frac{\partial N_j^w}{\partial x})w_j \end{bmatrix}. \tag{3.17}$$

Note that the B matrix is independent of the nodal variables and the C matrix is linear in $\{\delta_e\}$. The virtual work equation can now be written for a single finite strip as,

$$\int_V \{\tilde{\epsilon}\}^T \{\sigma\} \quad dvol = \{\tilde{\delta}_e\}^T \mathbf{p} \tag{3.18}$$

where,

$$\{\sigma\} = \begin{Bmatrix} \sigma_x \\ \sigma_y \\ \tau_{xy} \end{Bmatrix} \tag{3.19}$$

and $\mathbf{p}$ is the consistent load vector, calculated from the shape functions $[N]$.

Substitution of the equation 3.15 into the equation 3.18 results in the equilibrium equation for a single strip,

$$\int_V [[B] + [C]]^T \{\sigma\} \quad dvol = \mathbf{p} \tag{3.20}$$

. This equation can now be assembled strip by strip, with the introduction of a compatibility constraint setting nodal values in neighbouring strips equal to each other to get the structure

equilibrium equation,

$$\sum_{allstrips} \int_V [[B] + [C]]^T \{\sigma\} \quad dvol = \sum_{allstrips} \mathbf{p} = \mathbf{P} \tag{3.21}$$

where $\mathbf{P}$ is the structure load vector.

To solve equations 3.21, the stresses $\{\sigma\}$ have to be expressed in terms of displacements. Once this is done, the left hand side of the equations 3.21 will be non-linear in the nodal displacements, and thus has to be solved by an iterative procedure. This is explained in the next section.

3.7 Newton-Raphson Iterative Procedure

The equilibrium equation for a single strip can also be written as,

$$\{\phi\} = \mathbf{p} \tag{3.22}$$

where, $\{\phi\} = \{\phi(\delta)\}$ is the left hand side of the equation 3.20. $\{\phi\}$ can be expanded in a Taylor series, around a known solution $\{\delta_0\}$, as,

$$\{\phi(\delta_0)\} + \left.\frac{\partial\{\phi\}}{\partial\{\delta\}}\right|_{\{\delta\}=\{\delta_0\}} (\{\delta\} - \{\delta_0\}) + \ldots\ldots = \mathbf{p} \tag{3.23}$$

In equations 3.23, the differentiation $\frac{\partial\{\phi\}}{\partial\{\delta\}}$ is understood to be a vector operation, producing a matrix. This equation can be rearranged, after neglecting higher order terms, to get,

$$[K]\{\Delta\delta\} = \mathbf{p} - \{\phi(\delta_0)\} \tag{3.24}$$

where $[K]$ is a tangent stiffness matrix given by,

$$[K] = \left.\frac{\partial\{\phi\}}{\partial\{\delta\}}\right|_{\{\delta\}=\{\delta_0\}} \tag{3.25}$$

and $\{\Delta\delta\} = \{\delta\} - \{\delta_0\}$, is the incremental nodal displacement vector.

The iterative scheme proceeds as follows. An initial guess solution $\{\delta_0\}$ is substituted into equation 3.24 to obtain the displacement correction $\{\delta\}-\{\delta_0\}$. This correction, added to the initial guess solution results in the displacement solution vector after the first iteration, $\{\delta\}$. This iterative process is continued until the correction becomes sufficiently small.

$[K]$, the tangent stiffness matrix, is determined by differentiating the left hand side of equation 3.22 with respect to the vector of nodal displacements, and then, evaluating the result from the previous iteration. Differentiation of $\{\phi\}$ with respect to $\{\delta\}$ gives,

$$\begin{aligned}\frac{\partial\{\phi\}}{\partial\{\delta\}} &= \frac{\partial}{\partial\{\delta\}}\int_V \left[[B]+[C]\right]^T\{\sigma\} \quad dvol \\ &= \int_V \frac{\partial}{\partial\{\delta\}}\left(\left[[B]+[C]\right]^T\{\sigma\}\right) \quad dvol,\end{aligned} \tag{3.26}$$

assuming that the integrand is well behaved, so that the integration over the volume of the strip and the differentiation with respect to the nodal variables can be interchanged. The integrand of the above equation can be expanded as,

$$\begin{aligned}\frac{\partial}{\partial\{\delta\}}\left(\left[[B]+[C]\right]^T\{\sigma\}\right) &= \left[[B]+[C]\right]^T\frac{\partial\{\sigma\}}{\partial\{\delta\}} + \left(\frac{\partial}{\partial\{\delta\}}\left[[B]+[C]\right]^T\right)\{\sigma\} \\ &= \left[[B]+[C]\right]^T\frac{\partial\{\sigma\}}{\partial\{\epsilon\}}\frac{\partial\{\epsilon\}}{\partial\{\delta\}} + \left(\frac{\partial}{\partial\{\delta\}}[C]^T\right)\{\sigma\}\end{aligned} \tag{3.27}$$

since $[B]$ is not a function of $\{\delta\}$.

It is clear from the equations 3.5 and 3.15 that,

$$\frac{\partial\{\sigma\}}{\partial\{\epsilon\}} = [D_T] \tag{3.28}$$

and

$$\frac{\partial\{\epsilon\}}{\partial\{\delta\}} = [[B] + [C]], \tag{3.29}$$

respectively. The last term in the equation 3.27 can be expresed as

$$\left(\frac{\partial}{\partial\{\delta\}}[C]^T\right)\{\sigma\} = [U] \tag{3.30}$$

where,

$$U_{ij} = \sum_{k=1}^{3} \frac{\partial\left(C^T\right)_{ik}}{\partial\left(\delta\right)_j}\sigma_k \tag{3.31}$$

Derivation and the elements of U_{ij} are presented in Appendix B. Substitution of 3.28, 3.29 and 3.30 in 3.27 and then in 3.26 results in,

$$\frac{\partial\{\phi\}}{\partial\{\delta\}} = \int_V \left\{[[B] + [C]]^T[D_T][[B] + [C]] + [U]\right\} \quad dvol \tag{3.32}$$

Now, $[K]$, the tangent stiffness matrix is the evaluation of the above at $\{\delta_0\}$, which will be symmetric if $[D_T]$ is symmetric.

3.8 Numerical Integration

Evaluation of the volume integral in the equation 3.32 cannot be done analytically, as the stress-strain relationship is not known in an explicit form. Therefore, some form of numerical integration has to be employed. In the present analysis, Gauss quadrature is used.

The function to be integrated will be evaluated at a discrete number of points. The number of points necessary in one direction will be determined depending on the complexity

of the expression to be integrated. In Gauss quadrature, these sampling points are located at positions to be determined so as to achieve best accuracy for a polynomial integrand.

The limits of integration will be changed to -1 to +1 by transforming variables. Then, if the integrated result is I,

$$I = \int_{-1}^{+1} \int_{-1}^{+1} \int_{-1}^{+1} f(\alpha, \beta, \gamma)\, d\alpha\, d\beta\, d\gamma. \tag{3.33}$$

To evaluate the right hand side numerically, 3.33 will be replaced by,

$$I = \sum_{k=1}^{M} \sum_{j=1}^{M} \sum_{i=1}^{M} H_i H_j H_k f(\alpha_i, \beta_j, \gamma_k) \tag{3.34}$$

where, H_i, H_j and H_k denote the weight components and α_i, β_j and γ_k denote the sampling points respectively. In the above, the number of integrating points in each direction are assumed to be the same at M. This is not necessary, and on occasion it may be of advantage to use different numbers in each direction of integration. Considering only one direction of integration, M points can integrate a polynomial of order 2M-1 exactly. Therefore, if the integrand is a polynomial in all three directions, it is a trivial problem to find out the required number of Gauss evaluation points for an exact integration. When the integrand is not a polynomial, this evaluation has to be done by a trial and error procedure or by experience. Selection of the number of Gauss evaluation points for the present study will be discussed in the next chapter.

3.9 Computer Implementation

The finite strip formulation described in the preceeding pages is implemented in a computer programme. This programme is written in FORTRAN IV and has been test run through

the use of an AMDHAL 5850 computer.

The user has the option of selecting one or more displacement modes in each of the displacement variables u,v and w. The number of Gauss integration points necessary in any one direction is chosen by the computer programme depending on the complexity of the problem and the number of modes employed in the analysis. The final set of simultaneous equations are solved for the nodal variables by a Gauss elimination procedure. Convergence of the solution algorithm is determined by one of two criteria. In the maximum norm criterion, the solution is converged if,

$$\left|\frac{\Delta\delta_i}{\delta_i}\right|_{max} \leq TOLER \tag{3.35}$$

where δ_i denotes the displacement solution for the nodal variable i, $\Delta\delta_i$ is the correction for that variable at the present iteration, and $TOLER$ is the accepted tolerence which is specified by the user. On the other hand, in the Euclidian norm criterion, the solution is converged if,

$$\frac{\sum_{i=1}^{N}(\Delta\delta_i)^2}{\sum_{i=1}^{N}(\delta_i)^2} \leq TOLER^2 \tag{3.36}$$

where N is the total number of nodal variables. Selection of the convergence criterion for any particular problem was left to the user.

CHAPTER IV

NUMERICAL INVESTIGATIONS

4.1 Introduction

The finite strip formulation developed in the previous chapter was then used to investigate several example problems. Mode shapes used in the longitudinal direction of a strip are identified by the indices m, n and p, introduced in equation 3.2. The notation employed in this chapter is illustrated by the following examples.

(2,2,1)	one mode analysis $m = 2$, $n = 2$, $p = 1$
(2,2,1)+(4,4,3)	two mode analysis; second mode with $m = 4$, $n = 4$, $p = 3$
(2,2,1)+(4,-,-)	two modes for the u displacement, $m = 2$ and $m = 4$
	one mode for the v displacement, $n = 2$
	one mode for the w displacement, $p = 1$

Section 4.2 includes a discussion on the number of numerical integration points employed in different types of analyses. These numbers depend on the complexity of the expression to be integrated, as well as the desired accuracy.

It was decided to carry out a series of test runs on beam problems, before proceeding to plate problems, as there are very few, if any, analytical solutions available in the latter

case. A rectangular beam with various end conditions was analysed for linear elastic, non-linear geometry, and non-linear material behaviour. The finite strip results are compared with analytical and other numerical solutions in section 4.3.

I beams and T beams can be considered the least complicated stiffened panel structures presently in use. Moreover, there are numerous analytical and numerical procedures to solve for the deflections of these beams in both linear and non-linear realms. Several finite strips can be assembled to form an I beam as discussed in Chapter 3. The finite strip results for such a beam, are compared with analytical solutions in the case of linear analyses and against finite element results in the case of non-linear analyses in section 4.4.

Section 4.5 includes the numerical investigations on laterally loaded square plates which are not reinforced by stiffeners. In addition to the comparisons of the finite strip results with the other analysis procedures, the investigation extends to the determination of the number of finite strips necessary to adequately represent a given plate structure. The effects of various boundary conditions and the convergence of the displacements and strain energies as the number of strips is increased are also discussed in this section. Furthermore, the spread of plastic zones as the load increases was also examined.

Section 4.6 consists of the results of a detailed analysis on a stiffened panel. In the example problem, stiffeners, which are of the shape of an inverted T beam, run in one direction parallel to each other. The plate and the stiffeners are clamped all around. Deflections at the centre of the panel and at the top of the stiffeners and also the overall deflected shape of the panel, are compared with finite element results. Stresses at the top surface of the plate are also compared.

As explained in Chapter 2, the finite strip method uses continuously differentiable smooth series in the longitudinal direction of a strip. Most of the analyses in sections 4.2 through 4.6 are carried out by employing only one term of this series for each displacement

component u, v and w. However, the effect of adding more modes was also investigated in some example problems where it was considered necessary for more accuracy.

4.2 Numerical Integration

As discussed in section 3.8, it is often desirable to use different numbers of integration points in different directions of integration. If the number of Gauss evaluation points used in x, y and z directions (local) of a strip are r, s, and t respectively, the numerical integration will be denoted by $(r \times s \times t)$ in this chapter.

In Gauss quadrature, the sampling points are selected so as to integrate a polynomial expression exactly. Therefore, if the integrand is a polynomial, it is a trivial matter to determine the number of Gauss evaluation points necessary to obtain exact answers. However, when the integrand is not a polynomial, or when the explicit form of it is not known, there is no sure way to find out the required order of integration. In an elastic analysis, the integrand of equation 3.32 consists of the strain-displacement matrices $[B]$ and $[C]$ and the elasticity matrix $[D]$. Therefore, in such an analysis, it is possible to get the exact form of the expression to be integrated by examining the strain displacement relations and the displacement shape functions.

As described in chapter 3, the displacement variations in the strip direction consists of hyperbolic and circular functions. Therefore, it is clear that a typical higher order term one will encounter in equation 3.32 will look like $\sin^2 \pi\xi$, $\cos^2 \pi\xi$, $\sinh^2 \beta\xi$ or $\sinh \beta\xi \cosh \beta\xi$ in an elastic small deflection analysis, and $\sin^4 \pi\xi$, $\cos^4 \pi\xi$, $\sinh^4 \beta\xi$ or $\sinh^2 \beta\xi \cosh^2 \beta\xi$ in an elastic large deflection analysis if only one mode is employed in each of the three displacements. Results of integration of some of these terms by using different numbers of Gauss evaluation points are presented in Table 4.1. It is clear from this table

that 5 Gauss points are sufficient to obtain results accurate to five significant numbers in a small deflection analysis. Even in a large deflection problem, 5 point integration is in error only by about 0.5%. A similar analysis revealed that 7 Gauss points are sufficient in the strip direction if two displacement modes are employed in finite strip analysis.

TABLE 4.1 NUMERICAL INTEGRATION OF CIRCULAR AND HYPERBOLIC FUNCTIONS

$$\int_0^1 I d\xi$$

I	$\sin^2 \pi\xi$	$\sinh^2 \pi\xi$	$\cos^4 \pi\xi$
2 Gauss points	0.3857986652	17.5318815892	0.3772432796
5 Gauss points	0.5000154016	20.8061932632	0.3770682123
10 Gauss points	0.4999999999	20.8064616871	0.3749999995
Exact	0.5000000000	20.8064616871	0.3750000000

Considering widthwise and depthwise directions of a strip, equation 3.32 consists of quadratic polynomial terms in an elastic small or large deflection analysis. Therefore, it was concluded that 2 Gauss evaluation points are sufficient across the width of the strip and also through the thickness for exact integration in an elastic analysis.

When the plate material behaves in a non-linear manner, determination of r, s and t is more difficult. By observing the results of some example runs with varying number of integration points, it was decided to use the same r and s numbers as in the linear analysis even in non-linear material problems. However, as plastification of the material extends through the depth, a higher order of Gauss integration is required to capture the non-linear distribution of stresses. For thin beams of rectangular cross-section, Wu and Witmer[41]

found that 4 depthwise Gaussian points were sufficient to give an accurate representation of this non-linear stress distribution. This same order of Gauss integration is employed in the present analysis.

In summarising this section, the numerical integrations employed in the examples given in this chapter will be,

(5×2×2)	one mode analysis, linear material,
(7×2×2)	two mode analysis, linear material,
(5×2×4)	one mode analysis, non-linear material,
(7×2×4)	two mode analysis, non-linear material.

When more than two modes were employed, r was increased to 10.

Exceptions to the above will be seen in some example problems, where it was necessary to investigate the effect of using different orders of integration. The order of numerical integration used in these problems will be stated in the corresponding discussions.

Positions and weighting coefficients for Gaussian integration are presented in Table 4.2 for the different orders used in this thesis.

TABLE 4.2 ABSCISSAE AND WEIGHT COEFFICIENTS OF THE GAUSSIAN QUADRATURE FORMULA[19]

$$\int_{-1}^{1} f(x)dx = \sum_{j=1}^{N} H_j f(a_j),$$

N	$\pm a$	H
2	0.57735 02691 89626	1.00000 00000 00000
4	0.86113 63115 94053 0.33998 10435 84856	0.34785 48451 37454 0.65214 51548 62546
5	0.90167 98459 38664 0.53846 93101 05683 0.00000 00000 00000	0.23692 68850 56189 0.47862 86704 99366 0.56888 88888 88888
6	0.93246 95142 03152 0.66120 93864 66265 0.23861 91860 83197	0.17132 44923 79170 0.36076 15730 48139 0.46791 39345 72691
7	0.94910 79123 42759 0.74153 11855 99394 0.40584 51513 77397 0.00000 00000 00000	0.12948 49661 68870 0.27970 53914 89277 0.38183 00505 05119 0.41795 91836 73469
10	0.97390 65285 17172 0.86506 33666 88985 0.67940 95682 99024 0.43339 53941 29247 0.14887 43389 81631	0.06667 13443 08688 0.14945 13491 50581 0.21908 63625 15982 0.26926 67193 09996 0.29552 42247 14753

4.3 Analysis of a Rectangular Beam

4.3.1 Simply supported ends

The behaviour of a rectangular beam simply supported in bending, but restrained axially, subjected to a uniformly distributed load, was studied by the finite strip method using a single strip. Only one displacement mode was employed in the strip direction for

each of the three displacements u, v and w. i.e. in the notation described before, the analysis uses (2,1,1).

A Rayleigh-Ritz analysis can be conducted out to obtain the modal solutions for this problem by an energy minimization. The total potential energy of the beam is given by,

$$V = \frac{1}{2}\int_0^L \left[EI\left(\frac{\partial^2 w}{\partial x^2}\right)^2 - 2qw \right] \quad dx \tag{4.1}$$

where, x is the distance measured along the beam,

L is the length of the beam,

EI is the flexural rigidity of the beam,

q is the distributed load per unit length and

w is the lateral deflection.

Assuming a one mode solution of the form,

$$w = w_c \sin\frac{\pi x}{L}, \tag{4.2}$$

the potential energy can be minimized with respect to the central deflection w_c to get,

$$\begin{aligned} w_c &= \frac{4L^4 q}{\pi^5 EI} \\ &= \frac{5L^4 q}{382.525EI}. \end{aligned} \tag{4.3}$$

This result is slightly larger than the central deflection given by the exact solution, $5L^4q/384EI$. A comparison of the central deflection, strain energy, maximum bending moment and the maximum stress, obtained by the three methods is presented in Table 4.3, along with the geometric and material properties of the beam.

TABLE 4.3 LINEAR ELASTIC RESPONSE OF A SIMPLY SUPPORTED BEAM

beam length, L = 500 mm

beam width, b = 10 mm

beam thickness, h = 10 mm

elastic modulus, E = 220000 N/mm^2

Poisson's ratio, ν = 0.0

uniformly distributed load, q = 0.1 N/mm^2

	Beam Theory	One Mode Analytical	One Mode Finite Strip
Central Deflection(mm)	4.4389	4.4560	4.4560
Strain Energy(Nmm)	71.023	70.920	70.920
Maximum Moment(Nm)	3.1250	3.2251	3.2251
Maximum Stress(N/mm^2)	187.50	193.51	193.51

Error in deflection between the beam theory and the other two methods is 0.38% whereas that in energy is 0.15%. However, as one might expect in any approximate solution based on a displacement approach, bending moments and stresses show a higher error (3.2%) between the exact solution and the modal solutions.

Deflected shape of the beam and bending moment distribution along the beam obtained by finite strip analysis are plotted with the beam theory solutions in Figures 4.1 and 4.2 respectively. The non-dimensional length, ξ, is used in these plots as the abscissa. It is clear that in a linear analysis an accurate prediction of the displacement and moment distributions can be obtained by the present finite strip formulation using one mode, and that the finite strip integration scheme is correct for this linear problem.

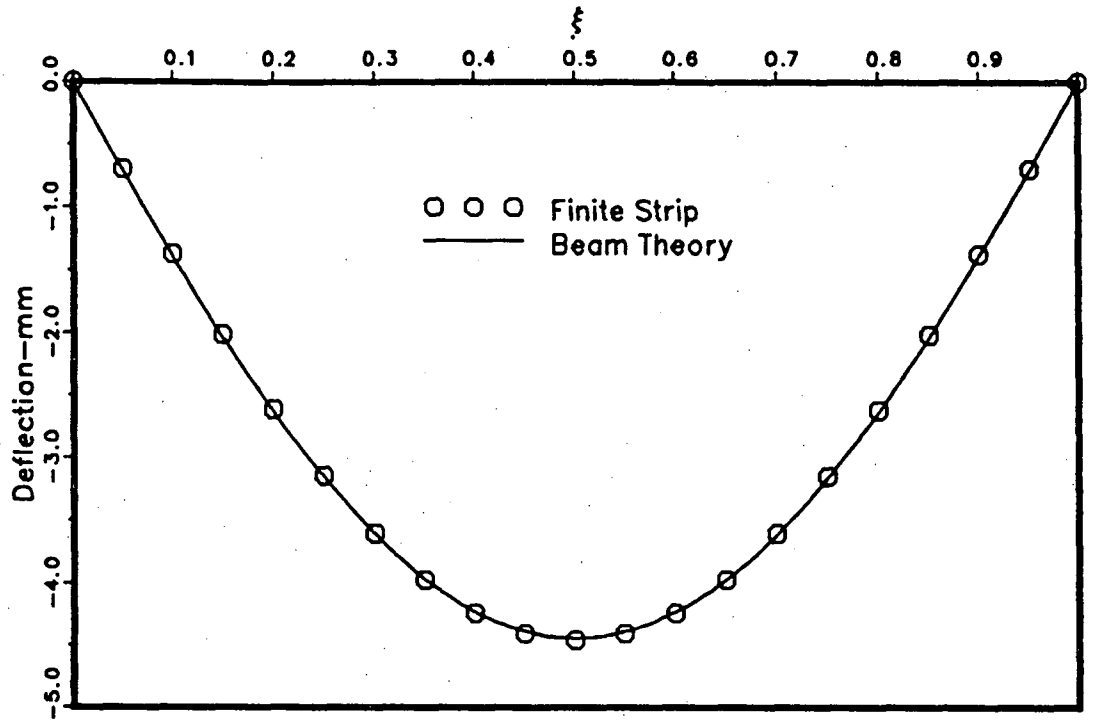

Figure 4.1 – Deflected shape of the simply supported rectangular beam

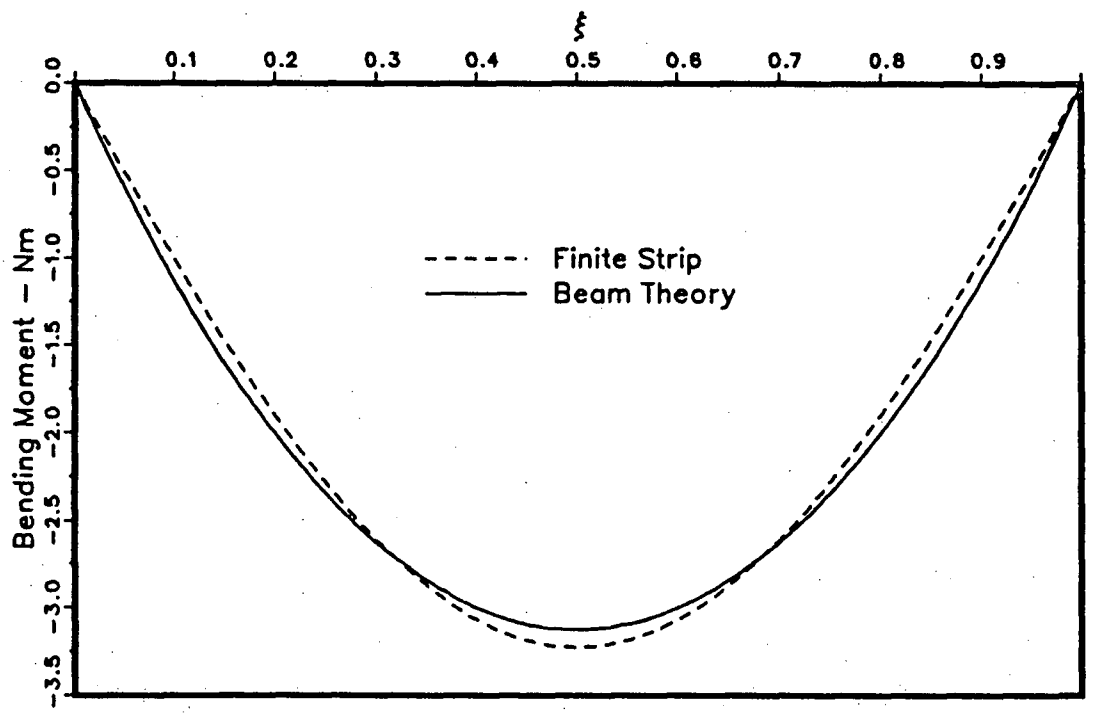

Figure 4.2 – Bending moment distribution of the simply supported rectangular beam

Timoshenko and Woinowsky-Krieger[2] present an exact solution for a uniformly loaded bar submitted to the action of an axial force. This solution takes the effect of the membrane forces into account. A large deflection finite strip analysis was carried out by employing only one mode (2,1,1). A comparison of these two methods in the form of a load deflection plot is included in the Figure 4.3. In this analysis, a Poisson's ratio of 0.3 was assumed. A very good agreement is seen between the one mode finite strip solution and the analytical solution. Finite strip results are slightly on the flexible side of the Timoshenko curve. A comparison of strain energies in these two methods is presented in Figure 4.4. It is clear from this plot that even in terms of energy, the finite strip model is more flexible than the Timoshenko theory. This result contradicts with the energy bound one might expect in a modal solution. This may be due to possible errors in numerical integration.

Figure 4.3 also includes the results of an elastic perfectly plastic analysis of the same problem. All the geometric and material properties are the same and a yield stress of 300 N/mm^2 is assumed. Soreide et al. [42] used a total Lagrangian finite element formulation including the effects of large deflections by incorporating von-Karman strain displacement relations. Plastic analysis was carried out by following the von-Mises yield criterion. Bäcklund[43] also attacked the problem in a similar manner, but used a different element. The present one mode finite strip result agrees very well with the solution by Soreide et al. and is similar to the Bäcklund solution. The loss of stiffness due to plastification is clearly demonstrated. Also shown in the Figure are the rigid plastic solution of Jones[44] and the rigid plastic horizontally free solution which depicts an uncontrolled deformation once the plastic collapse load is reached.

In a rigid plastic analysis, the stress in the beam cannot exceed the yield stress of the beam material. Therefore, once every section of the beam becomes plastic, the beam turns to a plastic string with constant tension if it is restricted against axial motion. The

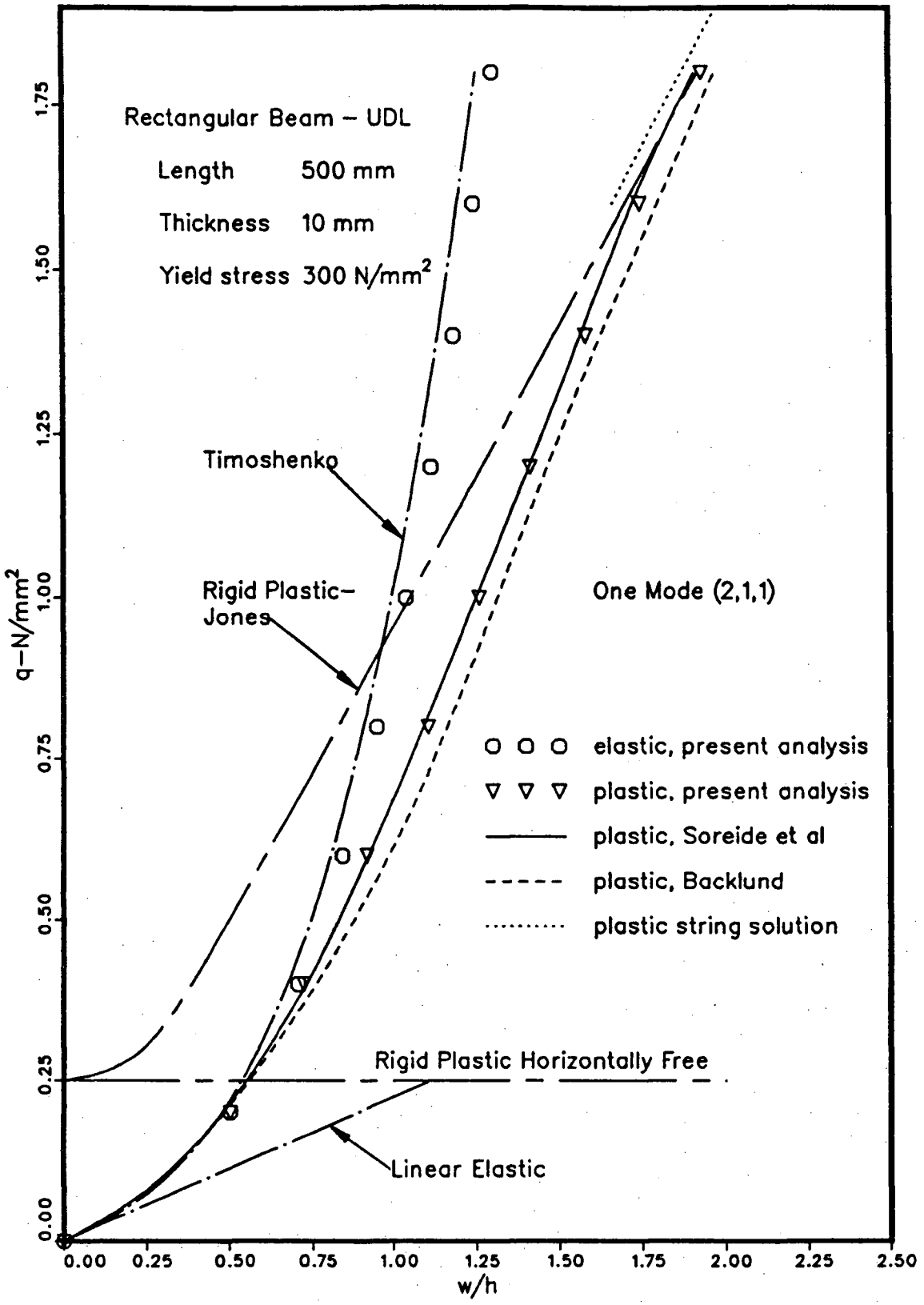

Figure 4.3 – Central deflections of the simply supported rectangular beam

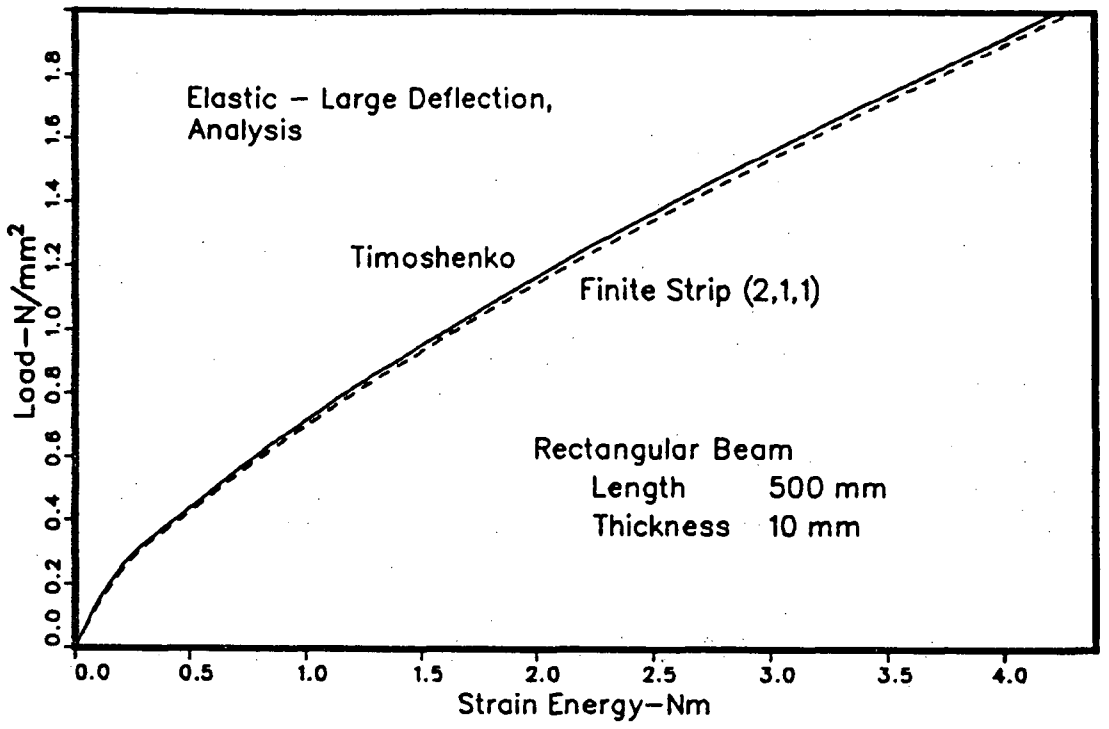

Figure 4.4 – Strain energy comparison in the simply supported rectangular beam

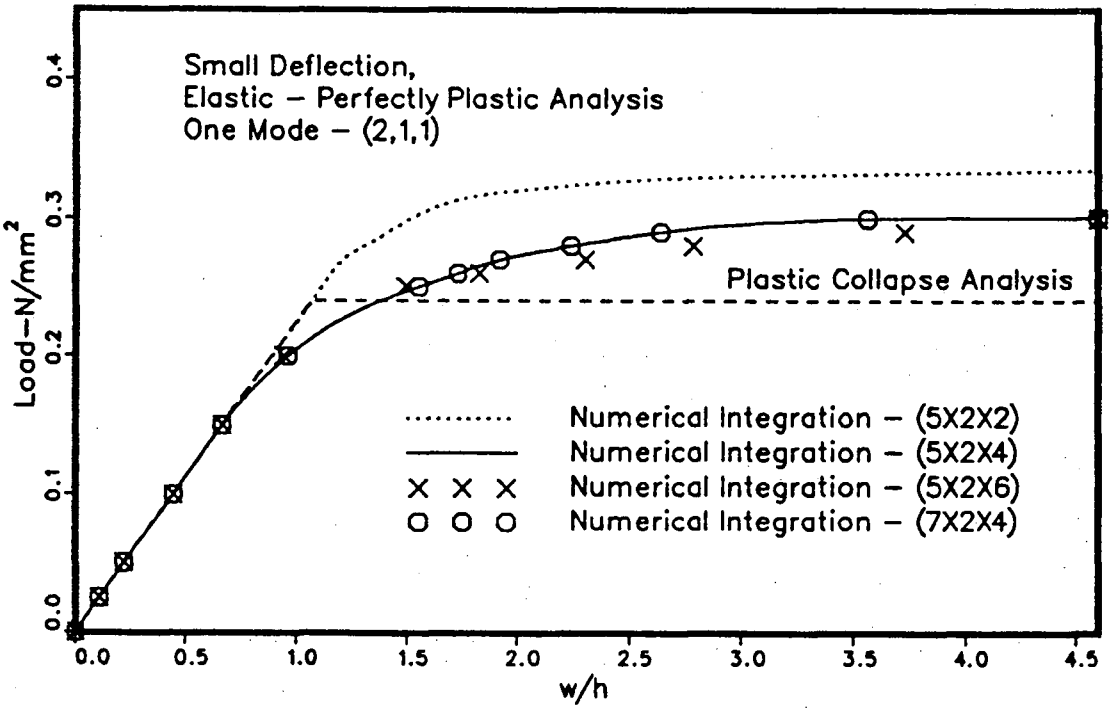

Figure 4.5 – Deflection response of the simply supported rectangular beam with varying numerical integrations

uniform tension T is equal to the cross sectional area times the yield stress. The central deflection of such a string can be calculated by considering the equilibrium of a small portion of the string. This results in a central deflection of $qL^2/8\sigma_y h$ for a uniformly distributed load of intensity q, where σ_y is the yield stress and h is the beam thickness. This solution is also presented in Figure 4.3. Finite strip and Soreide et al. curves are asymptotic to the plastic string solution when the central deflection exceeds two beam thicknesses, as one might expect in a plastic analysis. The other important factor to be noted is the difference between Jones's rigid plastic model and the elastic-perfectly plastic analysis when the central deflection is less than a beam thickness. Exclusion of the elastic deformation causes the rigid plastic model to underestimate the deflection. For example, when the finite strip central deflection is equal to a beam thickness, the rigid plastic model predicts a central deflection of 0.7 times the beam thickness.

For axially unrestrained beams, one of the simple and popular methods of plastic analysis utilises the concept of plastic hinges. A plastic hinge analysis on the example rectangular beam predicts a plastic collapse at a uniformly distributed load of $8M_p/L^2$ per unit length, where M_p is the fully plastic moment of the section. The load displacement curve obtained by plastic hinge analysis consists of two straight line segments. Figure 4.5 illustrates the comparison of this curve with several finite strip solutions obtained by varying the number of numerical integration points in a small deflection elastic-perfectly plastic analysis. The number of integration points across the width was kept constant at 2 as it was shown that 2 points are sufficient in that direction to integrate the expressions exactly. This analysis shows that the effect on displacements of increasing spanwise Gauss points from 5 to 7 is very minimal. However, it is seen that to capture the plastic stress distribution through the thickness at least 4 Gauss points should be employed in that direction. This is consistent with Wu and Witmer[41]'s observations. The finite strip solution does not show a kink and

it reaches a plateau at a load 25% higher than the plastic collapse load. This difference can be attributed to the difference between actual and assumed deflection patterns of the beam. When the central deflection is larger than about 50% of beam thickness, these small deflection analyses are no-longer valid for a beam with constrained ends. Therefore, it is unreasonable to expect any kind of agreement at deflections larger than one beam thickness.

4.3.2 Clamped ends

The same beam was analysed again by clamping its ends against rotation in the xz plane. The finite strip solution uses the beam vibration modes of a fixed ended beam for the lateral deflection. The analytical one mode solution can again be determined by an energy minimization procedure. One mode solution now takes the form,

$$w = w_c \left[\alpha_1 \left(\sinh \beta_1 x - \sin \beta_1 x\right) + \left(\cosh \beta_1 x - \cos \beta_1 x\right)\right] / A_1 \tag{4.4}$$

where, $A_1 = \alpha_1 \left(\sinh 0.5\beta_1 L - \sin 0.5\beta_1 L\right) + \left(\cosh 0.5\beta_1 L - \cos 0.5\beta_1 L\right),$

$$\alpha_1 = \frac{\cos \beta_1 L - \cosh \beta_1 L}{\sinh \beta_1 L - \sin \beta_1 L}$$

and, $\beta_1 L$ is the first solution of the transcendental equation, $\cosh \beta L = \sec \beta L$.

Substitution of 4.4 into 4.1 and the subsequent minimization gives,

$$w_c = \frac{L^4 q}{379.353 EI}, \tag{4.5}$$

which is slightly higher than the beam theory solution, $L^4 q/384EI$. A comparison of the central deflection, strain energy, maximum bending moment and the maximum stress, obtained by the three methods is presented in Table 4.4, along with the geometric and material properties of the beam.

TABLE 4.4 LINEAR ELASTIC RESPONSE OF A CLAMPED BEAM

beam length, L = 500 mm

beam width, b = 10 mm

beam thickness, h = 10 mm

elastic modulus, E = 220000 N/mm^2

uniformly distributed load, q = 1.0 N/mm^2

Poisson's ratio, ν = 0.3

	Beam Theory	One Mode Analytical	One Mode Finite Strip
Central Deflection(mm)	8.8778	8.9866	8.9866
Strain Energy(Nmm)	1183.7	1175.4	1175.4
Moment at Middle(Nm)	10.42	11.62	11.62
Moment at Support(Nm)	20.84	19.12	19.12
Maximum Stress at Middle(N/mm^2)	62.52	69.74	69.74
Maximum Stress at Support(N/mm^2)	125.0	114.7	114.7

The error in deflection between the beam theory and the other two methods is 1.23%, whereas that in energy is 0.70%. However, as one might expect in any approximate solution based on a displacement approach, bending moments and stresses show a higher error (11.52% at the centre and 8.25 % at the clamped end) between the exact solution and the modal solutions. The finite strip model predicts a larger bending moment at the middle of the beam and a smaller moment at the clamped ends than the exact solution. The ratio between these two moments is 1.645 whereas the exact ratio is 2.. These differences are due to the beam vibration mode assumed in the present analysis instead of the polynomial

shape obtained in plate theory for the deflected shape of the beam.

The deflected shape and the bending moment distribution of the beam obtained by finite strip analysis is plotted with the beam theory solutions in Figures 4.6 and 4.7 respectively. It is clear that in a linear analysis an accurate prediction of the displacement and moment distributions can be obtained by the present finite strip formulation using one mode.

The results of a large displacement analysis of the clamped beam are presented in Figure 4.8 where comparisons are made to an exact solution to the problem given by Timoshenko and Woinowsky-Krieger[2]. Only one displacement mode is employed in each of the three displacements u, v and w; however, the finite strip solution for this problem is sensitive to the selection of the shape functions for u, the in plane longitudinal displacement. For $g^u(\xi) = \sin 2\pi\xi$ and for $g^u(\xi) = \partial\phi_1/\partial x$ where $\phi_1 = g^w(\xi)$, the load displacement curves are almost identical, but are on the stiff side of the Timoshenko solution by about 12.5% for a deflection of one beam depth to about 17% for a deflection of twice the beam depth. However, for $g^u(\xi) = \sin 4\pi\xi$, there is very good agreement with the analytical solution. This can be explained by considering axial equilibrium of the fixed ended beam, which requires that the axial force be constant along the beam. Since the beam is of uniform cross section, this is the same as requiring the axial strain to be constant. The expression for axial strain is given by,

$$\epsilon_x = \frac{\partial u}{\partial x} + \frac{1}{2}\left(\frac{\partial w}{\partial x}\right)^2 \tag{4.6}$$

If the shape function for w, ϕ, is approximated by $(1 - \cos 2\pi\xi)$, then, $\left(\frac{\partial w}{\partial x}\right)^2$ will vary as $\cos 4\pi\xi$. Therefore, the shape function for the axial displacement should take the form,

$$g^u(\xi) = \sin 4\pi\xi \tag{4.7}$$

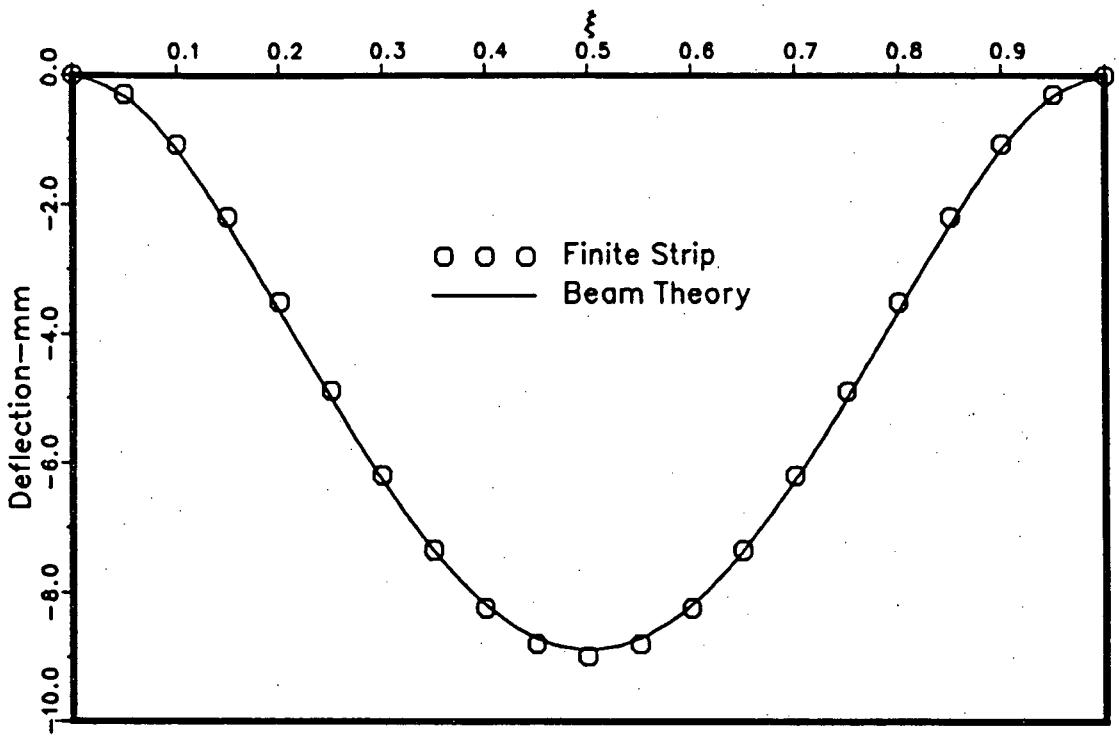

Figure 4.6 – Deflected shape of the clamped rectangular beam

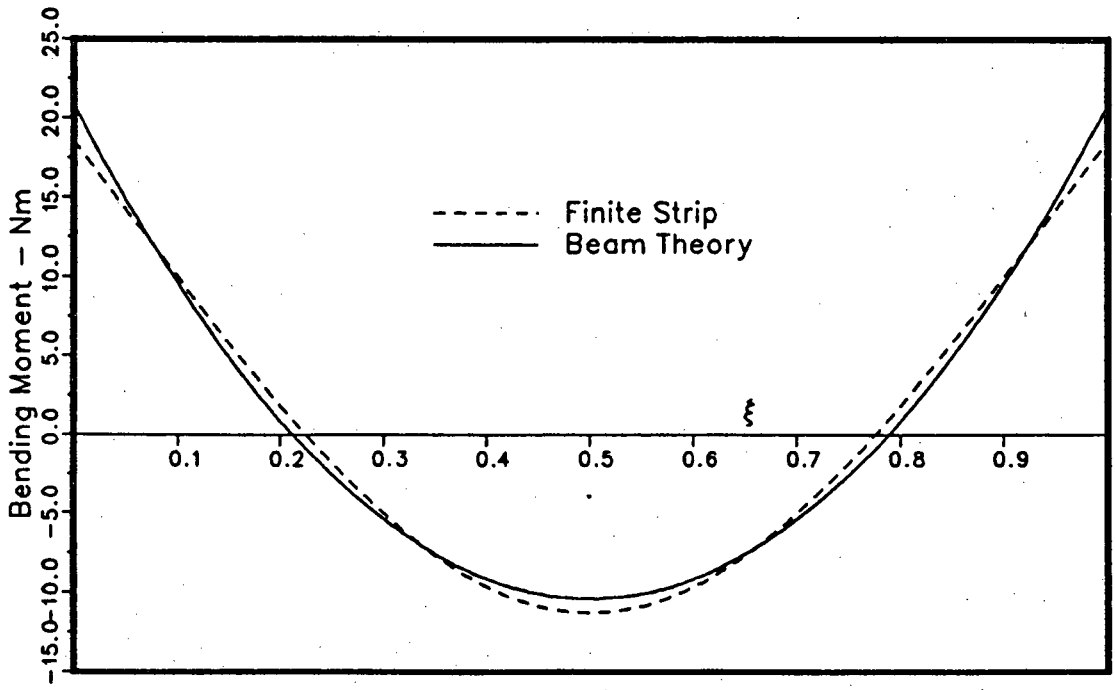

Figure 4.7 – Bending moment distribution of the clamped rectangular beam

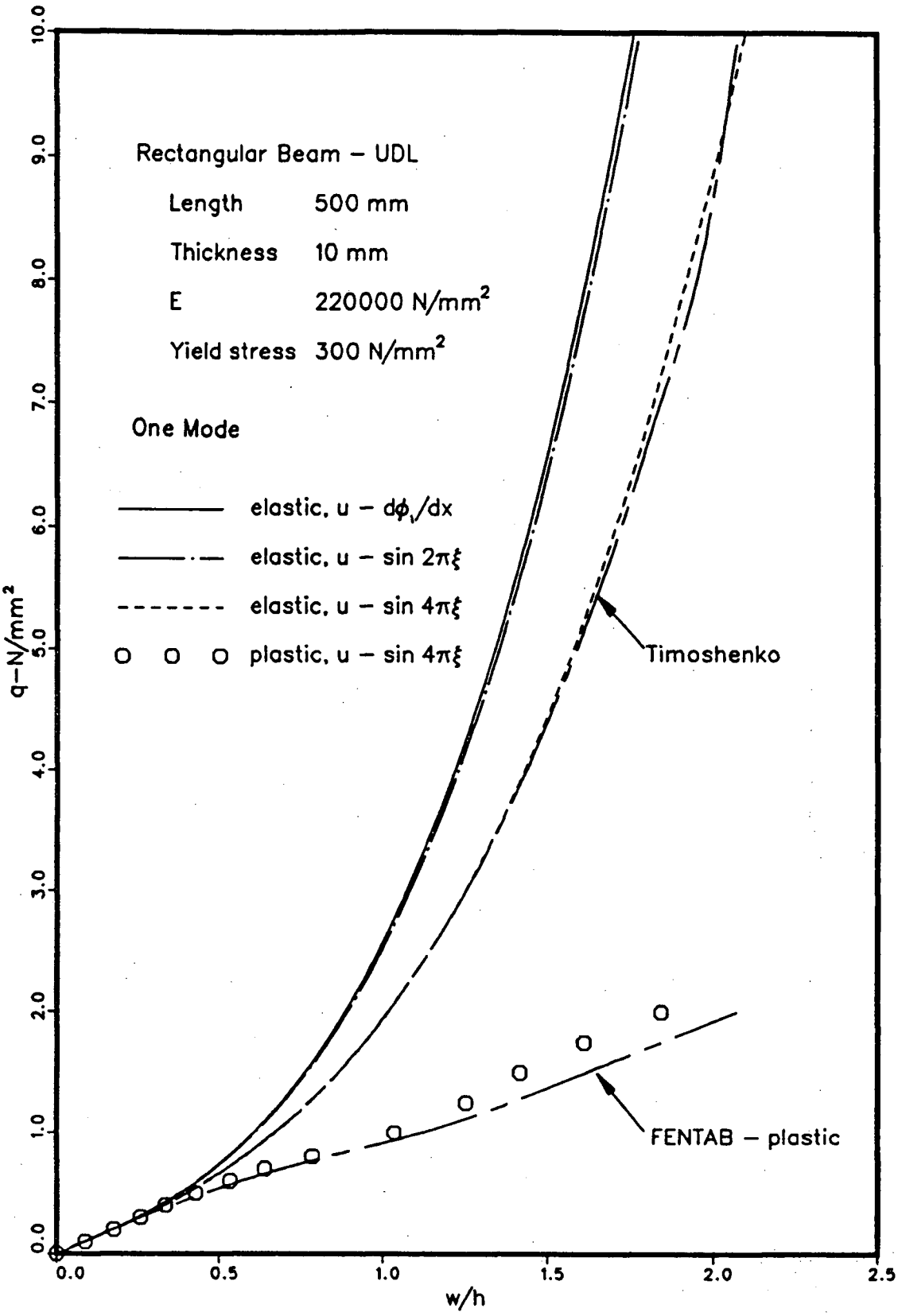

Figure 4.8 – Central deflections of the clamped rectangular beam

so that ϵ_x can be constant along the length. Note that this requirement can be used to select u variation corresponding to any given w shape function along the length of the strip.

To verify the shape of the u displacement along the beam strip, it was decided to carry out a finite element analysis incorporating geometric non-linearities. For this purpose, the finite element computer programme FENTAB[45] was used, which was developed at The University of British Columbia in 1986. FENTAB is capable of predicting the transient response of slender ductile beams exhibiting geometric and/or material non-linearities. Thus, FENTAB can be used to predict static response of beams by means of a dynamic relaxation procedure. For the present analysis, FENTAB was used with 10 elements per half span. 3 spanwise and 4 depthwise Gauss integration points were employed in each element to perform the numerical integrations. The FENTAB solution for u displacement along the beam at a uniformly distributed load of 2.5 N/mm^2 is plotted in Figure 4.9, along with a curve that varies as $\sin 4\pi\xi$. Although they are not identical, $\sin 4\pi\xi$ is a very close approximation to the FENTAB curve.

Strain energy predictions by the finite strip method for the present problem are compared with the Timoshenko solution in Figure 4.10. As in the case of a simply supported beam, finite strip results are more flexible than the analytical solution. Lack of an energy bound may be due to errors in numerical integration. Agreement between the two curves is satisfactory.

A comparison between the results of the finite strip programme and FENTAB for an elastic-perfectly plastic analysis is also included in Figure 4.8. Figure 4.11 is a large scale plot of the same results with the addition of the plastic string solution at larger displacements. Note that the FENTAB curve approaches the plastic string solution at a central deflection of about twice the beam depth. The finite strip solution is more stiff than the FENTAB curve. The two curves agree very well until a central deflection of about one beam depth.

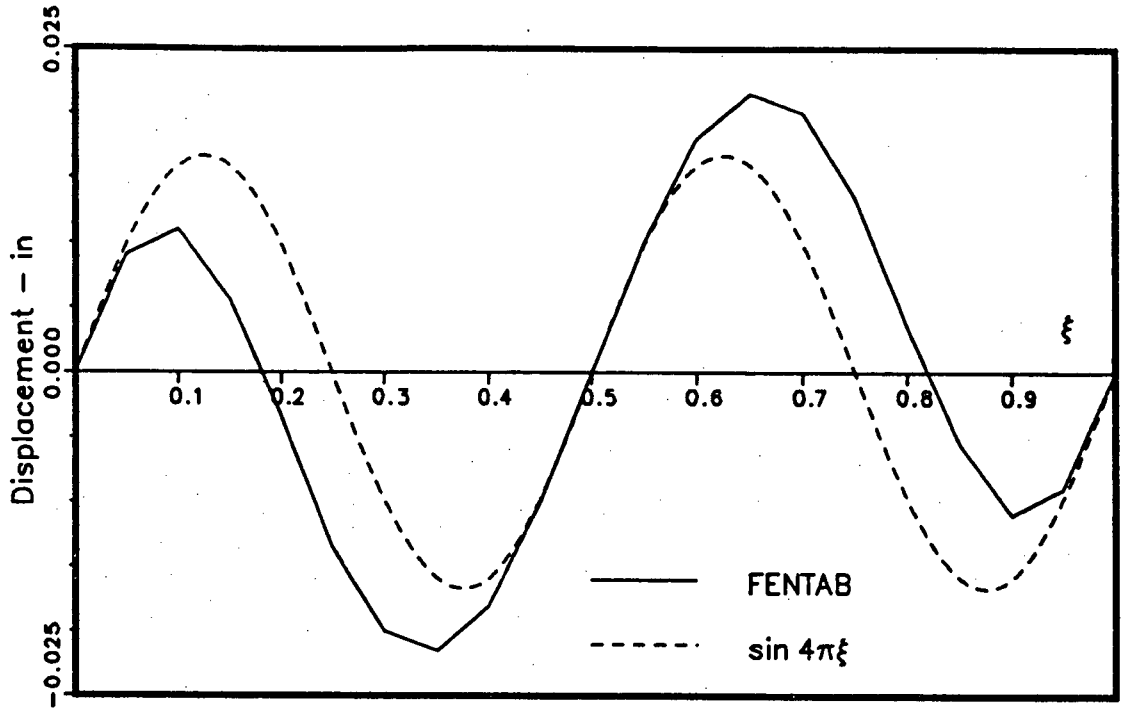

Figure 4.9 – u displacement along the clamped beam for q = 2.5 N/mm²

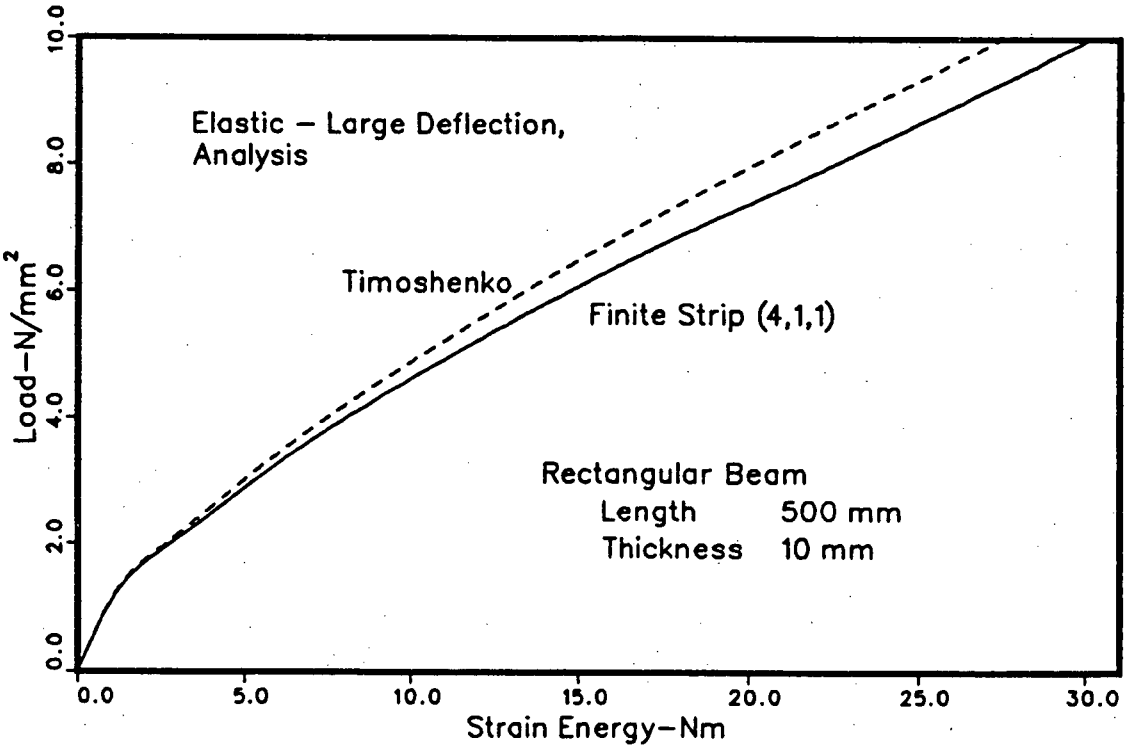

Figure 4.10 – Strain energy comparison in the clamped rectangular beam

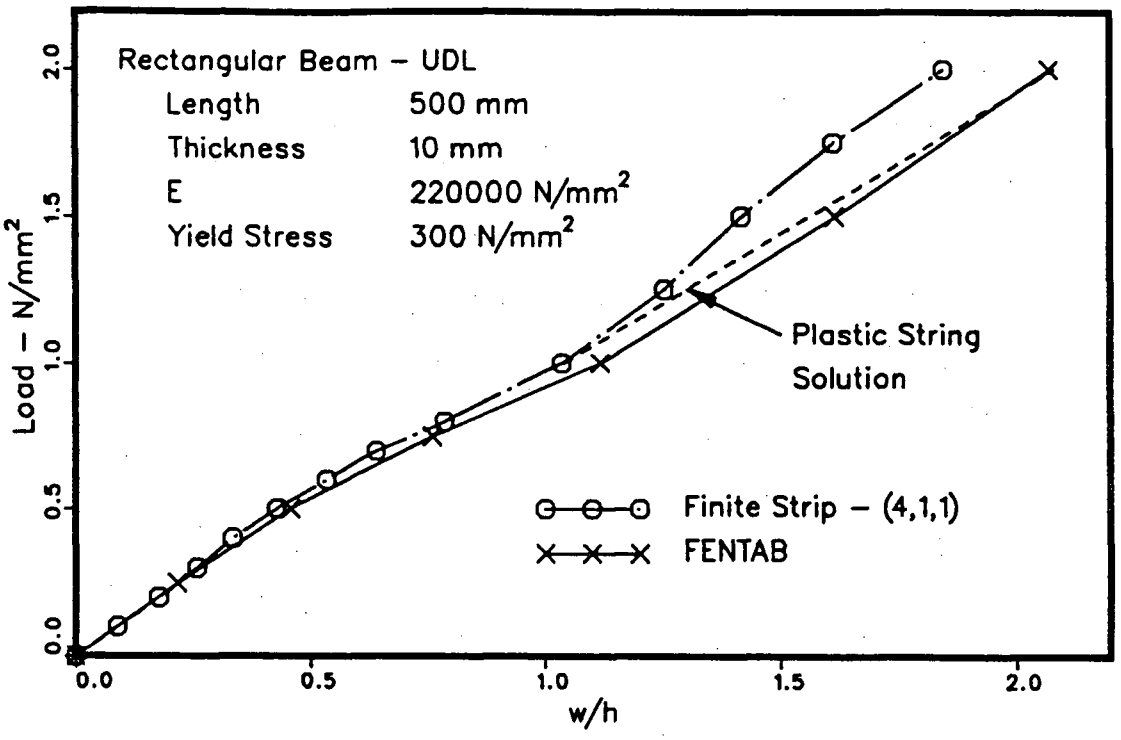

Figure 4.11 – Central deflections of the clamped beam in a large deflection, elastic–perfectly plastic analysis

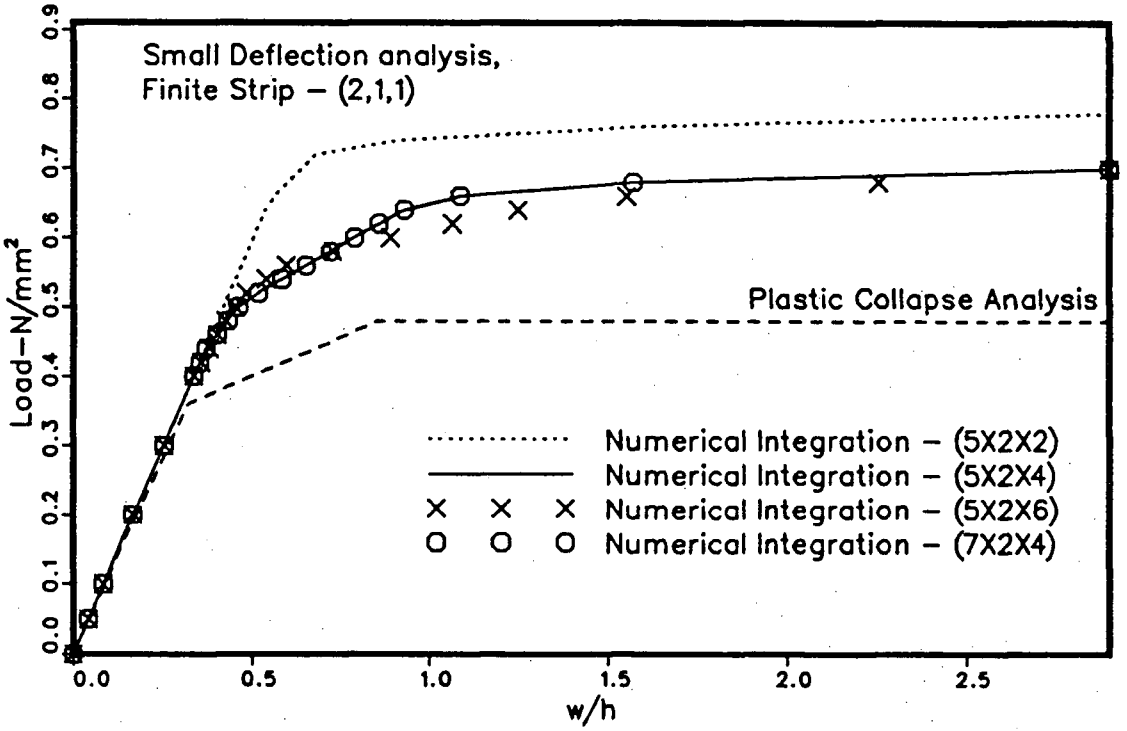

Figure 4.12 – Central deflections of the Clamped Beam with varying numerical integrations

The difference between these two curves increases from 6.33% to 11.18% when the central deflection increases from one to two beam thicknesses. At very high deflections the beam behaves as a plastic string, which has a parabolic shape. However, the finite strip solution always maintains the $\phi_p(\xi)$ shape, with zero slopes at both ends. On the other hand, FENTAB solution is capable of assuming a parabolic shape since a fine mesh has been used. This is the reason for the differences observed between FENTAB and the finite strip model at higher values of deflections.

The classsical three hinge collapse mechanism for a fixed ended beam predicts the occurence of the first two plastic hinges at a uniformly distributed load of $12M_p/L^2$ per unit length. Plastic collapse takes place at a uniformly distributed load of $16M_p/L^2$. For the example beam, these values correspond to 0.36 and 0.48 N/mm^2 respectively. These results are compared with the results of the finite strip model in Figure 4.12. In this figure, four finite strip curves, obtained by using different numerical integrations, are presented. These curves confirm that even when using the clamped beam vibration mode, 5 integration points are sufficient along the length of the strip, and at least 4 points are required through the thickness for plastic analysis. As it was observed in the simply supported beam example, finite strip curves lie above the plastic hinge solution throughout the loading history. The general shape of the curves are quite similar. The kinks in finite strip curves come later than those of the other, at loads of $16.67M_p/L^2$ and $21.67M_p/L^2$ respectively. In plastic hinge analysis, the beam is assumed to behave as a mechanism once the plastic collapse load is reached. On the other hand, as mentioned before, the finite strip solution maintains a zero slope at the ends of the beam throughout the loading history, and therefore is not capable of approximating the mechanism mode. Furthermore, the comparisons of Figure 4.11 are more practical than those of Figure 4.12 because of the inclusion of the effect of large deflections in the former, especially in regions where the differences occur.

4.4 Analysis of an I Beam

As the final example of beam analysis, an axially constrained steel I beam subjected to a uniformly distributed line load was considered. Geometric and material properties of the beam are presented in Figure 4.13(a). It is seen that the assembly process in the finite strip method adds an extra area to the beam cross section at the T joints as shown in Figure 4.13(b). This additional area increases the cross sectional area by 1.65% and the second moment of area by 1.87% in the example I beam. The flange width of the finite strip model was adjusted to give the correct second moment of area. In the analyses that follow, a flange width of 7.858 in. was used instead of the actual width of 8.022 in.

4.4.1 Simply supported ends

The example I beam was analysed with simply-supported boundary conditions first. In the initial linear elastic analysis, a five strip discretisation was employed (Fig. 4.13(c)) and the following shape functions were used for the three displacements u, v and w, in the longitudinal direction.

$$g_m^u(\xi) = \cos \pi\xi,$$

$$g_n^v(\xi) = \sin \pi\xi, \qquad \text{and}$$

$$g_p^w(\xi) = \sin \pi\xi, \qquad \text{i.e.} \quad (m, n, p) = (1, 1, 1)$$

These shape functions satisfy the necessary compatibility between v and w displacements and also between u and the slope of the w displacements (section 3.3.4). At the ends of the beam, the u displacement of the top flange is the negative of that of the bottom flange, thus ensuring an axial constraint at the middle of the web. Lines (a) and (c) of the

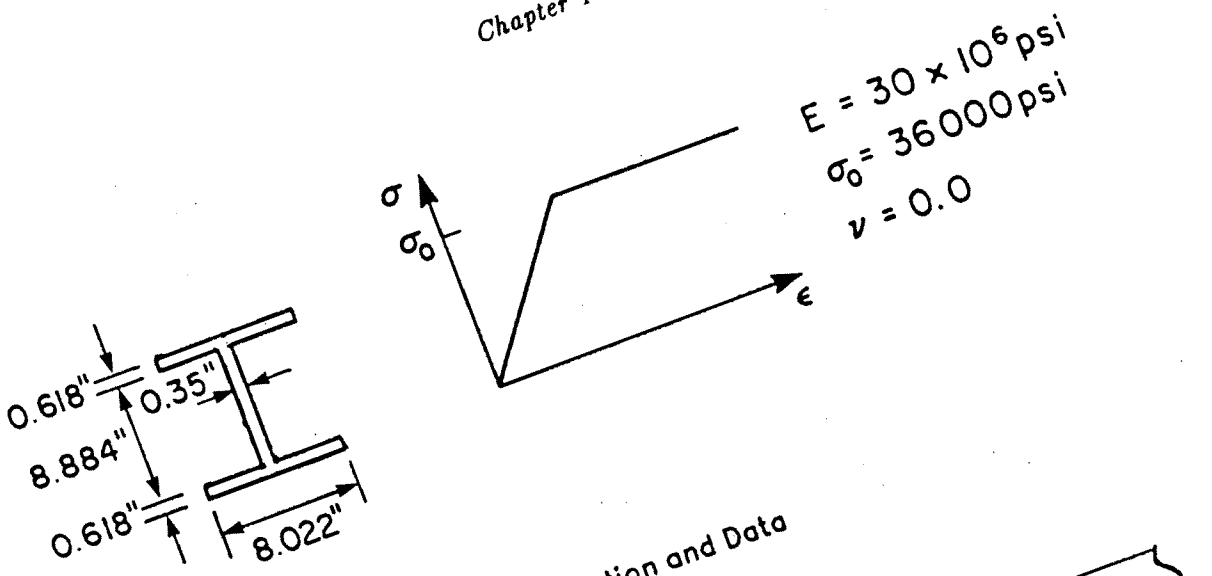

Figure 4.13 – Symmetric I beam example

Table 4.5 summarise the results of the linear elastic analysis. One mode analytical solutions were calculated following a Rayleigh-Ritz procedure, as discussed in the previous sections.

TABLE 4.5 LINEAR ELASTIC RESPONSE OF A SIMPLY SUPPORTED I BEAM

beam length, L = 400 in

elastic modulus, E = 30000000 lb/in^2

uniformly distributed load, q = 495 lb/in

		Beam Theory	One Mode Analytical	One Mode Finite Strip
Central	(a)	22.488	22.575	22.820
Deflection(in)	(b)	22.699	22.792	22.820
Strain	(c)	1.4249	1.4228	1.4363
Energy $\times 10^{-6}$(lbin)	(d)	1.4380	1.4357	1.4363

The finite strip solutions are more flexible than the other two solutions, in both central deflection and strain energy. A major difference between the finite strip analysis and the other two methods is the ability of the finite strip analysis to include shear displacements in the web strip.

The shear displacement at any section of the beam is given by[46],

$$\delta_s = F \int_0^L \frac{V v}{A G} \quad dx, \tag{4.8}$$

where V is the vertical shear due to the actual loads, v is the vertical shear due to a unit load acting at the section where the deflection is desired, A is the area of the cross section, L is the length of the beam, x is the distance measured along the beam, G is the modulus

of elasticity of the beam material, and F is a factor depending on the form of the cross section. For an I section, F is given by,

$$F = \left[1 + \frac{3\left(D_2^2 - D_1^2\right) D_1}{2D_2^3}\left(\frac{t_2}{t_1} - 1\right)\right]\frac{4D_2^2}{10r^2}, \tag{4.9}$$

where, D_1 = distance from the neutral axis to the nearest surface of the flange,

D_2 = distance from the neutral axis to the extreme fibre,

t_1 = thickness of web,

t_2 = width of flange, and

r = radius of gyration of section with respect to the neutral axis.

Equation 4.8 yields a shear displacement of 0.2106 in at the mid span of the example beam. Corrected values of the central displacements and the strain energies are given in lines (b) and (d) of the Table 4.5, where the beam theory and analytical solutions have been increased by the amount of shear displacement and shear energy. The finite strip solutions now compare very well with the one mode analytical solutions.

In order to investigate the effect of large displacements, it was necessary to include another u mode which allows for finite stretching between the two pinned supports. As was explained in the clamped rectangular beam example, the requirement of a constant axial strain can be used in selecting this new mode. $\sin 2\pi\xi$ was chosen for this purpose as it satisfies the above requirement and is also antisymmetric about the mid span of the beam. The web is modelled by two equal width strips (Fig. 4.13(d)). In the middle of the web, i.e. on the new nodal line, the u displacement of the first mode was constrained to be zero.

For the example beam, a FENTAB analysis was also carried out, by incorporating geometric non-linearities. In this analysis, one half of the span was modelled by 10 equal length finite elements. Numerical integration through the depth is performed by employing

4 Gauss points through the web and a simple mid point in each of the flanges. Each element had three Gauss points along the axis. Results of the large deflection finite strip analysis are compared with the FENTAB results in Figure 4.14. Agreement is very good. The slight increase in flexibility observed in the finite strip solution can be attributed to the shear deformation in the web.

The comparison of predicted central deflections with FENTAB for an elastic plastic material, including large deflections, is presented in Figure 4.15, where it is seen that the agreement is excellent. When the central deflection approaches twice the beam depth, the FENTAB solution runs asymptotic to the plastic string limit. The finite strip solution, on the other hand, agrees with the solution obtained using a one mode Galerkin procedure on the governing differential equation for a plastic string. This is expected as the assumed displacement variation in the Galerkin analysis is the same as in the finite strip, namely $\sin \pi\xi$.

Axially restraining an I beam at different locations along the depth makes a considerable difference to the load-deflection response. Results for central deflection of the same I beam in an elastic large deflection analysis are presented in Figure 4.16 for the different support points A, B, C, D and E. These results were obtained by modelling the web with four equal width finite strips. The support point was moved from A through E by changing the boundary conditions at the appropriate nodal line. In a linear elastic analysis, points A and E should yield the same displacement pattern as they are equidistant from the centroidal axis. Therefore, near the origin, both these curves have the same slope. This is also true for the points B and D. However, as the axial stretching starts to take place, point A produces the stiffest solution and point E produces the most flexible solution. This can be explained as follows.

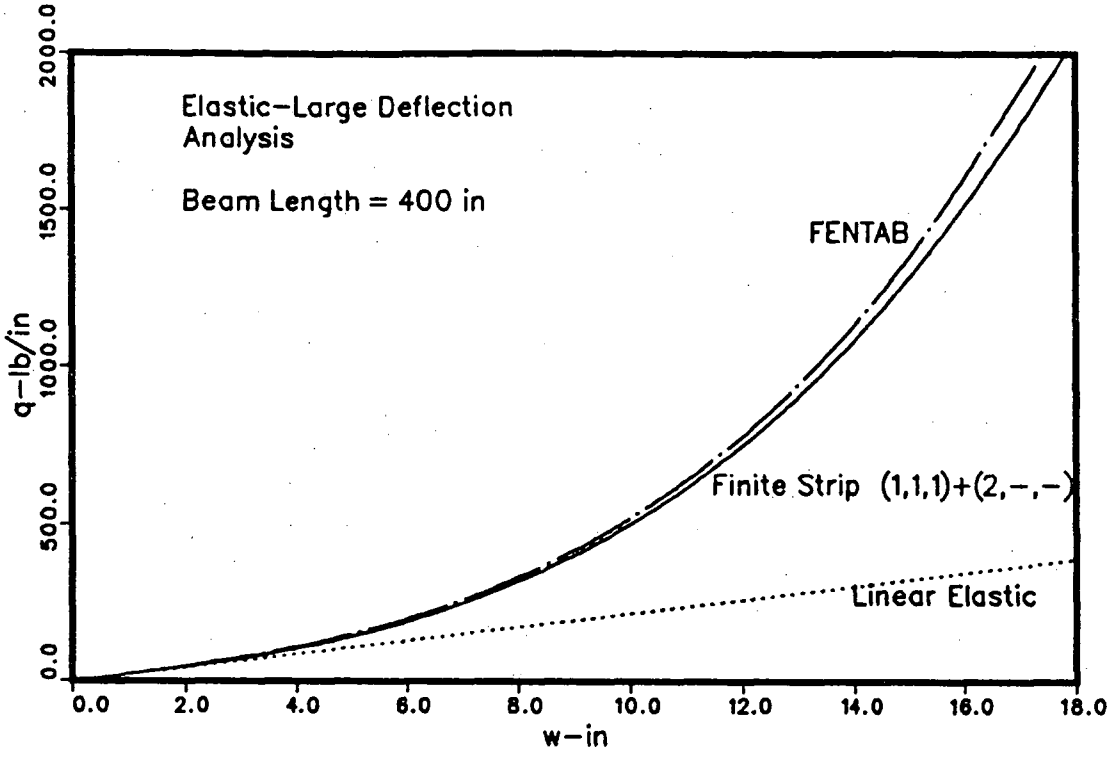

Figure 4.14 – Central deflections of the simply supported I beam in an elastic analysis

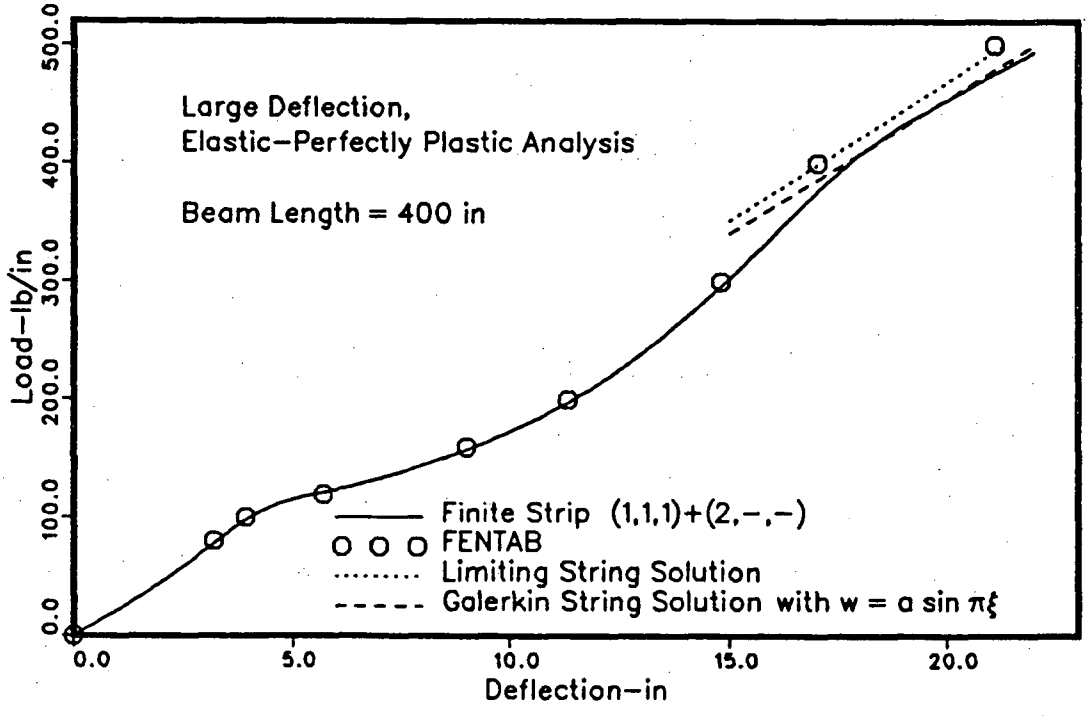

Figure 4.15 – Central deflections of the simply supported I beam in a elastic–perfectly plastic analysis

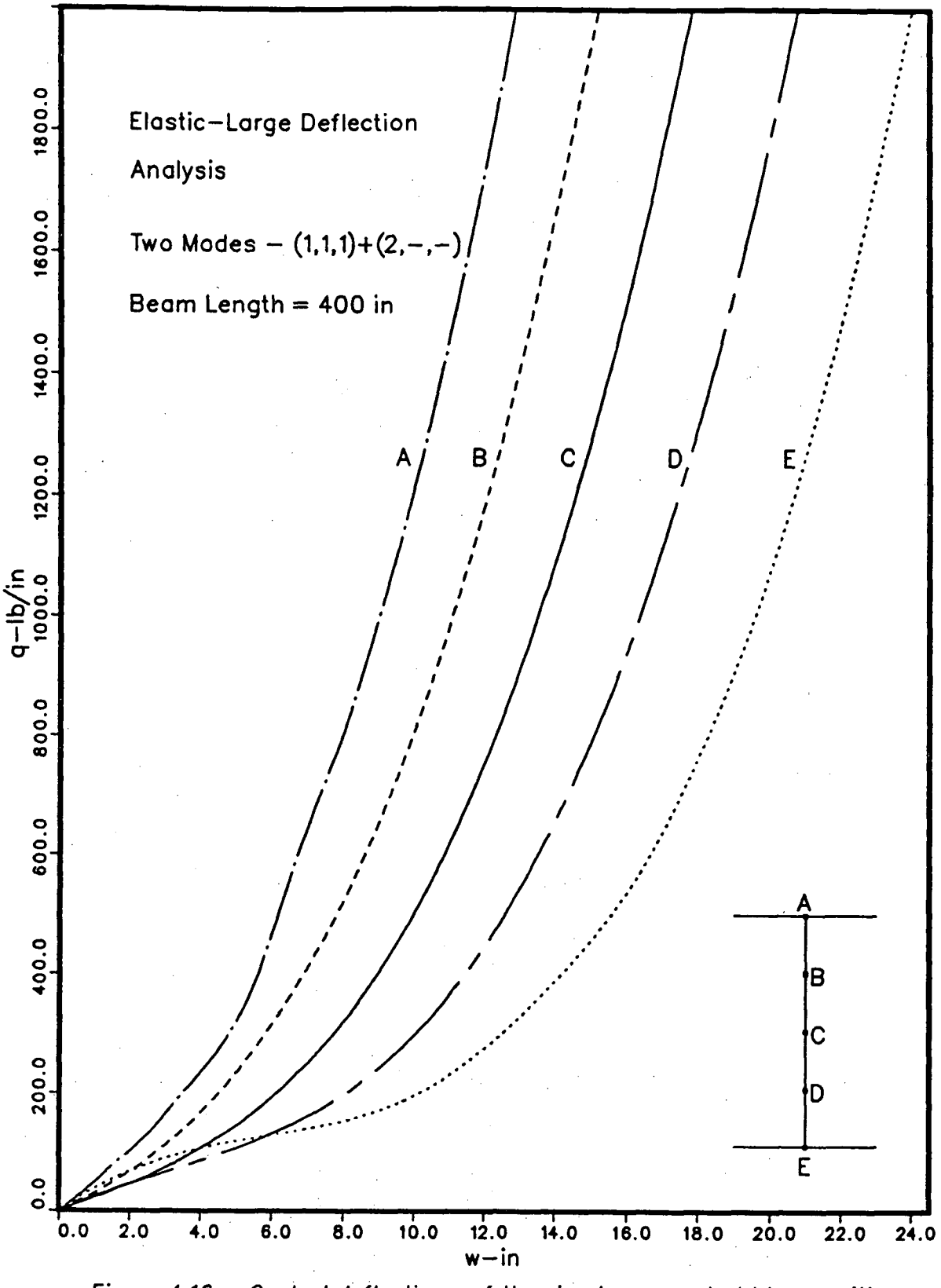

Figure 4.16 – Central deflections of the simply supported I beam with varying support points

When the beam is supported at the middle of the top flange(point A), the effect of the axial load at the support is equivalent to that of an axial load along, and a hogging bending moment about, the neutral axis (Fig. 4.17(a)). On the other hand, when the beam is supported at E, the axial load at the support can be replaced by an axial load along the neutral axis and a sagging bending moment about the neutral axis (Fig.4.17(b)). Therefore, in the former case, additional moment reduces the deflection due to lateral load, whereas in the latter case, it aids the deflection due to lateral load.

4.4.2 Clamped ends

The results of a one mode (1,1,1) linear elastic analysis of a clamped I beam are summarised in Table 4.6. The finite strip results were obtained by modelling the I beam with five strips as shown in Figure 4.13(c). To satisfy the linear requirement, the u displacement is assumed to be of the same shape as the slope of the w displacement in the longitudinal direction. The geometric and material properties are the same as for the simply supported case (Fig 4.13(a)). Once again, lines (a) and (c) of Table 4.6 present the central deflections and strain energies respectively before applying shear corrections. Corrected results are given in lines (b) and (d) respectively. The agreement between analytical and finite strip results is satisfactory.

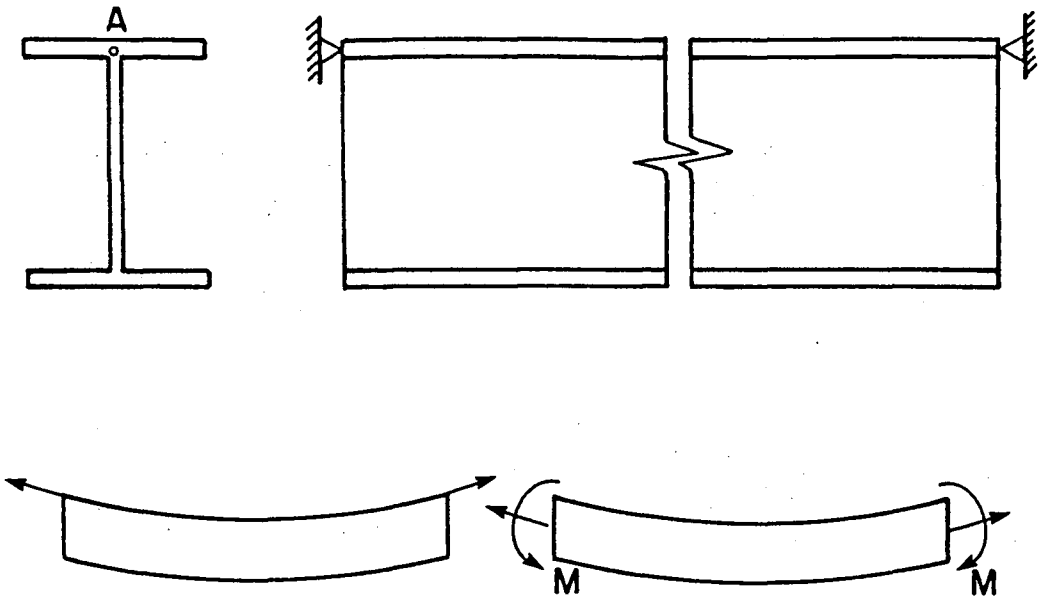

(a) Support point at A

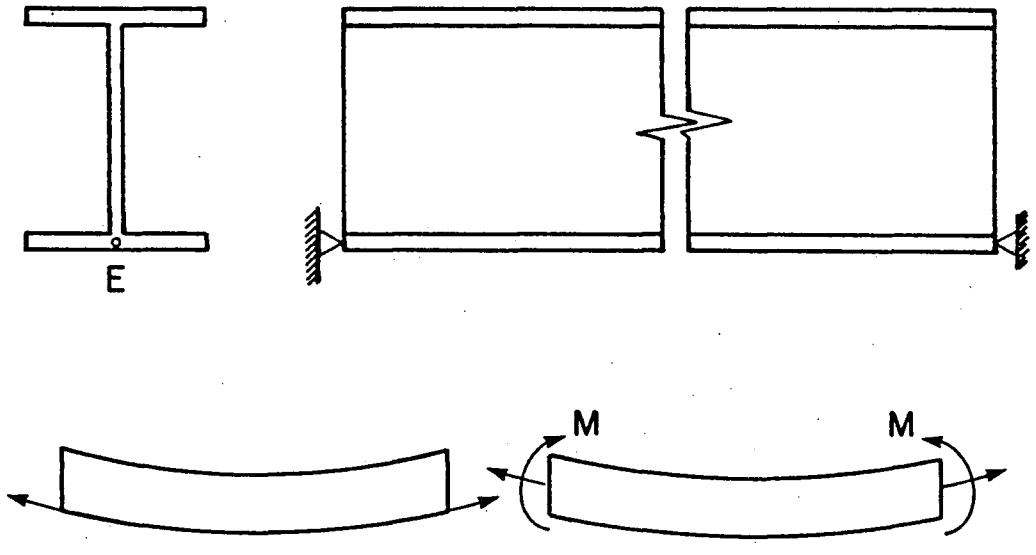

(b) Support point at E

Figure 4.17 – Varying support points

TABLE 4.6 LINEAR ELASTIC RESPONSE OF A CLAMPED I BEAM

beam length, L = 400 in

elastic modulus, E = 30000000 lb/in^2

uniformly distributed load, q = 495 lb/in

		Beam Theory	One Mode Analytical	One Mode Finite Strip
Central	(a)	4.4976	4.5528	4.7254
Deflection(in)	(b)	4.7082	4.7252	4.7254
Strain	(c)	2.3745	2.3579	2.4447
Energy $\times 10^{-5}$(lbin)	(d)	2.5054	2.4793	2.4447

The shear displacement along the beam is parabolic according to equation 4.8. However, v displacement of the web has the $\phi(\xi)$ shape along the beam (Section 3.3.2). It was revealed by a Rayleigh-Ritz analysis that the $\phi(\xi)$ shape underestimates the shear deflection at the mid span by 18.1% compared to the parabolic shape. Moreover, it is seen from Table 4.6 that for deflection the one mode analytical solution overestimates the beam theory by 1.21%. In the present example, shear constitutes 4.7% of the total deflection. Therefore, the total solution obtained by finite strip analysis should be $[(1.21 \times 0.955) - (18.1 \times 0.047)] = 0.33\%$ more flexible than the beam theory solution for the total deflection. This is in agreement with line (b) of Table 4.6.

Load deflection curves for the large deflection elastic behaviour of the example I beam are presented in Figure 4.18. FENTAB solutions were obtained by using the same number of elements and the same order of numerical integration as in the case of the simply supported I beam. One mode analysis (1, 1, 1) with the displacement patterns used in the linear

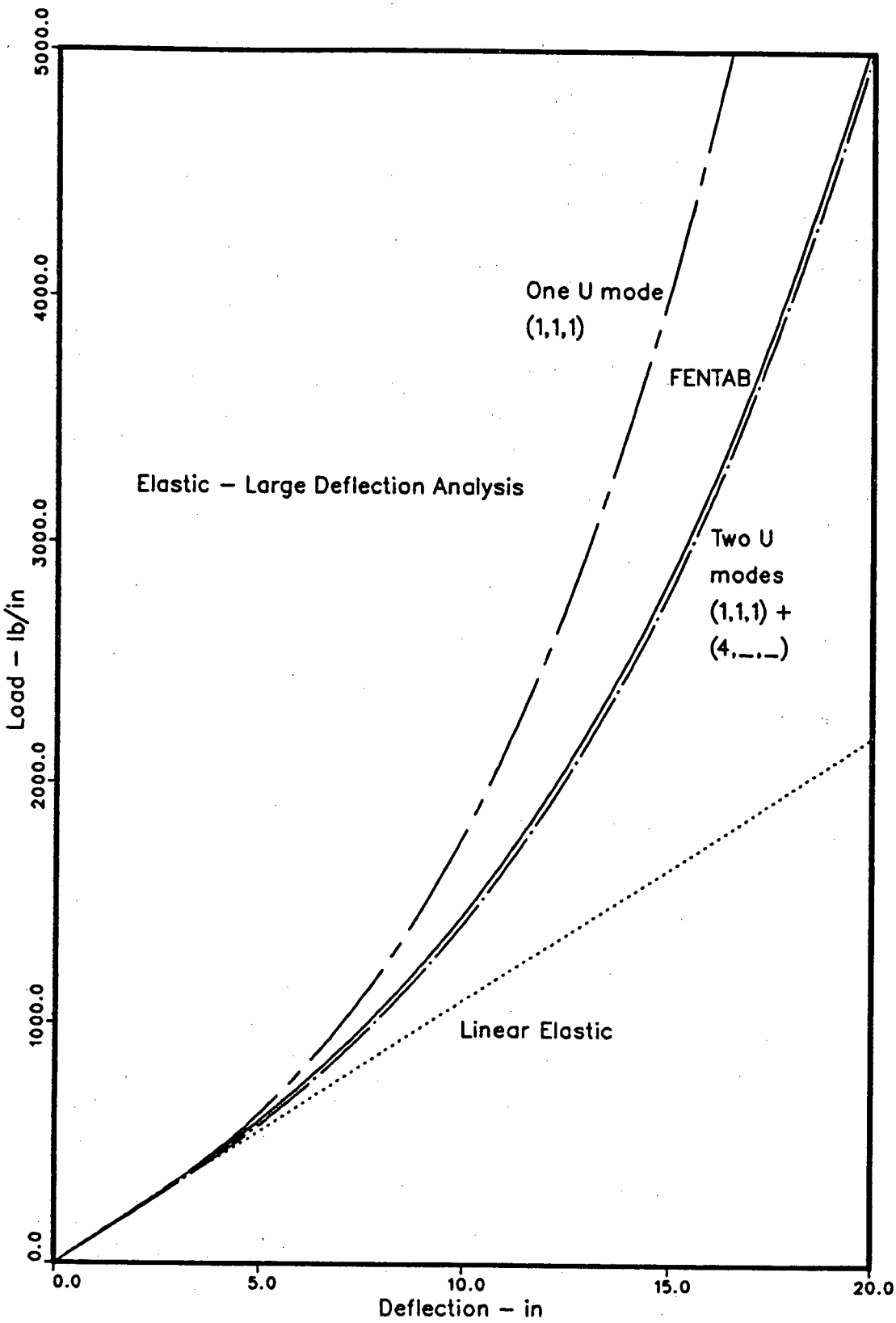

Figure 4.18 – Central deflections of the clamped I beam in an elastic analysis

elastic case, produces displacements which are stiffer than the FENTAB results. This is the same difference as was observed in the case of the clamped rectangular beam, where the u displacement varies as the slope of the w displacement in the axial direction (Fig.4.8). As explained before, this difference is due to the lack of ability of the present u mode to represent a constant axial strain. Accordingly, it was decided to add another mode for the u displacement which varies as $\sin 4\pi\xi$ in the longitudinal direction. A substantial improvement is seen after the addition of this mode, as shown in the Figure 4.18. The finite strip results now compare very well with the FENTAB analysis.

Results of an elastic-perfectly plastic analysis on the same beam are given in Figure 4.19. The FENTAB analysis represents the best estimate available for the exact results. The finite element discretisation and the order of numerical integration used in the FENTAB analysis are the same as before. In a small deflection analysis, the FENTAB curve follows the elastic-plastic hinge analysis very closely. However, the FENTAB curve exhibits a plateau at a load of 205 lb/in, about 6.5% higher than the rigid-plastic collapse load. The finite strip curve, although similar in shape, shows a very high load carrying capacity. The curve becomes almost horizontal at a load of 325 lb/in (at a load 58% higher than the FENTAB prediction). A similar difference was observed between the finite strip solution and plastic collapse solution in the case of a clamped rectangular beam (Fig. 4.12). There is a very slight slope in the finite strip curve at the collapse load, owing to the fact that some of the integration points will not become fully plastic, because of their locations.

Figure 4.19 also includes results of a large deflection elastic-plastic analysis. Compared to FENTAB, the finite strip results are in considerable error in the intermediate range of deflections, up to 200% higher in some locations. At larger deflections, when the beam is acting as a plastic string, agreement with FENTAB is much better, although the mode shape for w is quite different than the string mode shape.

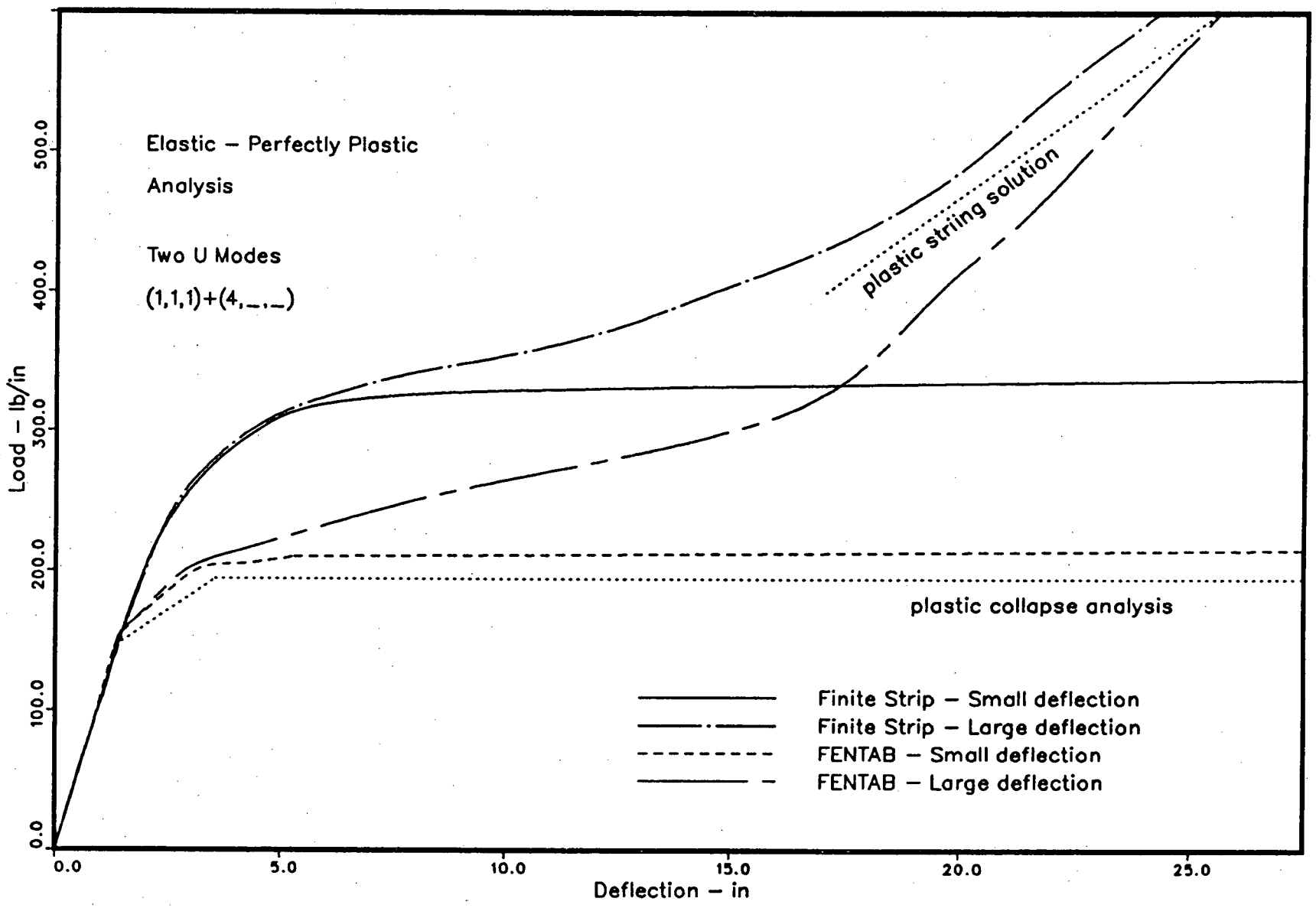

Figure 4.19 – Central deflections of the clamped I beam in an elastic–perfectly plastic analysis

To investigate the discrepancy at the intermediate range of deflections, it was decided to carry out a parametric study on the yield stress, while the elastic modulus was kept constant. Results of this analysis are presented in Figure 4.20 for $\sigma_0 = 36$, 72 and 108 ksi. When the yield stress is doubled to 72000 lb/in^2, the maximum difference in central displacements reduces to 106% (at a load of 600 lb/in) and to 62% for the yield stress of 108000 lb/in^2 (at a load of 946 lb/in). On the other hand, the maximum difference in the applied load for a given displacement remain essentially constant at about 38%.

Even though it was possible to increase the ratio of membrane to bending action by increasing the yield stress, overall differences between the two analyses were not reduced. Therefore, it can be concluded that the reason for the observed differences between finite strip and finite element results are due to the inability of the beam vibration mode to simulate the deflected shape of the beam when plastic action takes place.

Since the one mode representation of the example I beam did not produce satisfactory results, it was decided to study the effect of adding more displacement modes. Results of this analysis are presented in Figure 4.21. Addition of a second bending mode, i.e. two u modes and two w modes, reduces central displacements at a given load as compared to the previous solution (two u modes and one w mode). However, as stated before, it is necessary to have a u displacement shape which varies as the slope of the w variation, to satisfy linear requirements. Deflection response after the inclusion of this mode is represented by the dashed line in Figure 4.21. Note that the second w mode has a shape close to $(\cos 4\pi\xi - \cos 2\pi\xi)$. Therefore, the requirement of a constant axial strain can be satisfied by including a fourth u mode, which varies as $\sin 8\pi\xi$ along the strip. The solid line in Figure 4.21 is the load-deflection curve after introducing this new mode. It is clear now that the solution cannot be improved much by adding just a few more modes, presumably because of the zero slope boundary conditions.

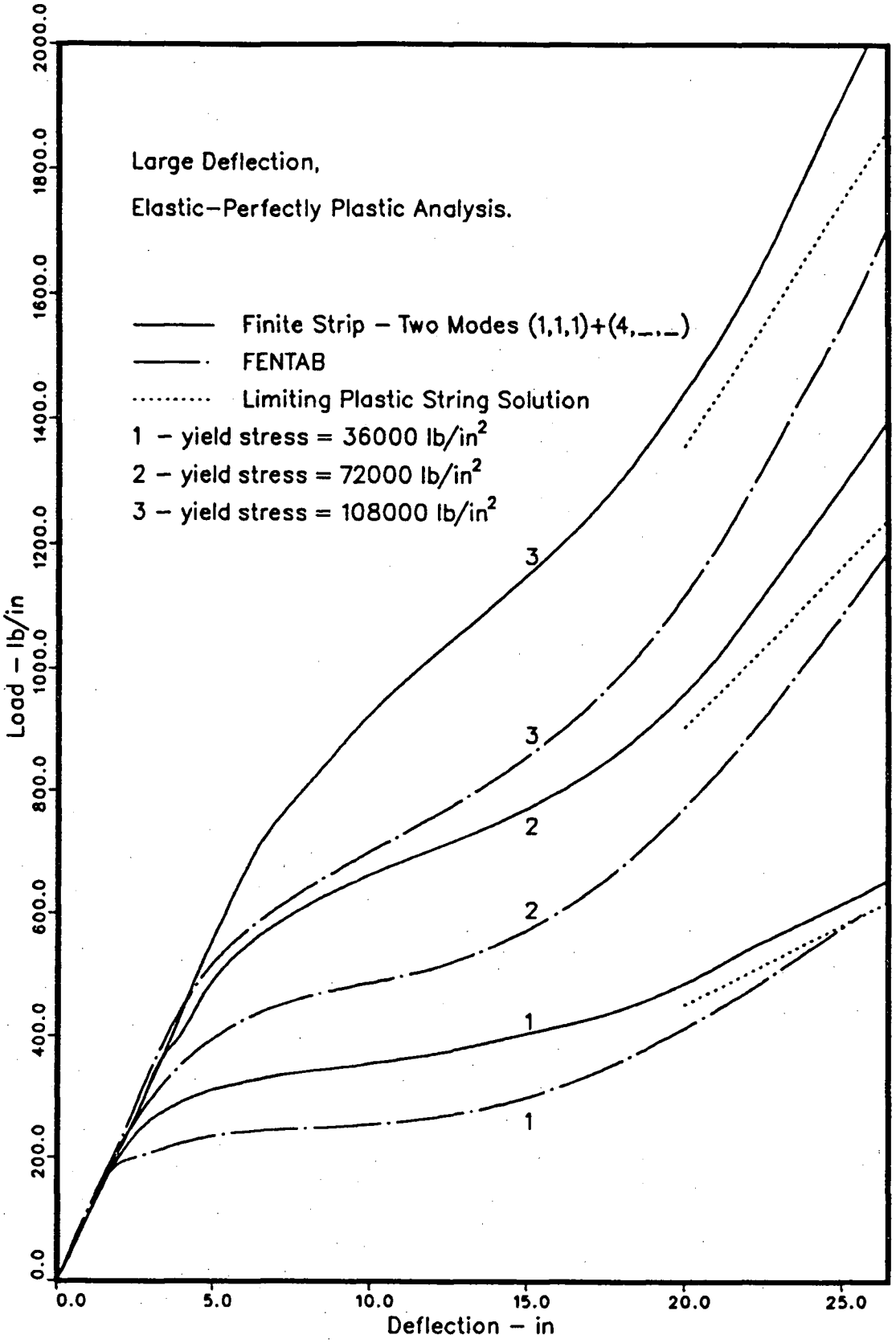

Figure 4.20 – Parametric study on the clamped I beam

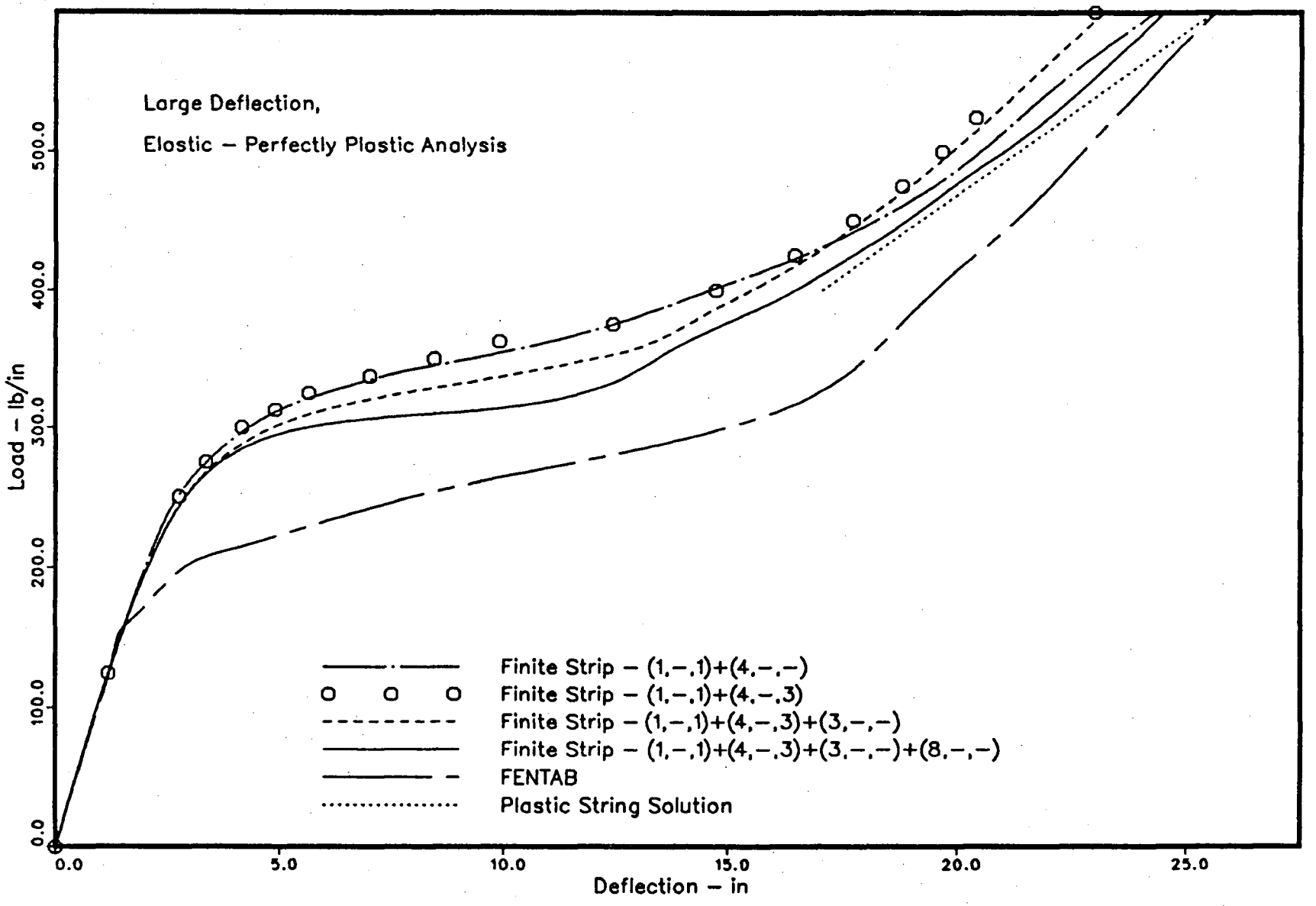

Figure 4.21 – Central deflections of the clamped I beam with varying displacement modes

Variation of strain energy in "two u one w" and "four u two w" finite strip models are presented in Figure 4.22, along with the FENTAB results. Energy variations in the other two finite strip models discussed in the previous paragraph fall between the dashed line and the solid line. As in the case of central deflections, a large discrepancy is seen between finite strip and FENTAB results. It is again realised that the improvement of solution by adding more modes of the type used in present analysis is very small. Therefore, it is believed that one has to resort to a different set of mode shapes in order to be able to represent plastic behaviour of a clamped beam.

As the final analysis on a clamped I beam, it was decided to examine the pattern of plastification in the beam. This can be observed by keeping track of the stress-strain behaviour of every integration point. Numerical integration was increased to $(7 \times 4 \times 4)$ from $(7 \times 2 \times 4)$ to obtain a more accurate description of the plastic flow. The spread of plastic zones as the load is increased is presented in Figure 4.23 for the large deflection elastic-perfectly plastic case with a yield stress of 36000 lb/in^2. These results were generated by employing a $(1,-,1)+(4,-,-)$ mode combination. This figure also includes the locations of the Gauss integration points in the beam. Vertical sections 1 through 7 are taken at the 7 spanwise Gauss evaluation points. Plastic action starts at the ends of the beam (sections 1 and 7) and at the integration points furthest from the centroidal axis. Once the two end sections are close to full plasticity, the mid-section (section 4) starts to show plastic action. Note that at a load of 250 lb/in, both end and centre sections have nearly formed plastic hinges, yet the displacement is very small(Fig. 4.19). This is again due to the restricted deflected shape. These results also show that the spread of plastic zones is modelled well by the present analysis, but unfortunately at load levels higher than the correct ones.

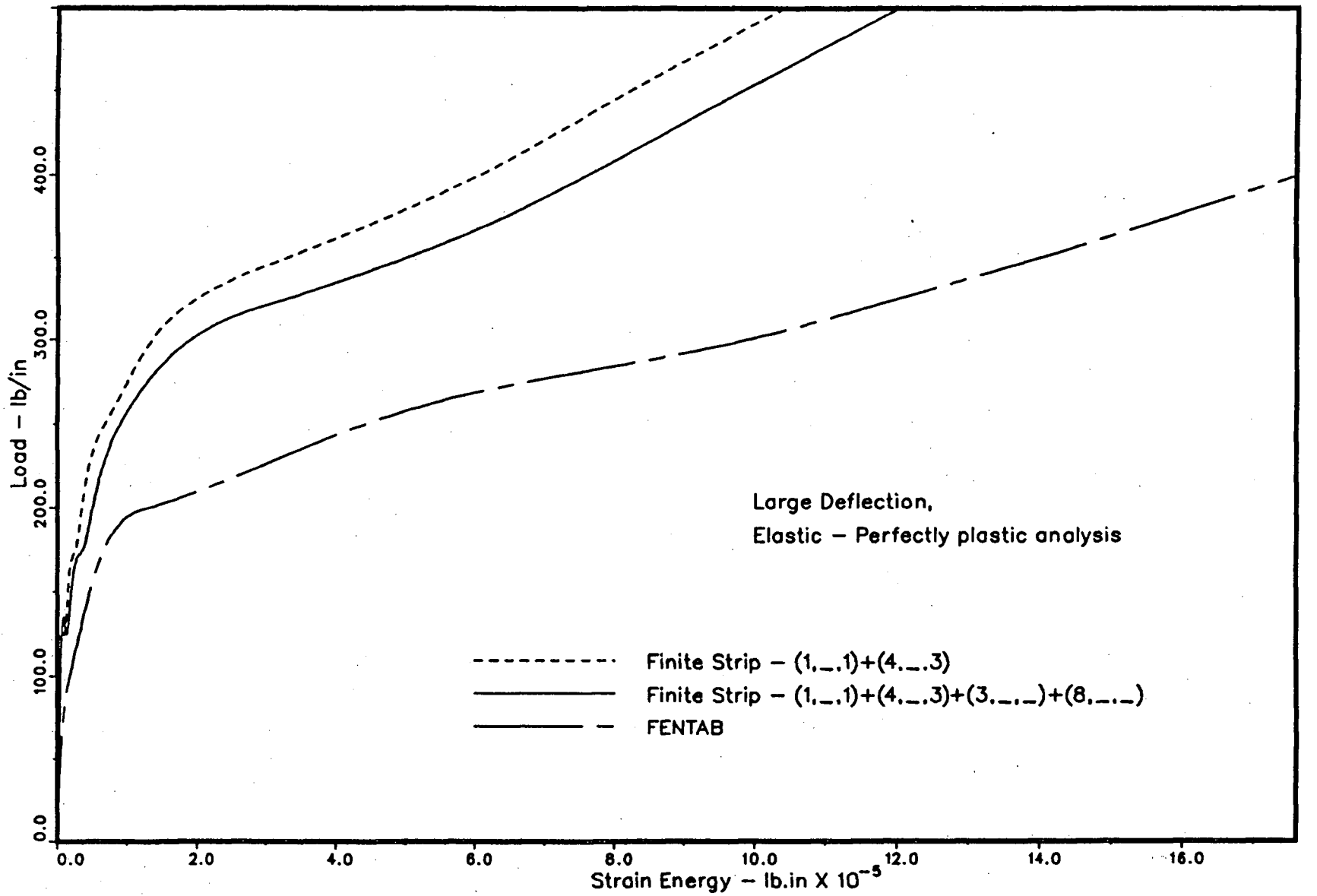

Figure 4.22 – Strain energy variation in the clamped I beam

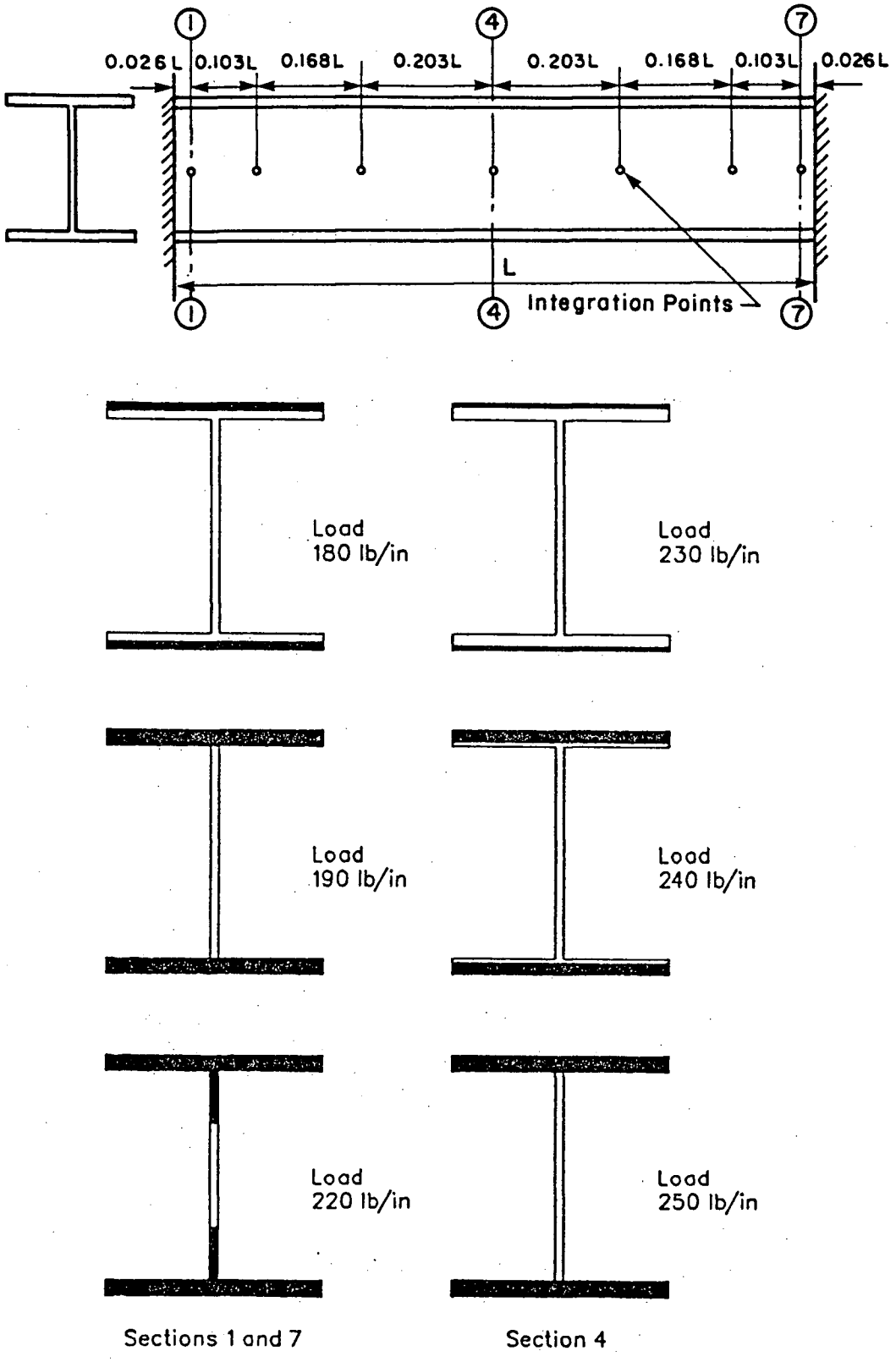

Figure 4.23 – Spread of plastic zones in an I beam

4.5 Analysis of Unstiffened Plates

4.5.1 Square plate with all four edges simply supported

The differential equation for the lateral deflection of a rectangular isotropic plate is,

$$\frac{\partial^4 w}{\partial x^4} + 2\frac{\partial^2 w}{\partial x \partial y} + \frac{\partial^4 w}{\partial y^4} = \frac{q}{D} \tag{4.10}$$

where, w is the lateral deflection,

q is the lateral load,

D is the flexural rigidity, and

x and y are the rectangular cartesian co-ordinates as shown in Figure 4.24.

Equation 4.10 can be solved for simply supported edge conditions by following Navier's method [2]. Navier's solution for the lateral displacement of a rectangular plate of size $a \times b$ is,

$$w = \frac{16 q_0}{\pi^6 D} \sum_{m=1,3,5}^{\infty} \sum_{n=1,3,5}^{\infty} \frac{\sin \frac{m\pi x}{a} \sin \frac{n\pi y}{b}}{mn\left(\frac{m^2}{a^2} + \frac{n^2}{b^2}\right)^2}. \tag{4.11}$$

Hence, the central deflection of a square plate ($a = b$) can be expressed as,

$$w_c = \frac{16 q_0 a^4}{\pi^6 D} \sum_{m=1}^{\infty} \sum_{n=1}^{\infty} \frac{(-1)^{\frac{m+n}{2}-1}}{mn\left(m^2 + n^2\right)^2} \tag{4.12}$$

This series converges very fast and can be summed to get,

$$w_c = \frac{4.0623527 q_0 a^4}{10^3 D} \tag{4.13}$$

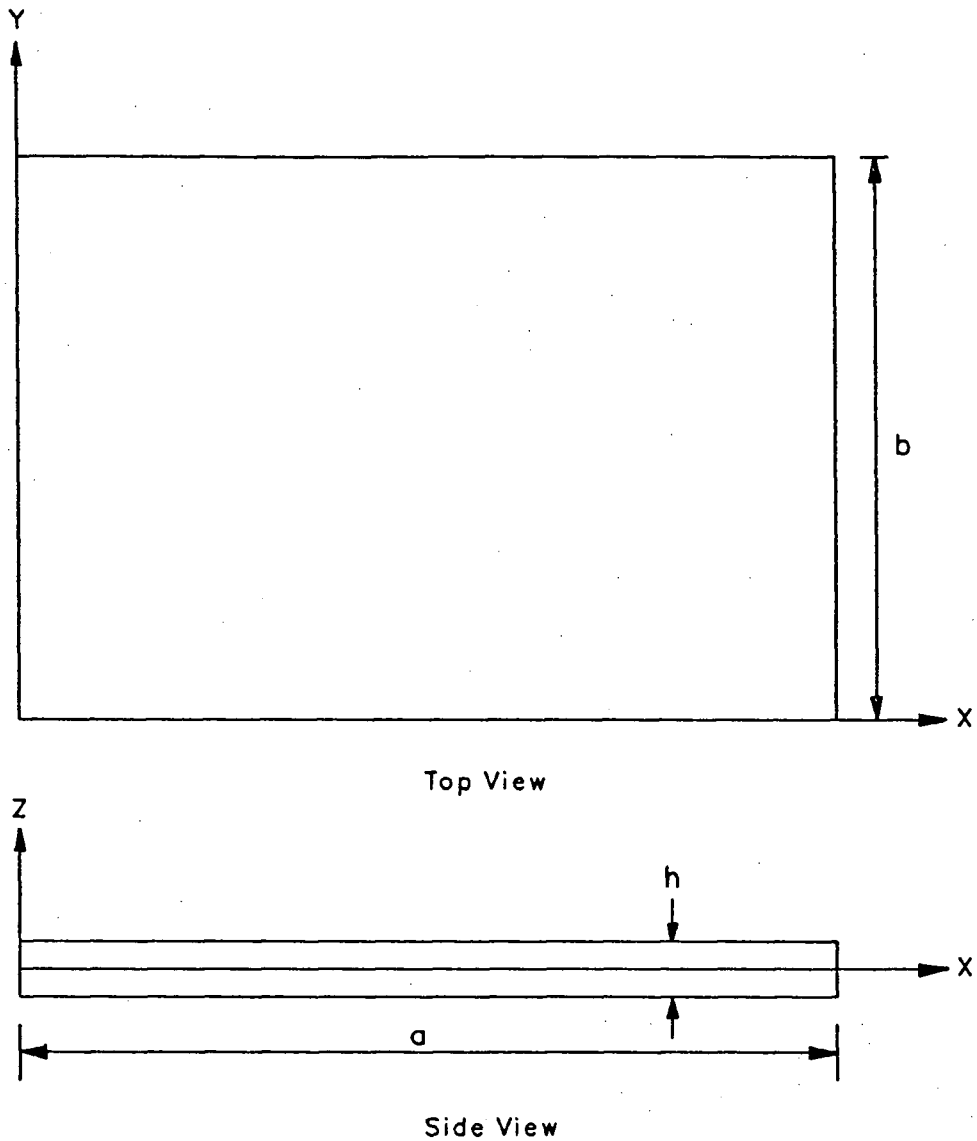

Figure 4.24 – Rectangular plate configuration

Once the expression for the deflection, equation 4.11, is known, it is possible to get an equation for the total strain energy stored in the plate. The total strain energy for a square plate of side a is,

$$U = \frac{1}{2}\int_0^a \int_0^a q_0 w \quad dx \quad dy$$
$$= \frac{8.5125526 q_0^2 L^6}{10^4 D} \tag{4.14}$$

A square plate was analysed by the finite strip programme assuming small deflections and linear elastic behaviour. Only one displacement mode is employed in this analysis (2,1,1). The central deflection and the total strain energy in the plate for various number of strips are presented in Table 4.7.

TABLE 4.7 LINEAR ELASTIC RESPONSE OF A SIMPLY SUPPORTED PLATE

dimensions	= 100 mm ×100mm ×1mm
elastic modulus, E	= 205000 N/mm^2
uniformly distributed load, q	= 0.1 N/mm^2
Poisson's ratio, ν	= 0.3

Number of Strips	2	4	6	8	Exact
Central Deflection(mm)	2.2071	2.1898	2.1891	2.1890	2.1639
error %	1.996	1.197	1.165	1.160	
Strain Energy(Nm)	0.4495	0.4511	0.4512	0.4512	0.4535
error %	0.864	0.527	0.496	0.491	

It is evident that both the central deflection and the total strain energy approaches a solution away from the exact value as the mesh is refined. The difference is due to the finite

strip approximation of the deflected shape in the longitudinal direction, namely that of one mode. Note that the central deflection is on the flexible side, whereas the strain energy is on the stiff side, of the respective exact solutions. Table 4.7 also includes the percentage errors at every stage of the discretisation. An inspection of this reveals that the % errors in energy are very small and are lower than those in central displacement, at any one level of finite strip discretisation. Therefore, it can be concluded that the present analysis with only a single mode is capable of predicting the response of a simply supported square plate very accurately. Furthermore, it is seen that there exists a bound on strain energy from below.

Bending moment distributions of the simply supported square plate along two mutually perpendicular centre lines are presented in Figures 4.25 through 4.28. Bending moments obtained by the present analysis with the four strip discretization are compared to the plate theory solutions. Note that M_y moment agrees more closely with theoretical predictions than M_x moment, although the errors are very small in both cases. This is due to the fact that there are four strips in the y direction and also that a cubic displacement pattern is allowed in that direction within a strip, as opposed to the predetermined sinusoidal variation in the x direction.

Timoshenko and Wo'nowsky-Krieger[2] present a method, recommended by Föppl[47], to analyse large deflection behaviour of a simply supported plate. If the plate deflects solely as a non-linear membrane, an energy minimization procedure yields the following expression for the central deflection[2] of a square plate of side $2a$.

$$w_c = 0.802a\sqrt[3]{\frac{q_1 a}{Eh}} \tag{4.15}$$

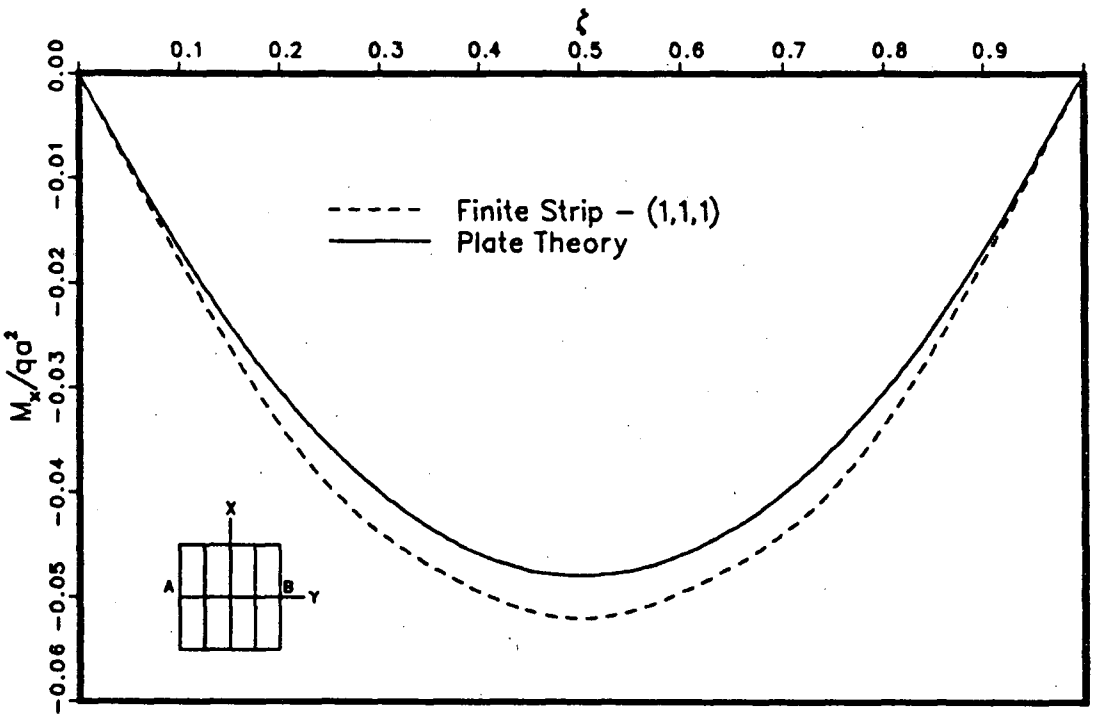

Figure 4.25 – Bending moment distribution along AB, in the simply supported square plate – M_x

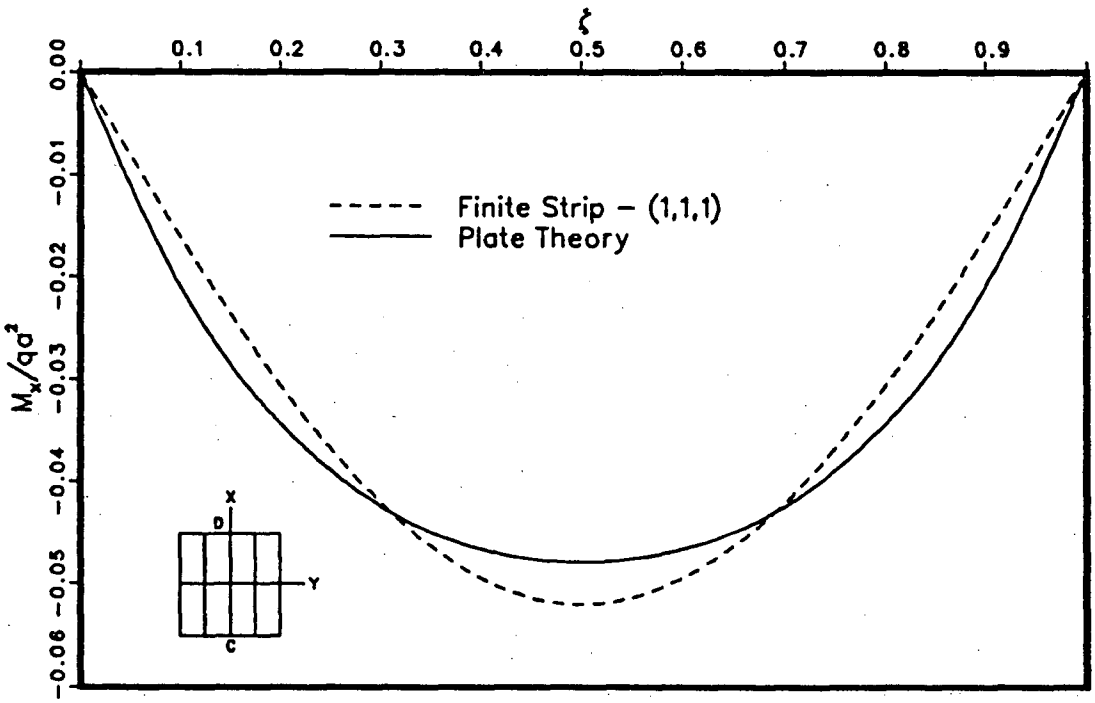

Figure 4.26 – Bending moment distribution along CD, in the simply supported square plate M_x

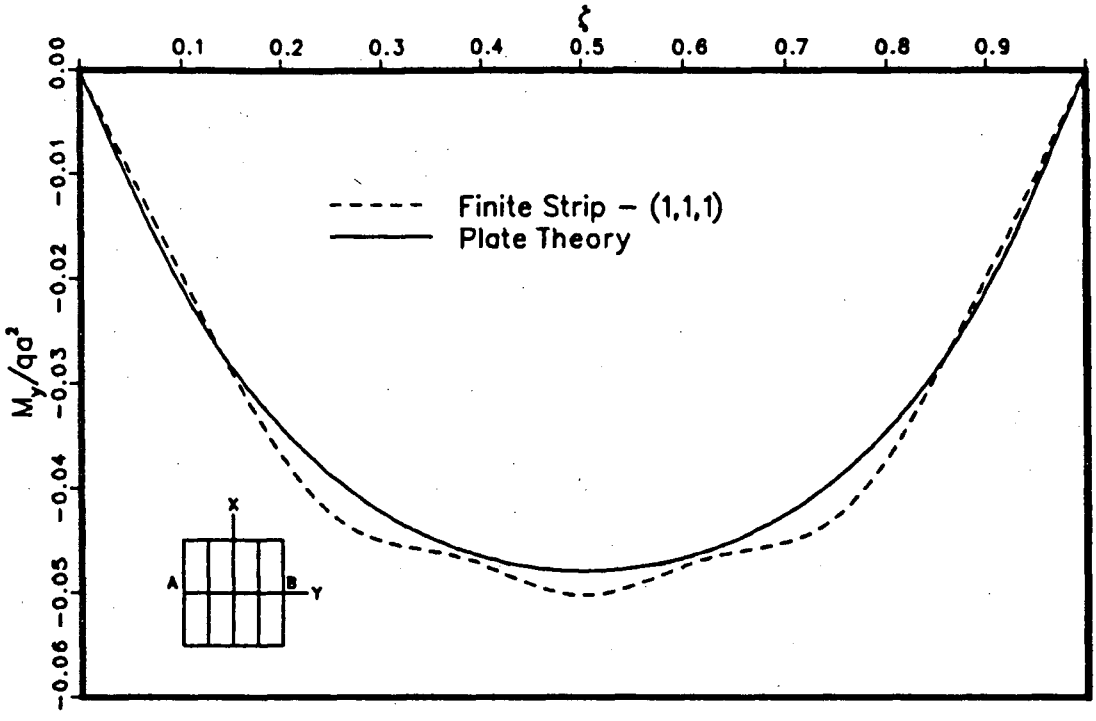

Figure 4.27 – Bending moment distribution along AB, in the simply supported square plate – M_y

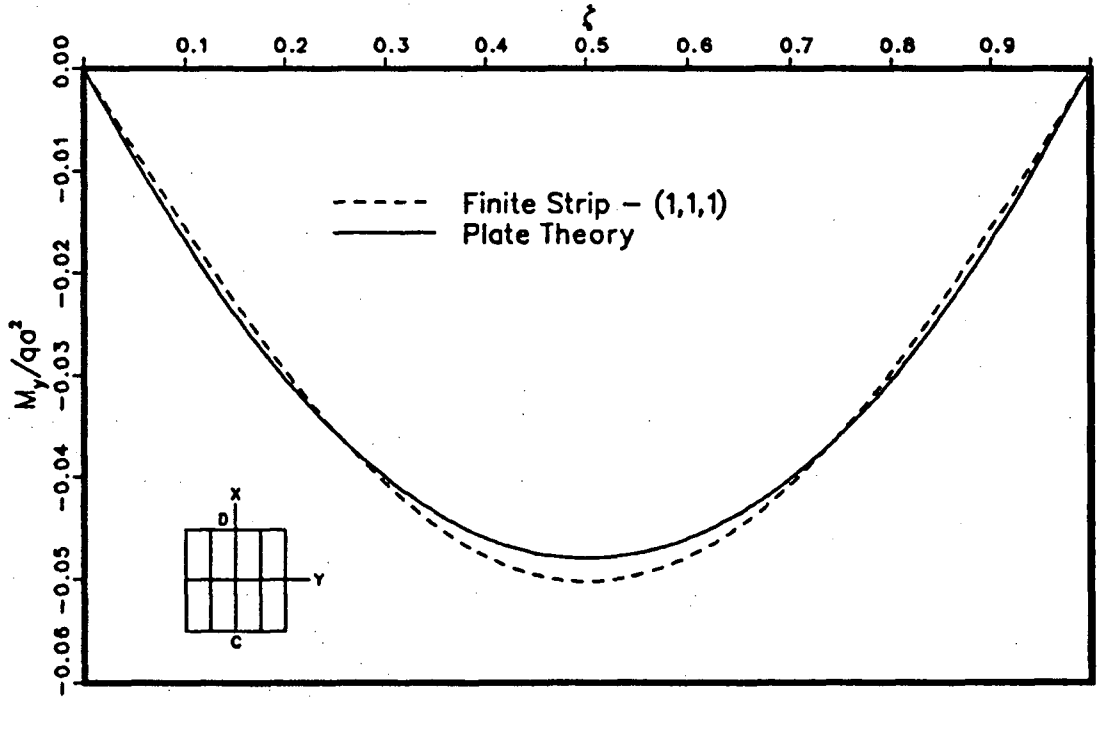

Figure 4.28 – Bending moment distribution along CD, in the simply supported square plate – M_y

where, q_1 is the uniformly distributed load,

E is the elastic modulus, and

h is the plate thickness.

Equation 4.15 was derived by assuming a Poisson's ratio of 0.25. If it is assumed that a uniformly disributed load q can be resolved into two parts q_0 and q_1 in such a manner that part q_0 is balanced by the bending and shearing stresses calculated by the theory of small deflections, part q_1 being balanced by the membrane stresses, one can write,

$$q = q_0 + q_1. \tag{4.16}$$

Substituting for q_0 and q_1 from 4.13 and 4.15 respectively, the above expression can be written in the form,

$$q = \frac{w_c E h^3}{a^4}\left[1.37 + 1.94\frac{w_c^2}{h^2}\right], \tag{4.17}$$

for a square plate of side $2a$, assuming Poisson's ratio of 0.25 for the plate material[2].

A large deflection elastic analysis is now performed on the example plate by using the finite strip programme. Results of this analysis are compared with the analytical solution given by the equation 4.17. Load - deflection plots are given in the Figure 4.29. Central displacements obtained by the eight strip discretisation are nearly identical with those of the analytical calculations. Results of the four strip discretisation are also very good compared to the Timoshenko solution. These strips include only a single mode for each of u, v and w.

The load deflection plot given in Figure 4.30 displays the effect of adding a second displacement mode in the four strip finite strip analysis. For a uniform load, the second mode tends to reduce the central deflection. However, this mode increases the deflections in the outer two thirds of the span (Figure 4.31).

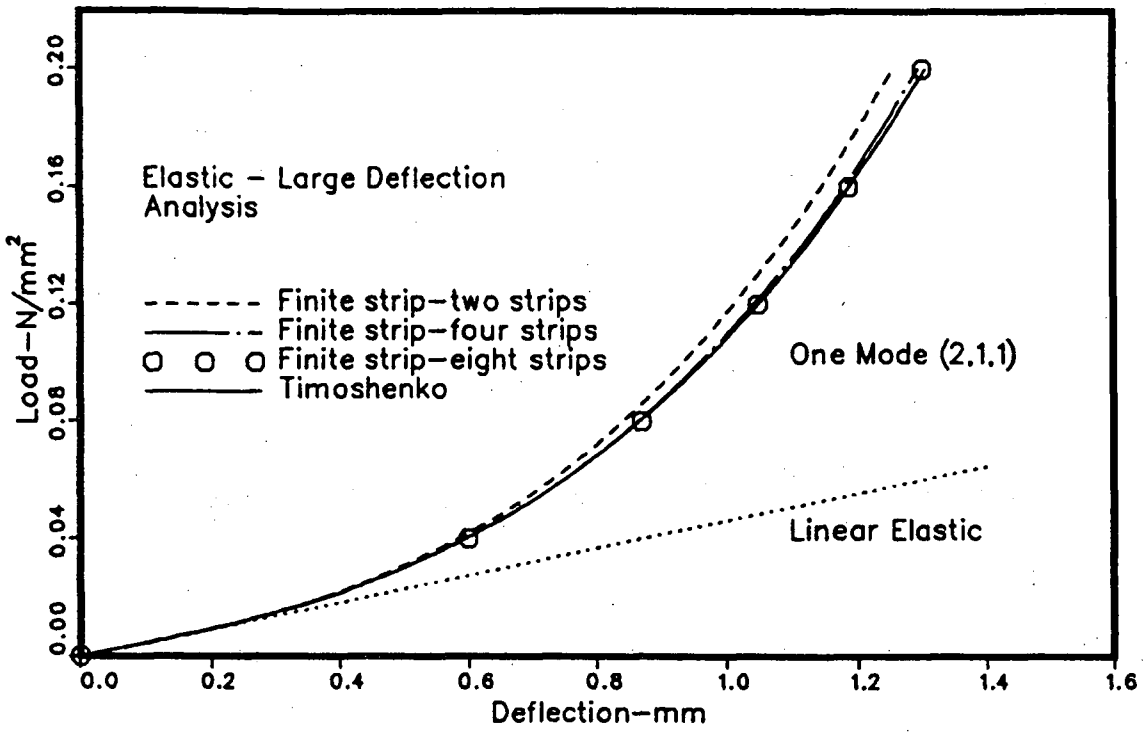

Figure 4.29 – Variation of central deflection response of the simply supported square plate with different discretizations

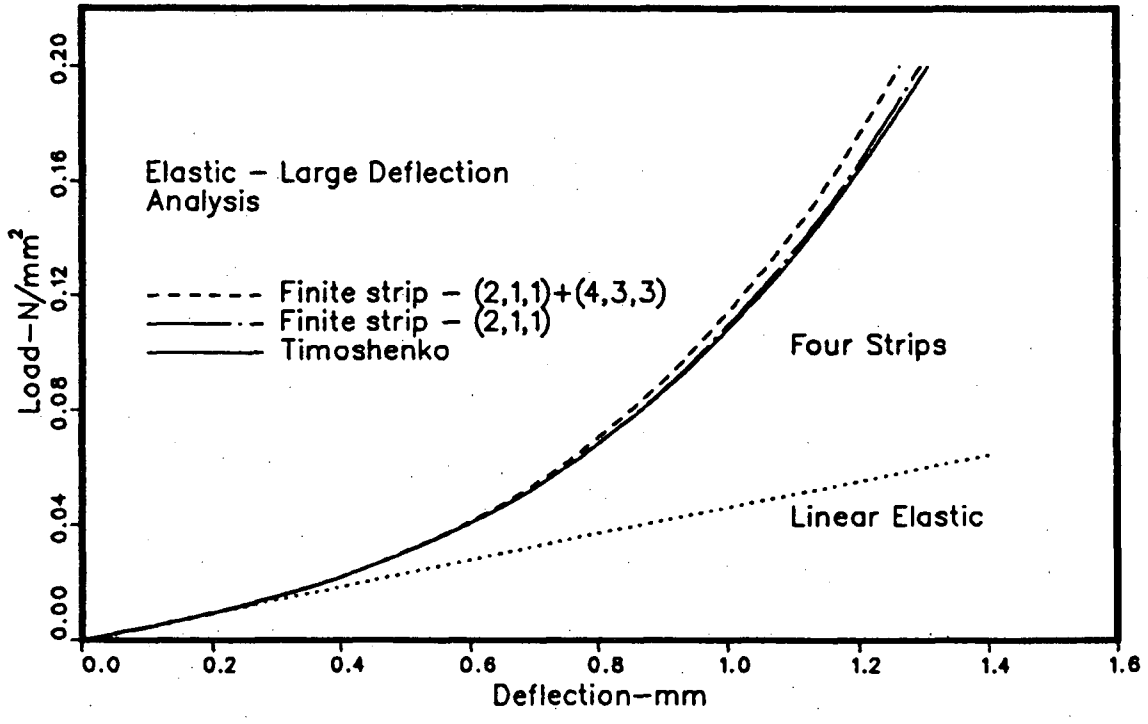

Figure 4.30 – Central deflection response of the simply supported square plate in one and two mode analyses

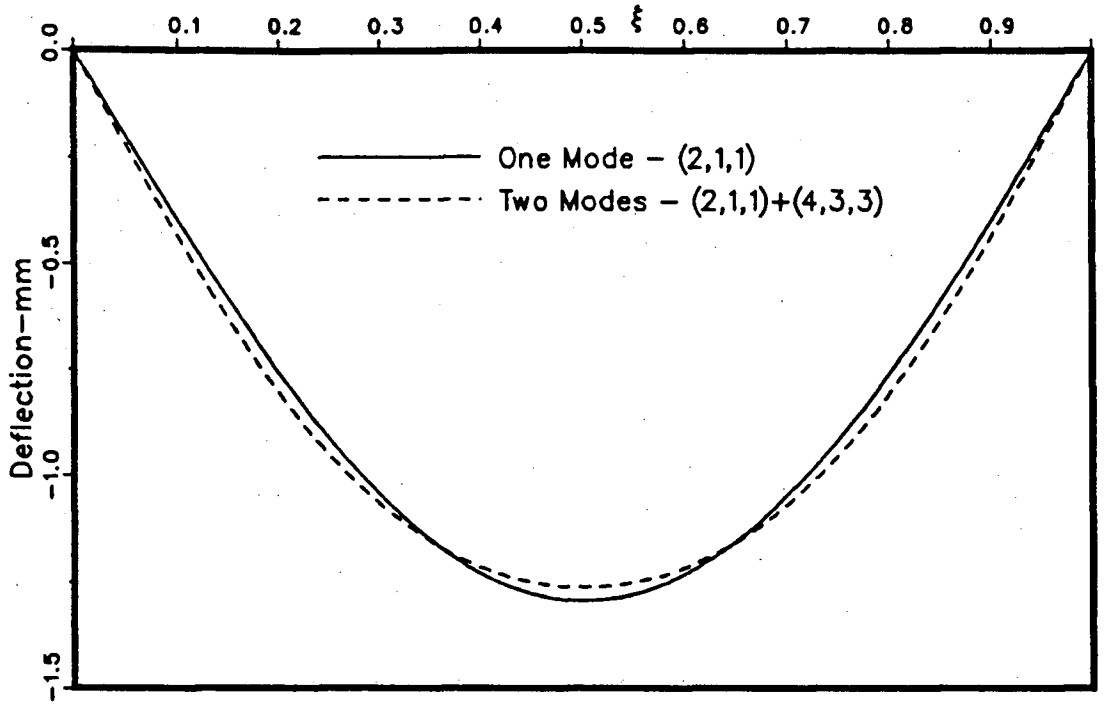

Figure 4.31 – Deflected shape of the simply supported square plate along a centre line in the direction of the strips at 0.2 N/mm²

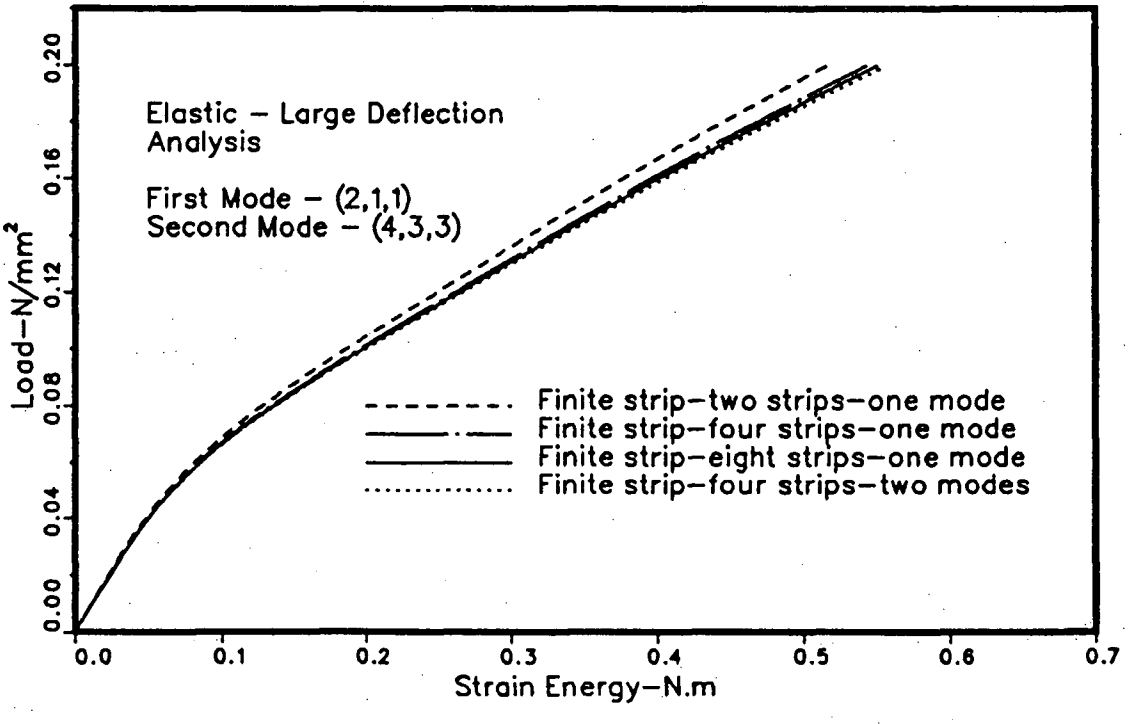

Figure 4.32 – Strain energy variation of the simply supported square plate

Figure 4.32 is a plot of load vs. strain energy calculated by the finite strip programme. It is apparent that there is a monotonic convergence in the strain energy as the mesh is refined. Furthermore, the effect on energy of increasing the number of strips from four to eight is almost the same as that of adding a second mode to the same four strip discretization.

Results of the present analysis are compared with those of a finite element computer programme, ADINA[48](Bathe and Bolourchi,1980), in Figure 4.33. In this diagram, loads and the central displacements are non-dimensionalized by introducing the load parameter $K = qa^4/Eh^4$ and the displacement parameter w_c/h, respectively, where q is the uniformly distributed load, a is the side length of the plate, E is the elastic modulus of the plate material, h is the plate thickness and w_c is the central deflection. The ADINA analysis was performed by using four 16 node shell elements to represent one quater of the plate. Also presented in the figure is the Timoshenko analytical solution given by equation 4.17. The two mode finite strip results agree very well with the ADINA results, especially at large deflections. Furthermore, the difference between the Timoshenko solution and the curves predicted by the numerical procedures is never more than about 5%.

The comparison of the present results with those of another finite strip computer programme developed by Azizan and Dawe[32] is presented in Figure 4.34. In this plot, the non-dimensional load parameter $Q = qa^4/Dh$ and the non-dimensional displacement parameter $100 \times w_c/a$ were used as the ordinate and the abscissa respectively. Azizan and Dawe employ Mindlin plate theory, which incorporates through-the-thickness shear deformation effects. They have also provided an improved classical plate theory(CPT) solution based on the Rayleigh-Ritz procedure, with more terms used in assumed series expression for u,v and w than the solution by Levy[49]. These points are identified as the CPT points in Figure 4.34. While the finite strip results are identical with each other for a given number of modes, the agreement with the Rayleigh-Ritz solution is also excellent.

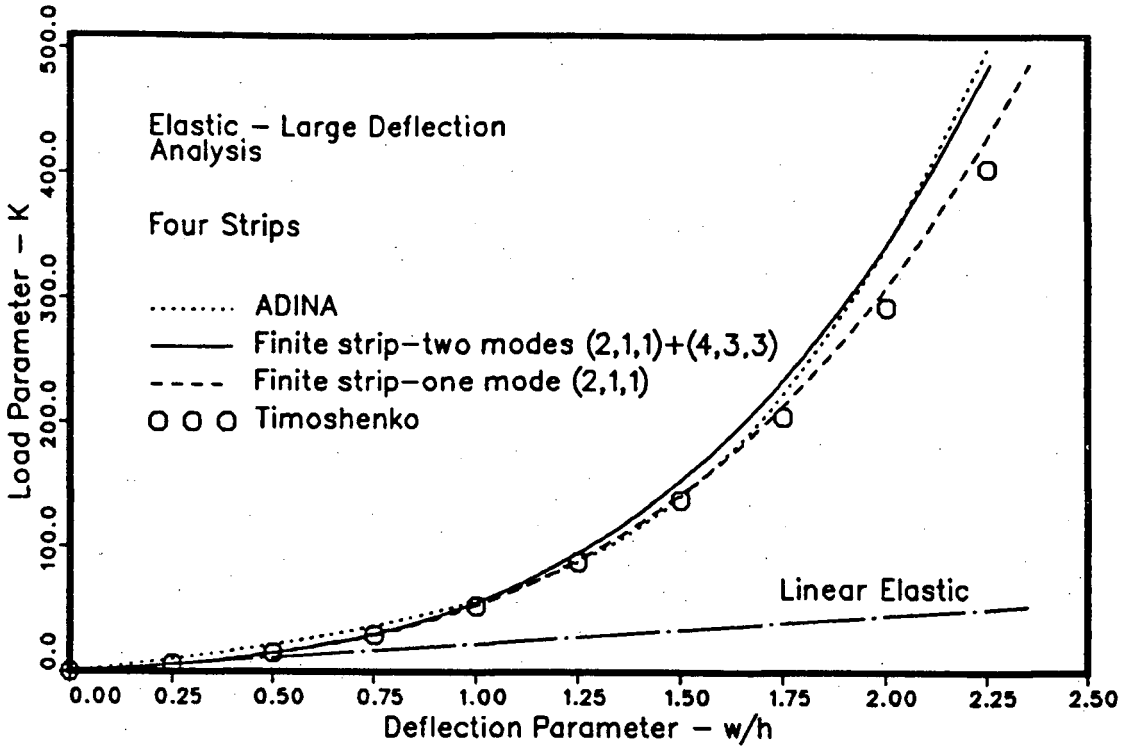

Figure 4.33 – Comparison of central deflections of a simply supported square plate with ADINA

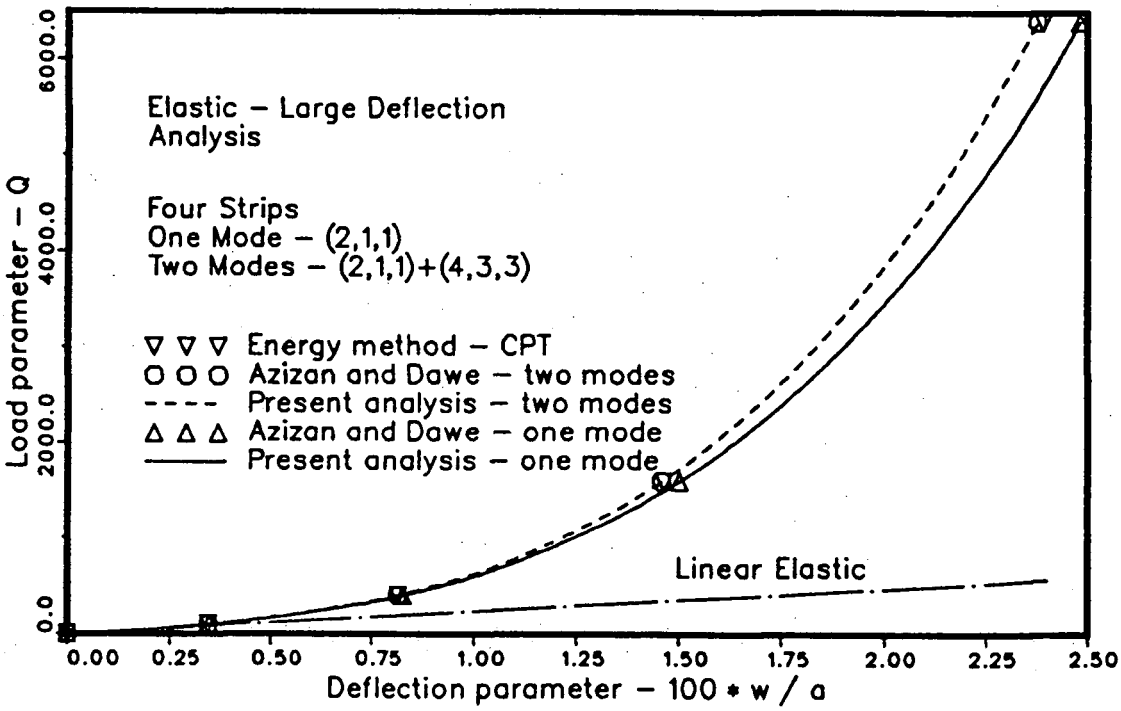

Figure 4.34 – Comparison of central deflections of a simply supported square plate with another finite strip solution

A simply supported square plate of size 6m × 6m × 0.2m is now analysed by assuming an elastic-plastic material with strain hardening. This example is chosen to match a comparison example presented in the next section. The plate material was assumed to possess the following values.

$$\begin{aligned} \sigma_0 &= 40 \text{ MN/m}^2, \\ E &= 30000 \text{ MN/m}^2, \\ E_T &= 300 \text{ MN/m}^2, \\ \nu &= 0.3, \end{aligned}$$

where, σ_0, E and E_T are the yield stress, elastic modulus and the slope of the plastic segment of the bi-linear stress-strain curve (Chapter 3) respectively. ν is the Poisson's ratio. In this analysis, the geometric non-linearity is ignored. Load deflection plots obtained by using three finite strip discretizations are presented in Figure 4.35. In this plot, a non dimensional load parameter $Q = a^2 q/10M_p$ and a non dimensional deflection parameter $W = 100Dw_c/a^2M_p$ are used as the ordinate and abscissa respectively, where M_p is the full plastic moment of a section and q is the uniformly distributed load. All three finite strip analyses provide nearly identical results.

The spread of plastic zones as the load is increased is given in the Figure 4.36. Q is again the non-dimensional load parameter. It is clear from this figure that if there exists a yield line pattern, such lines will form along the diagonals of the plate. The collapse load calculated by following a rigid plastic analysis with diagonal yield lines is $24M_p/a^2$, where a is the side length. This value corresponds to a Q of 2.4 for the present example. According to Figure 4.36, at $Q = 2.4$ there still is a middle layer to be yielded, even along the diagonals of the panel. At $Q = 3.0$, most of the panel has yielded, except at some points near the corners and some points at the middle of the sides. However, as the yield line theory is based on a non-strain hardening material, no valid comparisons can be made.

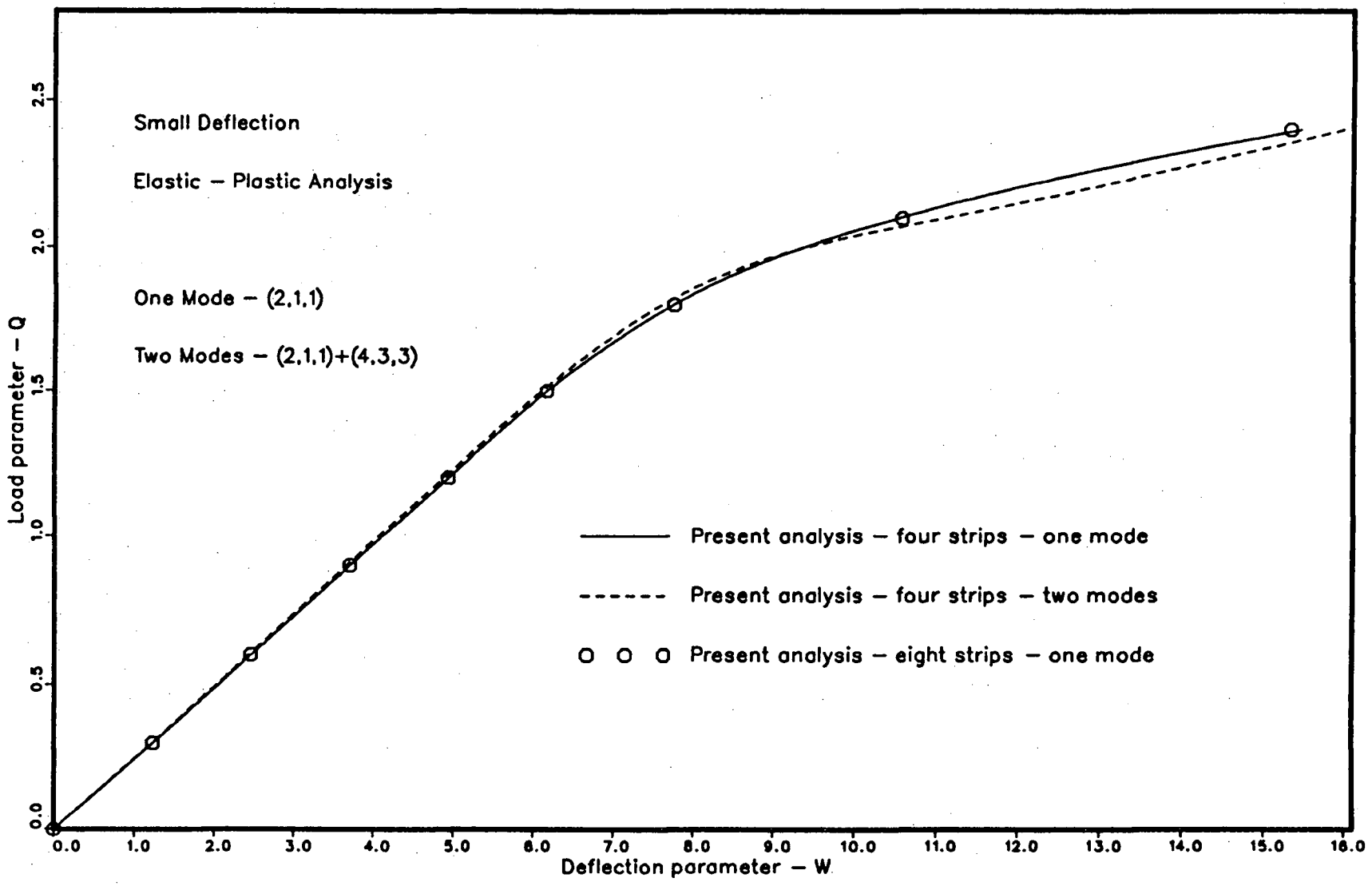

Figure 4.35 – Central deflections of a simply supported square plate in an elastic plastic analysis

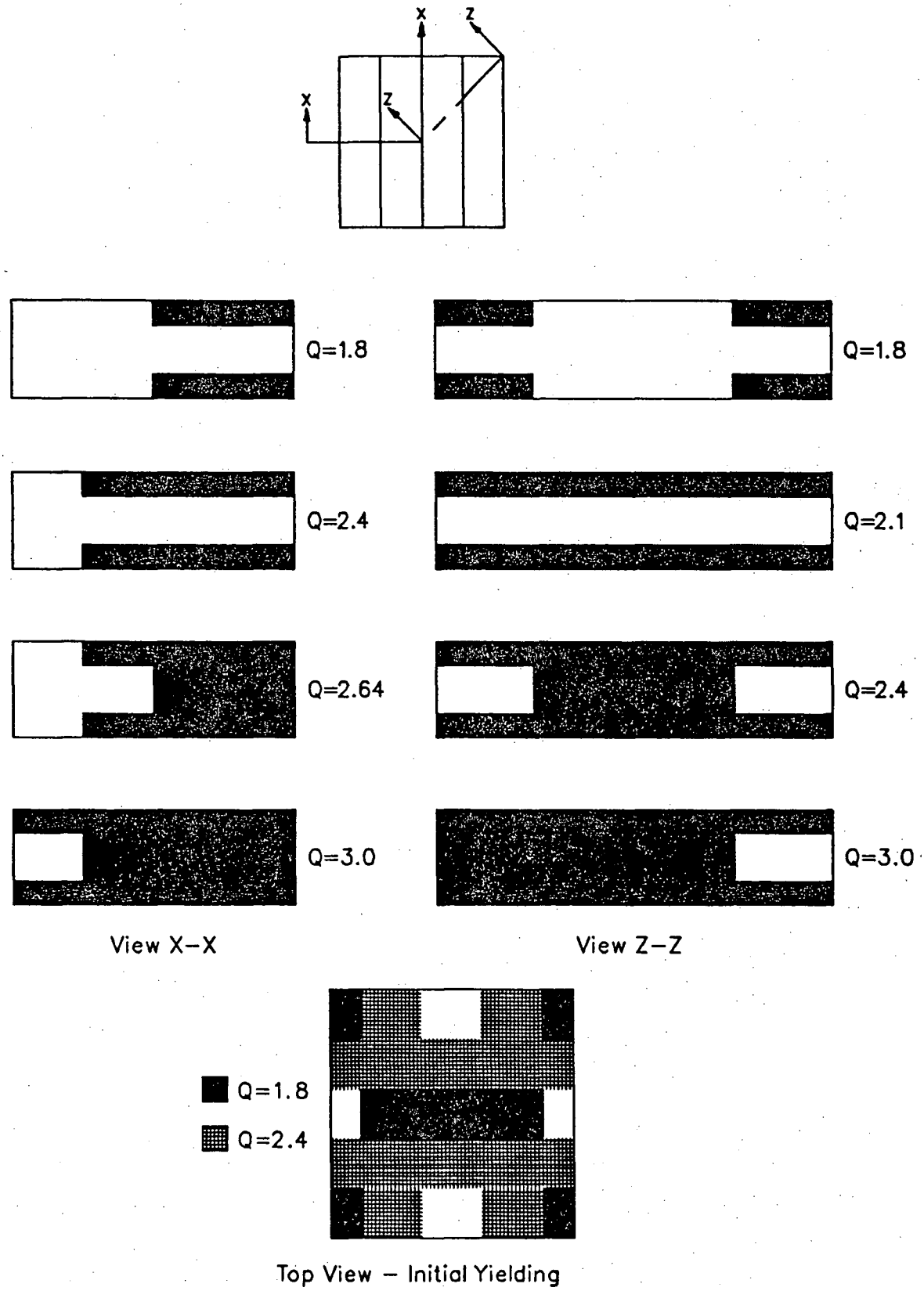

Figure 4.36 – Spread of plastic zones in a simply supported square plate

To compare with the yield line analysis, the last example was repeated with no strain hardening. A load-deflection plot is presented in Figure 4.37. Note that the finite strip model depicts a late yielding compared to the yield line solution, as observed in the simply supported beam example (Fig. 4.5).

Results of a large deflection elastic-perfectly plastic analysis on the same example plate are shown in Figure 4.38. Also shown in the figure is a membrane solution obtained by solving Poisson's equation for a membrane, assuming the plate becomes fully plastic with a membrane stress equal to the yield stress of the material. The membrane solution is in error because a rectangular plate always possesses some amount of shear stresses, especially close to the boundaries. This is the reason for the substantial difference between the two solutions.

Although the chosen functions for a simply supported strip are capable of reproducing zero moments at the ends of the strip in an elastic analysis, this condition is not strictly satisfied in a plastic analysis. However, the actual moments obtained at the ends of the strips are still negligible compared to the moments at the middle as indicated by the example calculation given in Appendix C.

4.5.2 Square plate with all four edges clamped

Clamped boundary conditions can be achieved by restricting the rotation at the edges of a simply supported plate. Thus, one can start with the solution of the problem for a simply supported plate and then can superpose on the deflection of such a plate by moments distributed along the edges. These moments are now adjusted in such a manner as to satisfy zero slopes at the boundary of the clamped plate. Timoshenko and Woinowsky-Krieger[2] followed this procedure and presented the following expression for the central deflection of

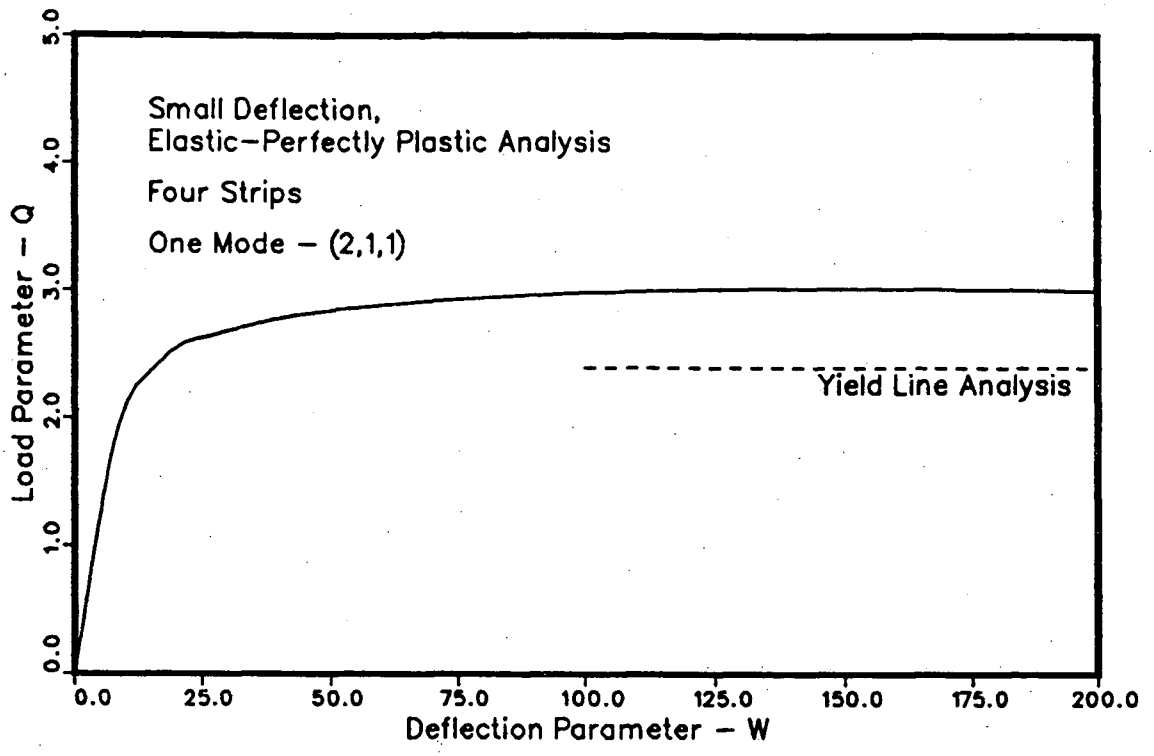

Figure 4.37 – Comparison of central deflections of a simply supported square plate with the yield line solution

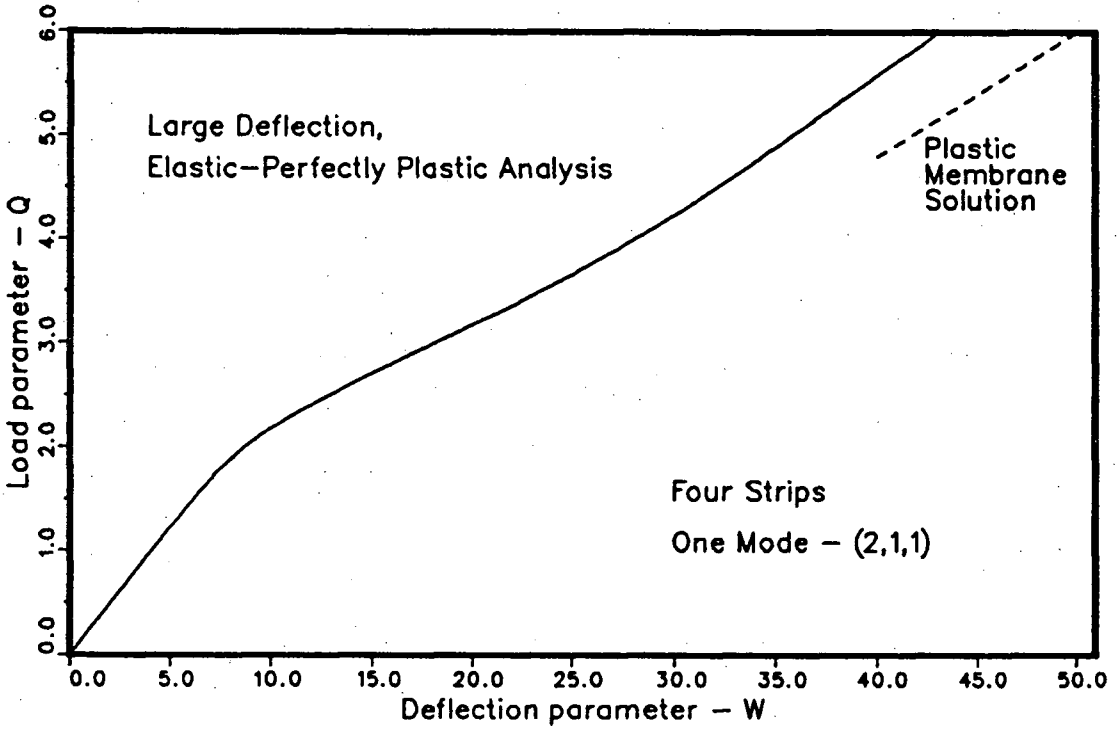

Figure 4.38 – Comparison of central deflections of a simply supported square plate with plastic membrane solution

a clamped plate of side a under a uniformly distributed load q_0.

$$w_c = \frac{0.00126 q_0 a^4}{D} \tag{4.18}$$

The equation for the deflection at any point on the plate surface is not given by Timosenko and Woinowsky-Krieger. Therefore, an exact calculation of the strain energy stored in the plate is not possible. However, an accurate value for the strain energy can be obtained by utilizing one of the many finite element computer programmes available for the linear elastic analysis of plates. Cowper et al.[50] present the following relationship between the strain energy U and the uniformly distributed applied load q_0 for a square plate of side a.

$$U = \frac{1.9455936 q_0^2 a^6}{10^4 D} \tag{4.19}$$

Finite strip results of a small deflection, linear elastic analysis, of a built-in plate by incorporating one mode (4,1,1), are summarised in Table 4.8.

TABLE 4.8 LINEAR ELASTIC RESPONSE OF A BUILT-IN PLATE

dimensions = 100 mm ×100mm ×1mm

elastic modulus, E = 205000 N/mm^2

uniformly distributed load, q = 0.1 N/mm^2

Poisson's ratio, ν = 0.3

Number of Strips	2	4	6	8	Exact
Central Deflection(mm)	0.7028	0.6916	0.6915	0.6915	0.6715
error %	4.66	2.99	2.97	2.97	
Strain Energy(Nm)	0.0919	0.0998	0.1002	0.1003	0.1036*
error %	11.32	3.70	3.24	3.22	

* (finite element)

It is clear that both the central deflection and the total strain energy approaches a solution away from the exact value as the mesh is refined. The difference is due to the finite strip approximation of the deflected shape in one direction, namely that of one mode. Note that the central deflection is on the flexible side, whereas the strain energy is on the stiff side, of the respective exact solutions, as was observed in the simply supported plate example. The relative errors are higher in the case of the clamped plate than in that of the simply supported plate with the same mesh. Similar differences were observed between simply-supported and clamped ends in rectangular and I-beam examples. There is also an energy bound from below, even in the case of the built-in plate.

Bending moment distributions of the built-in plate obtained by present analysis are compared with theoretical results and a finite difference solution[51] in Figures 4.39 through 4.42. Finite strip results are obtained by employing four strips across the width and moments are plotted along two mutually perpendicular directions. As seen in the simply supported plate example, a better comparison was observed in the direction perpendicular to the strips than in the direction of the strips. This is again due to the better approximation of the displacement pattern in the former direction.

Timoshenko and Woinowsky-Krieger[2] use an energy method to determine the solution of a large deflection analysis of a uniformly loaded rectangular plate with clamped edges. In and out-of plane displacements are expressed in polynomial forms with a total of 11 coefficients. A subsequent energy minimization results in a set of 11 non-linear equations to be solved for these coefficients. Table 4.9 is prepared by taking values off the non-dimensional plot given by Timoshenko and Woinowsky-Krieger[2] of w_c/h vs. qa^4/Dh for a square plate of side a.

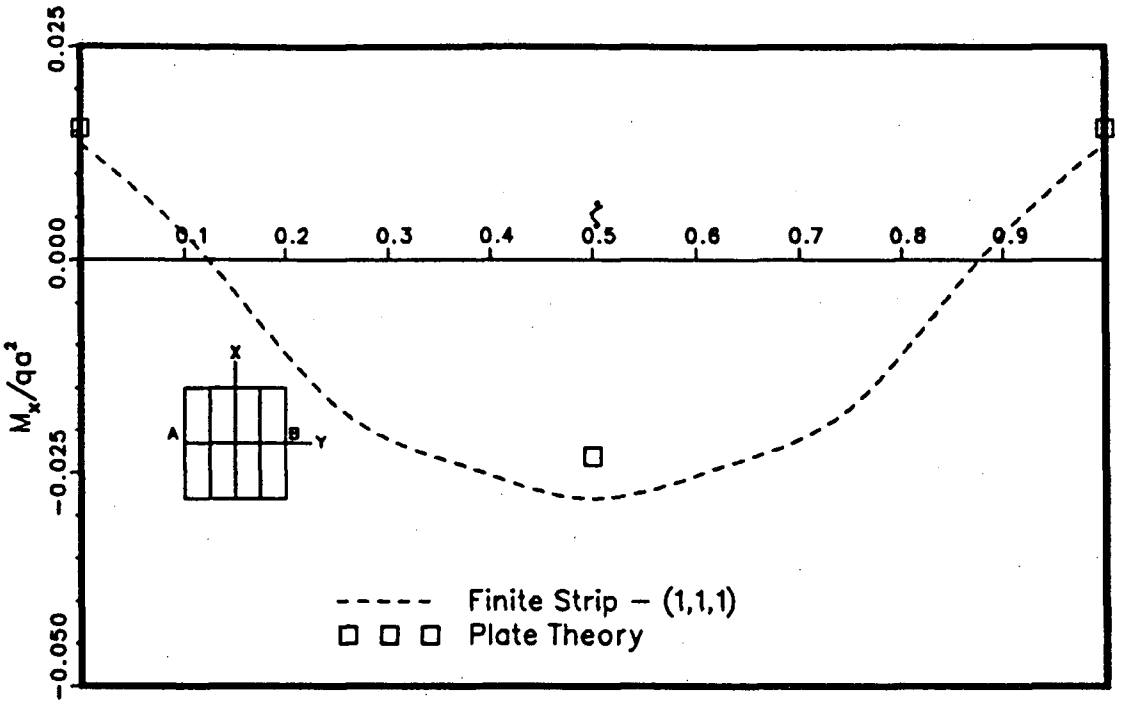

Figure 4.39 – Bending moment distribution along AB, in the clamped square plate – M_x

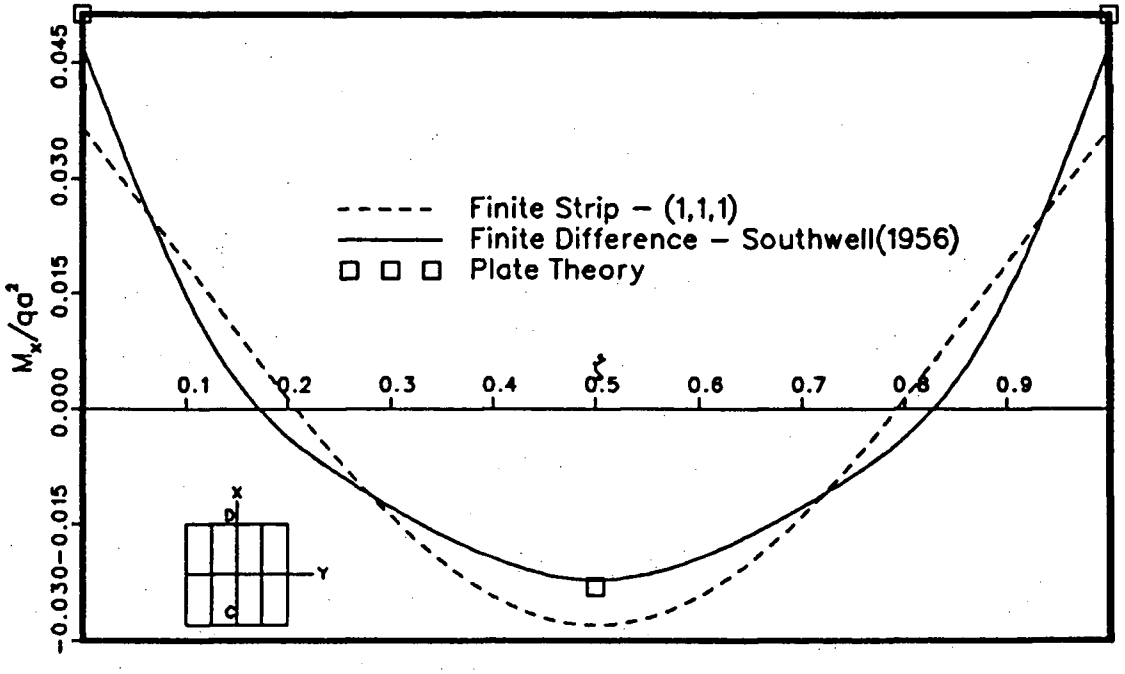

Figure 4.40 – Bending moment distribution along CD, in the clamped square plate – M_x

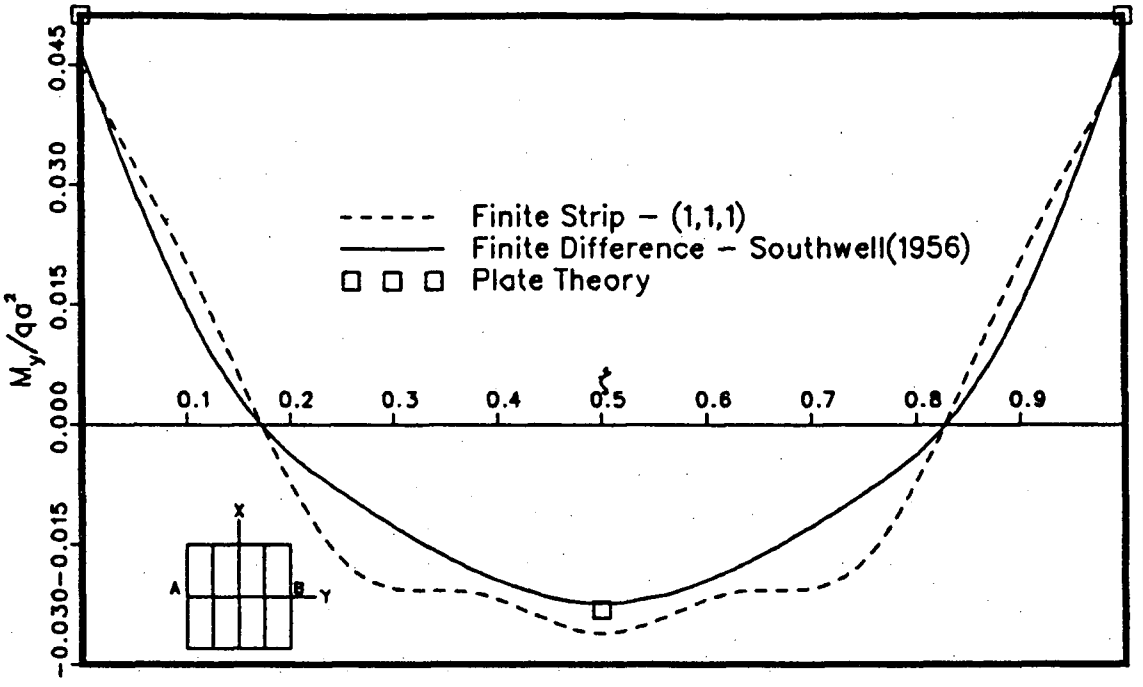

Figure 4.41 – Bending moment distribution along AB, in the clamped square plate – M_y

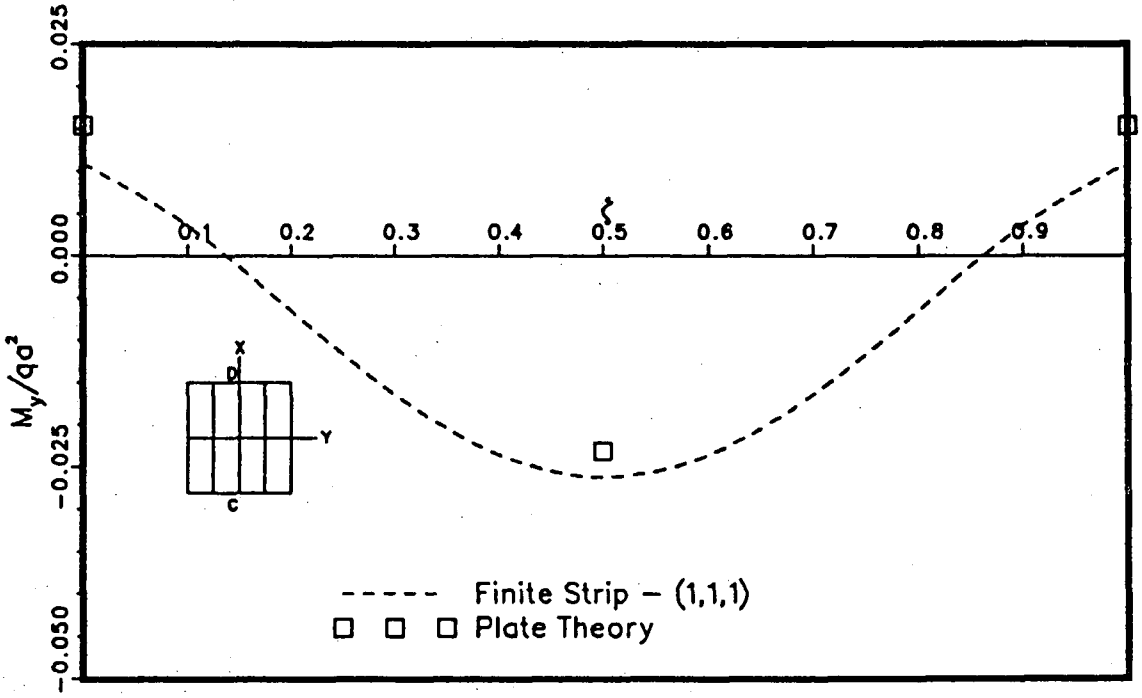

Figure 4.42 – Bending moment distribution along CD, in the clamped square plate – M_y

TABLE 4.9 CENTRAL DEFLECTIONS OF A BUILT-IN PLATE

LARGE DEFLECTION ANALYSIS

(Taken from Timoshenko and Woinowsky-Krieger[2])

Poisson's ratio, ν $= 0.3$

qa^4/Dh	50.0	100.0	150.0	200.0	250.0
w_c/h	0.75	1.15	1.40	1.60	1.77

The results of Table 4.9 are plotted along with the finite strip solutions obtained via a (4,1,1) analysis in Figure 4.43. An excellent agreement is noted when eight strips are used across the plate. The central deflection at any one load decreases when going from two strips to four strips, but increases again with the eight strip discretisation. i.e. the central deflection does not converge monotonically.

A load-deflection plot of a four strip analysis with one and two displacement modes is presented in Figure 4.44. Variation of strain energy, calculated by using different finite strip models is plotted against the load in Figure 4.45. Unlike the case of the central deflection, a monotonic convergence of the strain energy is seen as the mesh is refined. Furthermore, the effect of adding a second mode is more pronounced in the case of strain energy than in displacement.

As the last example on unstiffened plates, small deflection, elasto-plastic behaviour of a clamped square plate was considered. The example was chosen from a paper by Owen and Figuerias[52]. The geometric and material properties for this example are given below.

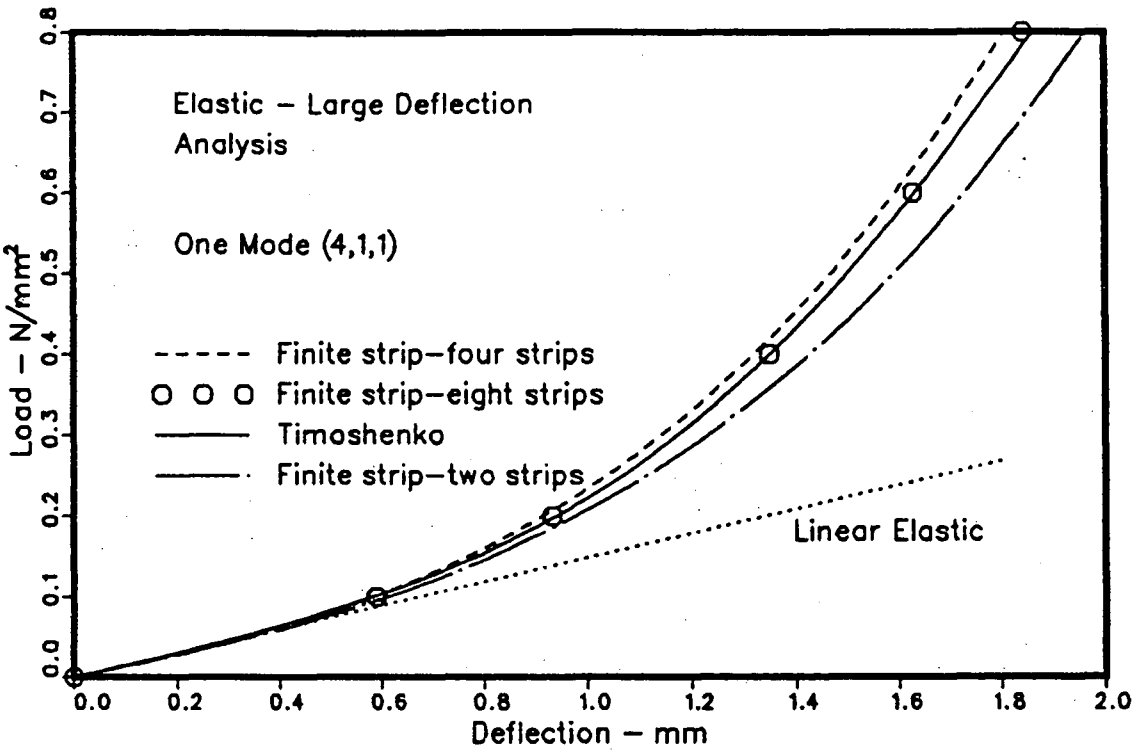

Figure 4.43 – Central deflections of the clamped square plate by different descretizations

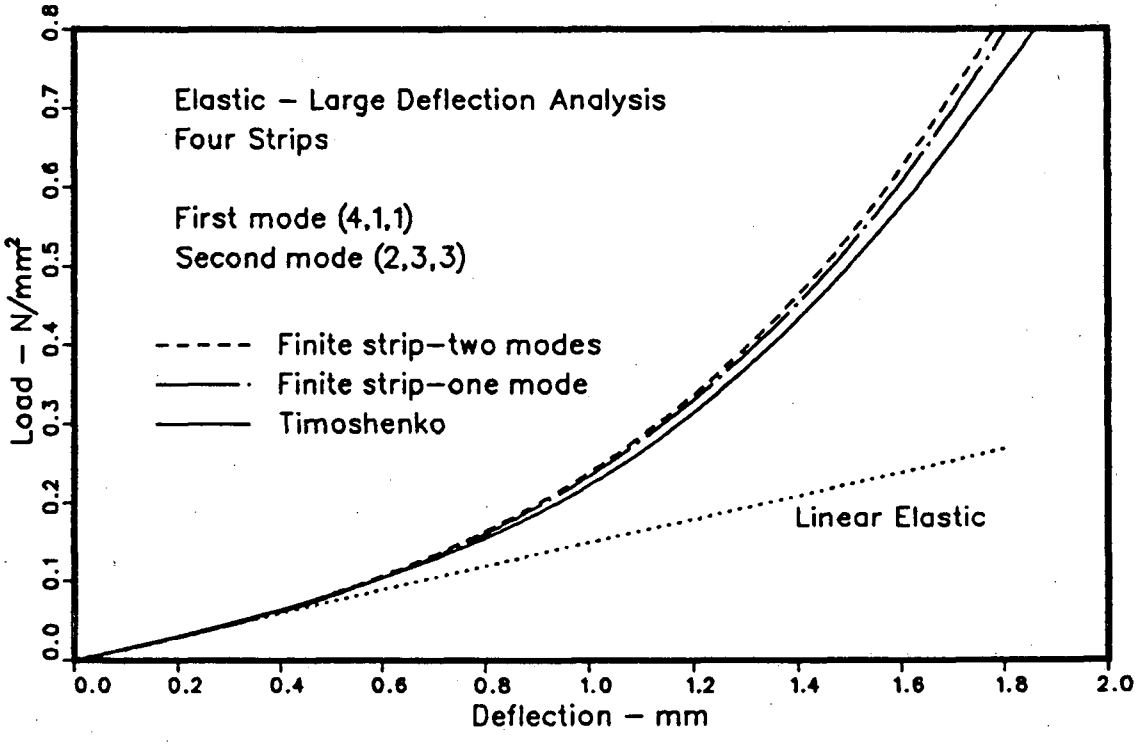

Figure 4.44 – Central deflection of the clamped plate by one and two modes

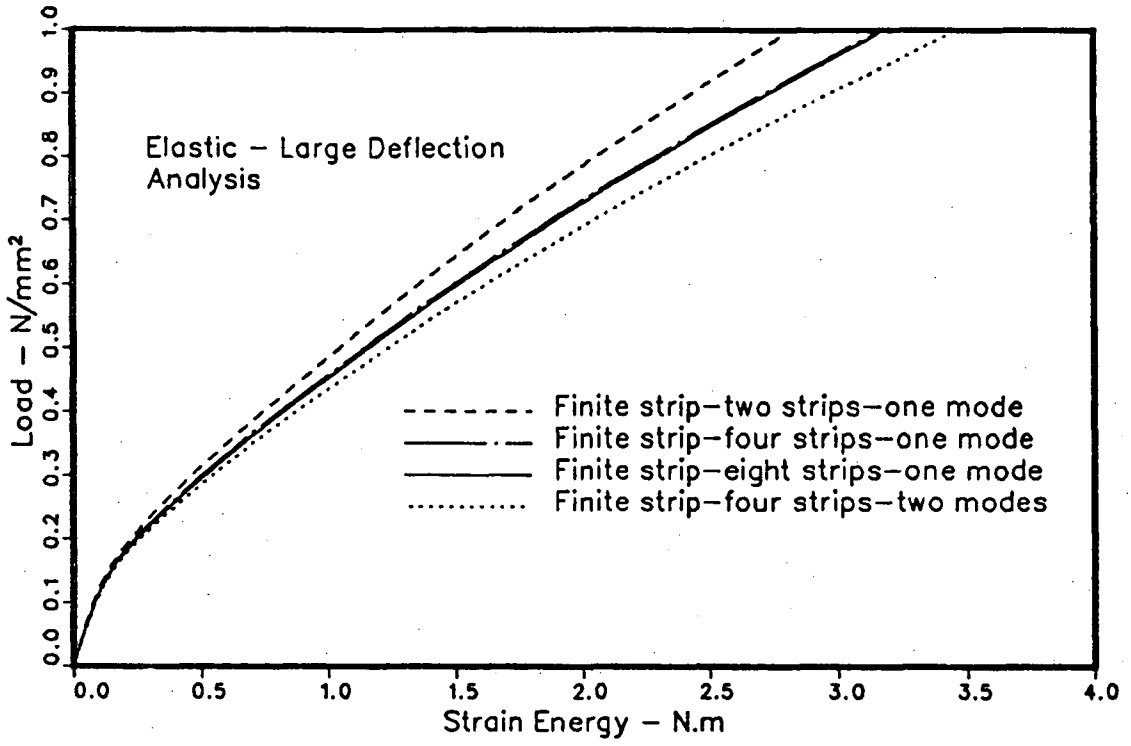

Figure 4.45 – Strain energy variation of the clamped square plate

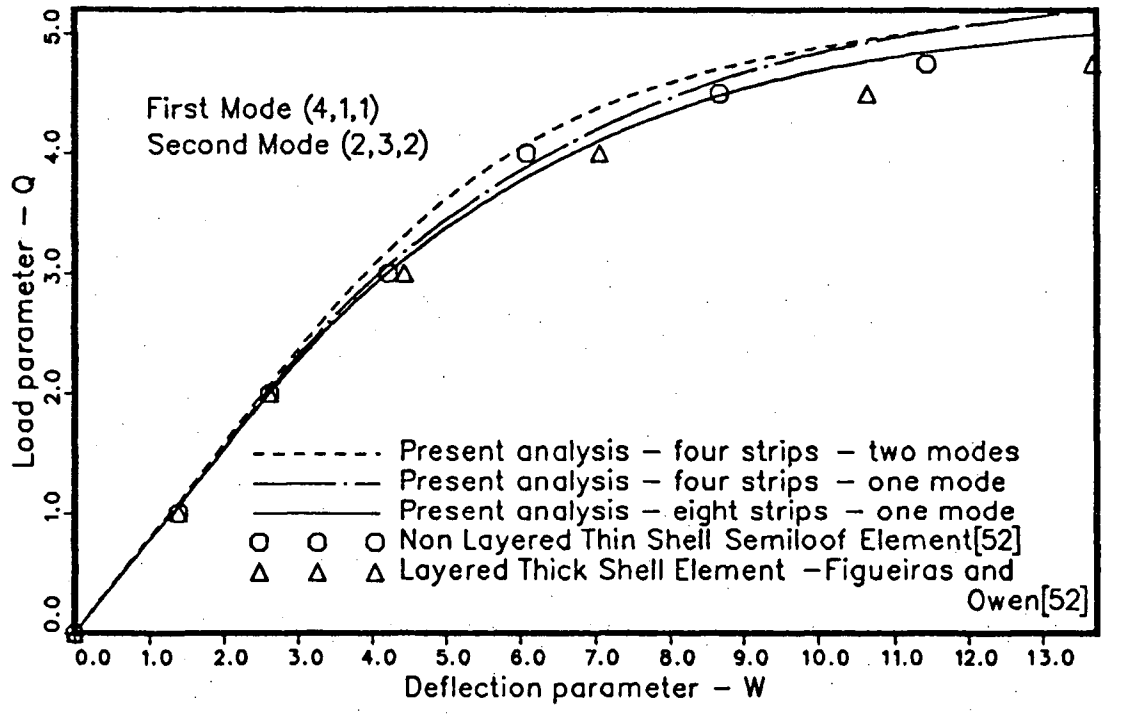

Figure 4.46 – Central deflection of the clamped square plate in a small deflection, elastic–plastic analysis

side length a	=	6.0m,
thickness h	=	0.2m,
σ_0	=	40 MN/m^2,
E	=	30000 MN/m^2,
E_T	=	300 MN/m^2,
ν	=	0.3.

Results of the present analysis by employing a (4,1,1) mode and 4 finite strips are compared with two finite element solutions in Figure 4.46. In this plot, a non dimensional load parameter $Q = a^2 q/10M_p$ and a non dimensional deflection parameter $W = 100Dw_c/a^2M_p$ are used as ordinate and abscissa respectively, where M_p is the full plastic moment of a section and q is the uniformly distributed load. The finite strip results appear slightly stiff at high load levels when compared to the finite element results, although the error is very small.

Owen and Figuerias[52] have also presented a figure showing the spread of plastic zones of the example plate. Finite strip prediction of plastic flow is compared with these results in Figure 4.47. Plastic zones are shown with increasing load parameter Q. In the finite strip analysis, two widthwise and four depthwise Gauss integration points were employed per strip. Therefore, when looking at section XX (Fig 4.47), one can see 16 Gauss points. Plastic flow was monitored by following the stress strain behaviour of these points. The patterns of plastification obtained by the two methods are comparable.

A small deflection, elastic-perfectly plastic analysis was also performed on the same example plate. Results of this analysis are presented in Figure 4.48. Plastic collapse load, calculated by following the yield line theory, is also shown in the figure. As observed in the clamped beam example, the finite strip model shows a higher load carrying capacity than that predicted by the yield line theory.

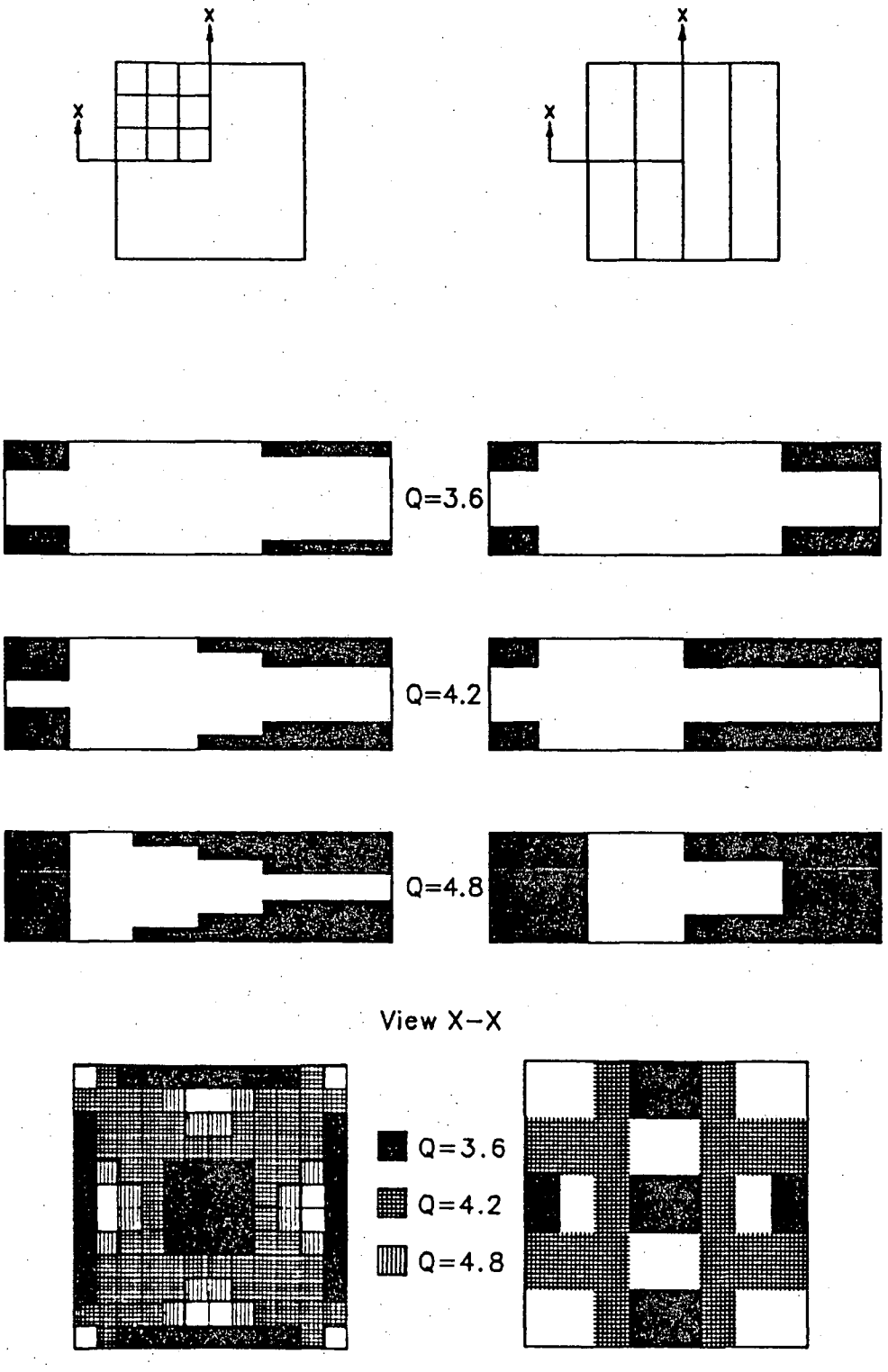

Figure 4.47 – Spread of plastic zones in a clamped square plate

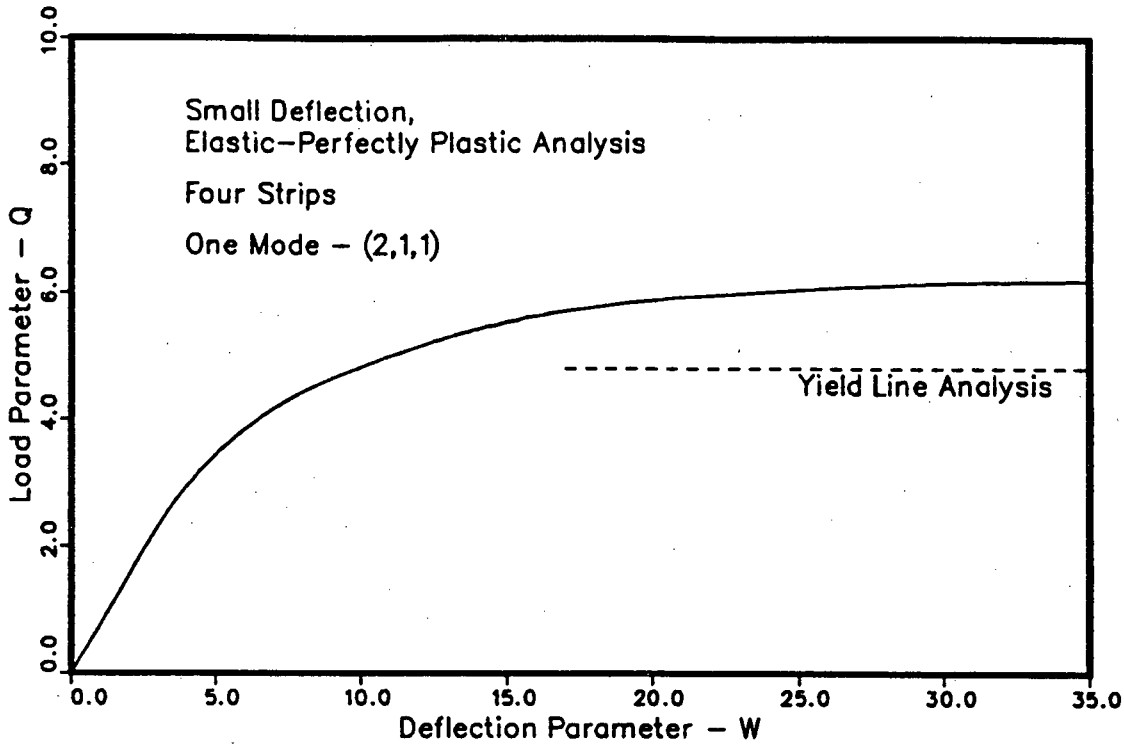

Figure 4.48 – Comparison of central deflections of a clamped square plate with the yield line solution

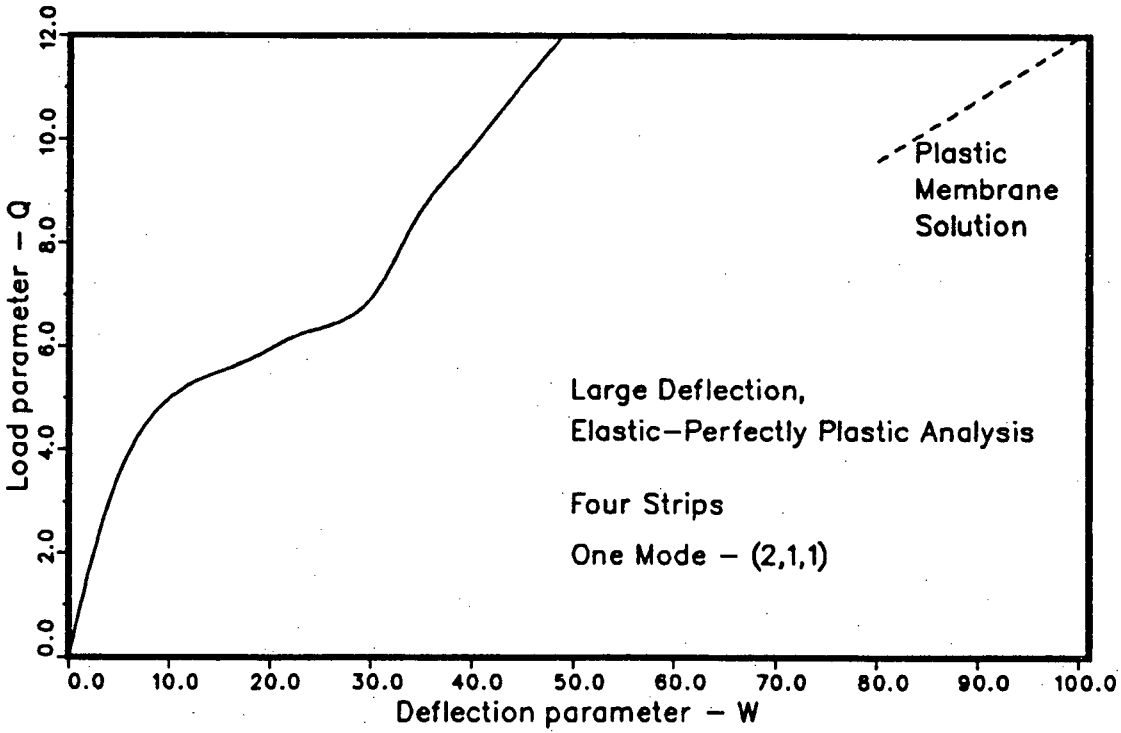

Figure 4.49 – Comparison of central deflections of a clamped square plate with plastic membrane solution

The finite strip results obtained by a large deflection, elastic-perfectly plastic analysis are presented in Figure 4.49, along with the membrane solution calculated for the same square plate. Note the large difference between membrane solution and the finite strip solution. This difference is much higher than that of the simply supported plate. Again, this result is due to the slope restrictions imposed by the mode shapes at the ends of the strips.

4.6 Analysis of a Stiffened Panel

The Defence Research Establishment in Suffield, Alberta (DRES) has tested a stiffened panel under blast loading conditions. A finite element analysis of the test panel was carried out by MARTEC Limited by employing the all purpose finite element computer programme ADINA[53]. On leading to the dynamic solution, a static analysis was performed and reported[54] on the test panel. On account of this, the DRES panel was chosen as the stiffened panel example to be analysed by the finite strip method. Properties of the panel material are given below.

Young's Modulus	=	30×10^6 lb/in^2
Hardening Modulus	=	0.178×10^6 lb/in^2
Poisson's Ratio	=	0.3
Yield Stress	=	45×10^3 lb/in^2

A top and a side view of the panel are presented in Figure 4.50, along with the geometric properties. The panel is clamped all around. A finite strip analysis was first carried out on half of the panel (ABCD in Figure 4.50) by utilising symmetry conditions. i.e. clamped boundary conditions are applied along AD and in-plane displacement v and rotation θ were forced to be zero along BC. In the following, this analysis is referred to as the DRES analysis.

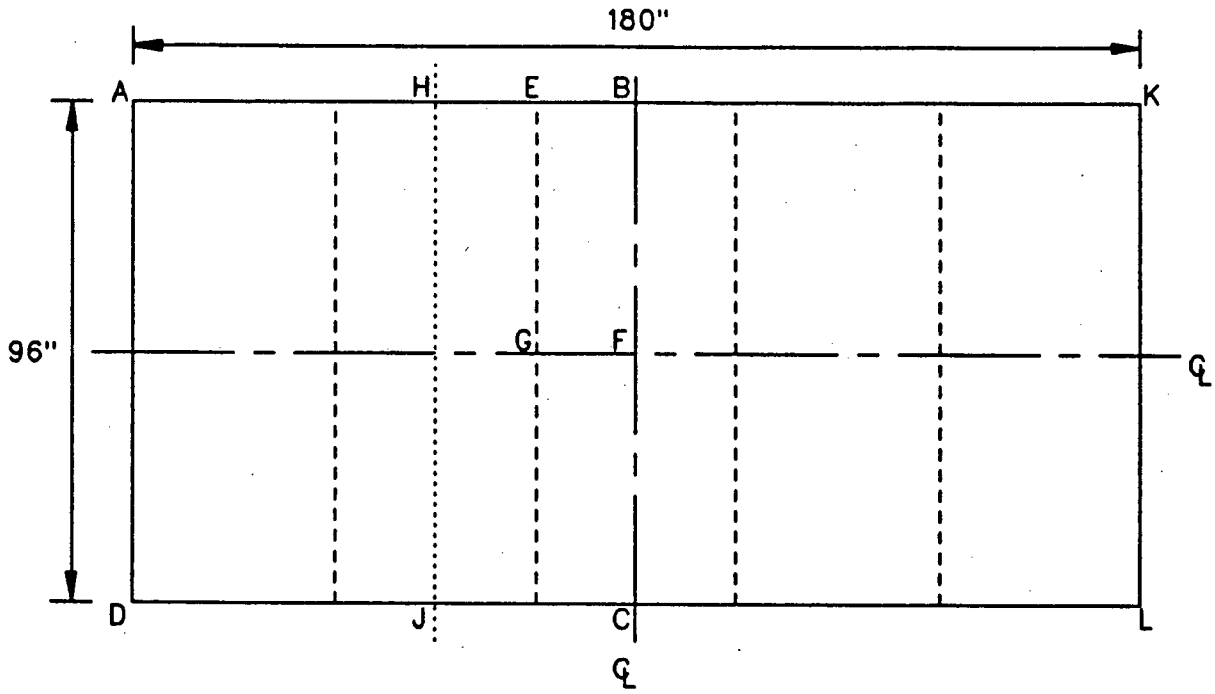

Plate Thickness	= 0.25"
Web Thickness	= 0.28"
Bottom Flange Thickness	= 0.50"

Figure 4.50 – Stiffened panel configuration

The ADINA results have been obtained by considering one quarter of the middle bay of the panel (EBFG in Figure 4.50). A three node triangular plate element based on discrete Kirchoff theory was used in the analysis. The finite element grid is presented in Figure 4.51. This grid consists of 964 elements, 336 for the plate and 528 for the stiffener. 8 elements were used through the depth of the web. ADINA uses a full section yield criterion proposed by Ilyushin, in contrast to the von-Mises criterion employed in the present analysis.

As the ADINA analysis incorporated only one bay of the panel, two other finite strip models were selected for comparison with ADINA, reflecting only the middle part of the panel (Figure 4.52). In the first model, the section HBCJ in Figure 4.50 was analysed with four equal width finite strips between the two lines HJ and BC. In the second, eight equal width strips were employed between these two lines. These two models will be referred to as DRES1 and DRES2 respectively (Figure 4.52). DRES1 and DRES2 analyses were carried out by making the in-plane v displacement and the rotation θ to be zero along the boundaries HJ and BC. In both DRES1 and DRES2, the stiffener was modelled by three strips, one for the web and two for the bottom flange. Initial finite strip calculations were carried out by employing (1,1,1)+(4,-,-) mode combination in all strips.

A linear elastic analysis was conducted initially, with a uniform load of 50 lb/in^2 on the top surface of the panel. Lateral deflections at the centre of the central bay (point F in Figure 4.50) and at the mid span of the stiffener (point G in Figure 4.50) are tabulated in Table 4.10. Results obtained by three finite strip analyses are presented, along with results from ADINA. In the finite strip analysis performed with (1,1,1)+(4,-,-) mode combination, nearly identical results were obtained by the three discretisations, DRES, DRES1 and DRES2. When additional modes were included, the analyses were performed only with the DRES2 model. As shown in Table 4.10, deflections at the centre of panel are overpredicted by 16% using the finite strip model with one w mode, as compared to ADINA. However, when

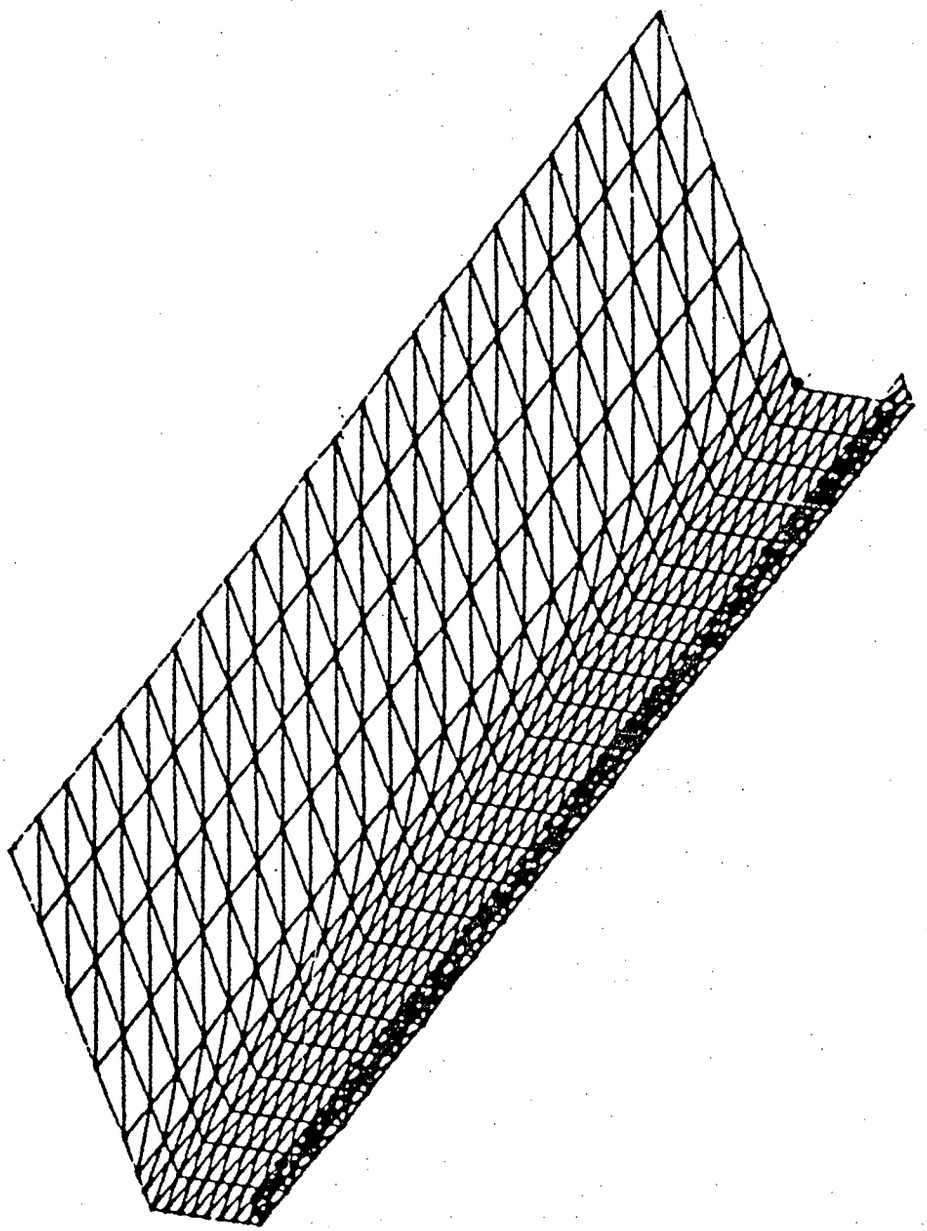

Figure 4.51 – Finite element grid

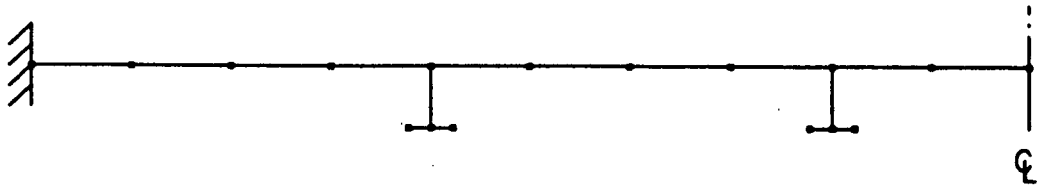

DRES – 16 Strip Model

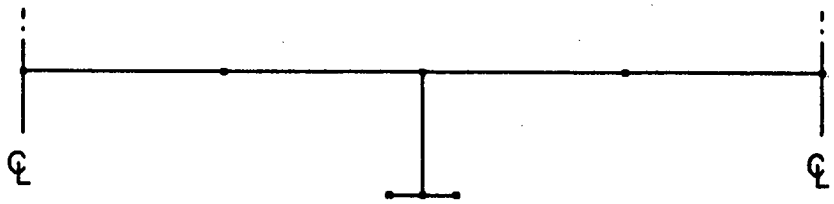

DRES1 – 7 Strip Model

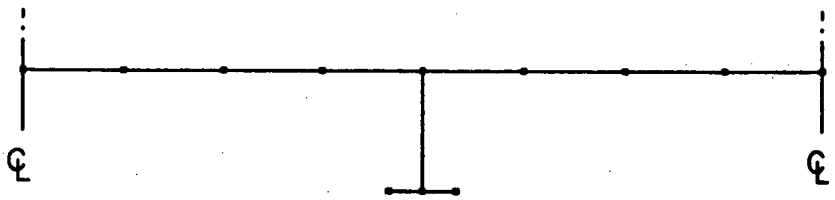

DRES2 – 11 Strip Model

Figure 4.52 – Finite strip models

a second w mode was included, central deflection response was stiffer than the ADINA result by 4.8%. A third w mode made the solution very close to the ADINA result. Deflections at the mid span of the stiffener were overestimated by 11%, 9% and 10% with one,two and three w modes respectively.

TABLE 4.10 DEFLECTIONS OF THE STIFFENED PANEL IN A LINEAR ELASTIC ANALYSIS

	Deflection at F	Deflection at G
ADINA	5.60 in	0.400 in
Finite strip $(1,1,1)+(4,-,-)$	6.51 in	0.444 in
Finite strip $(1,1,1)+(4,-,3)$	5.33 in	0.436 in
Finite strip $(1,1,1)+(4,-,3)+(-,-5)$	5.65 in	0.440 in

In order to investigate the differences observed in the mid span deflections of the stiffener in a linear elastic analysis, analytical calculations were made by treating section HBCJ (Fig. 4.50) as a wide flange I beam. The effective width of the top flange of such an I beam is 18.1% of the total span, as given by Timoshenko and Goodier[55]. With this value as the top flange width, linear elastic beam theory yields a central deflection of 0.38 in. at the mid span of the stiffener. Shear deflection at the mid span as calculated by equation 4.8 is 0.12 in., giving a total mid span deflection of 0.50 in. Therefore, it is seen from Table 4.10 that the finite strip solution for the stiffener top deflection compares more favourably than the ADINA result, with the beam theory solution. However, the finite strip solution is still 11.4% stiffer than the theoretical calculation. This may be due to possible errors in the expression for shear lag, Poisson's ratio effects of the plate, and the additional area at

the T joints.

The DRES analysis includes the effect of the fixed boundaries, AD and KL (Figure 4.50) as half the panel is considered. In contrast, in the ADINA, DRES1 and DRES2 analyses, the example panel is assumed to behave as an infinitely long plate structure in the direction perpendicular to the stiffeners. In order to study the applicability of the latter, a geometrically non-linear analysis was performed by using the two models DRES and DRES1. Lateral deflections at the center of the central panel are plotted against the applied distributed load in Figure 4.53. As the solutions are almost identical, the use of a wide flange I section instead of half the panel is justified.

Panel centre deflection responses in a large deflection analysis, with and without including material non-linearities, are shown in Figure 4.54. Deflection response predicted by DRES2 are slightly on the stiff side of those predicted by DRES1, as one might expect with a finer discretisation. The finite strip curves are on the stiff side of the ADINA curve in a linear material analysis. In a non-linear material analysis, the finite strip results cross to the flexible side of ADINA curve at high loads. As ADINA employes a large number of elements and therefore a large number of degrees of freedom, the flexibility of ADINA is expected. The flexiblity in finite strip solutions in a non-linear material analysis at high loads may be caused by the differences in yield criteria. A similar comparison for the deflection at the mid span of the stiffener top is presented in Figure 4.55. Figures 4.54 and 4.55 are drawn to the same scale. Therefore, it is easy to note the large difference between the deflections at the panel centre and at the mid span of the stiffener for a given load.

In both the Figures 4.54 and 4.55, the non-linear material curve branches away from the linear material curve at a load of approximately 35 lb/in^2 in all three analyses. The general shape of all the curves are quite similar.

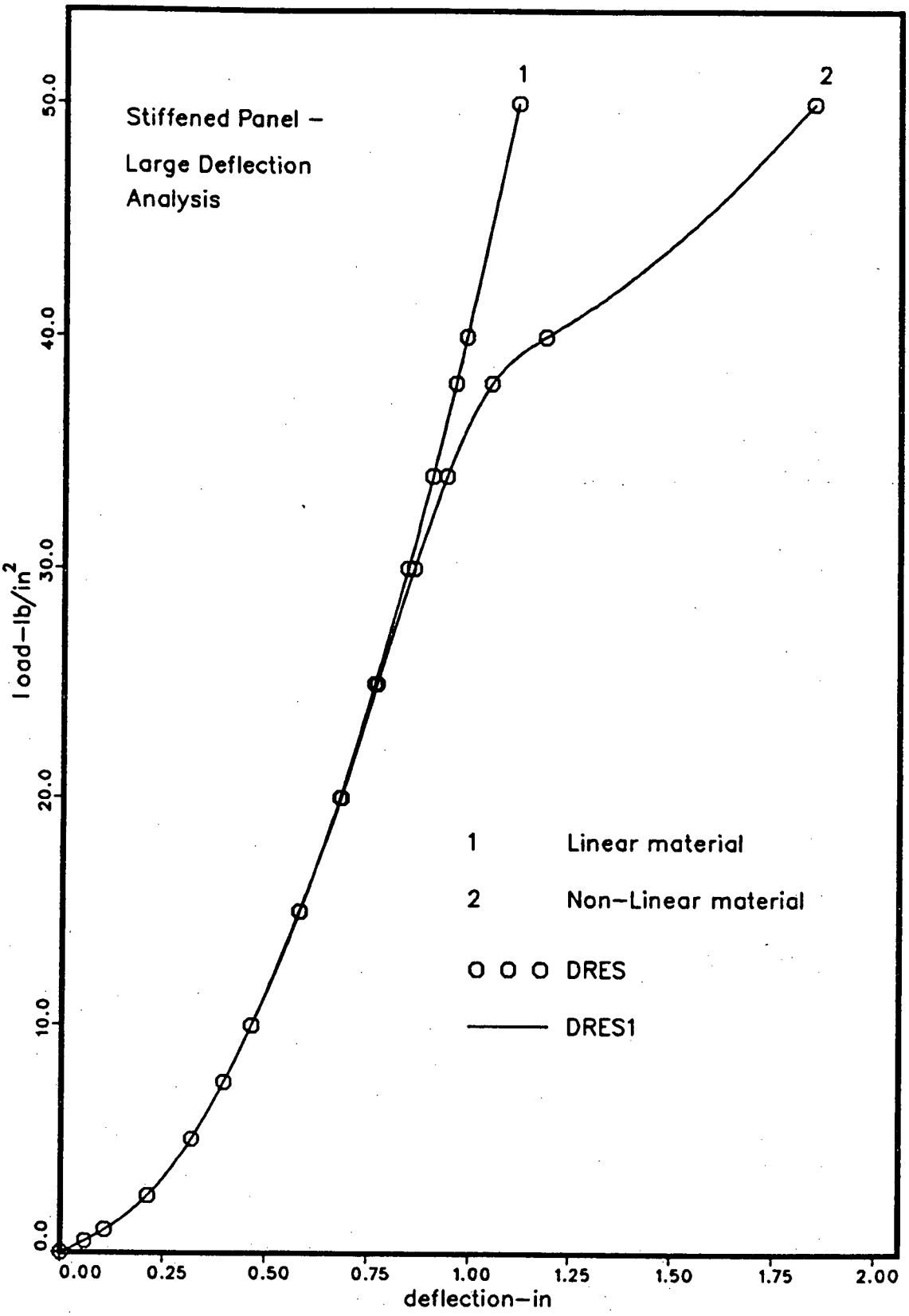

Figure 4.53 – Panel centre deflections with DRES and DRES1 models

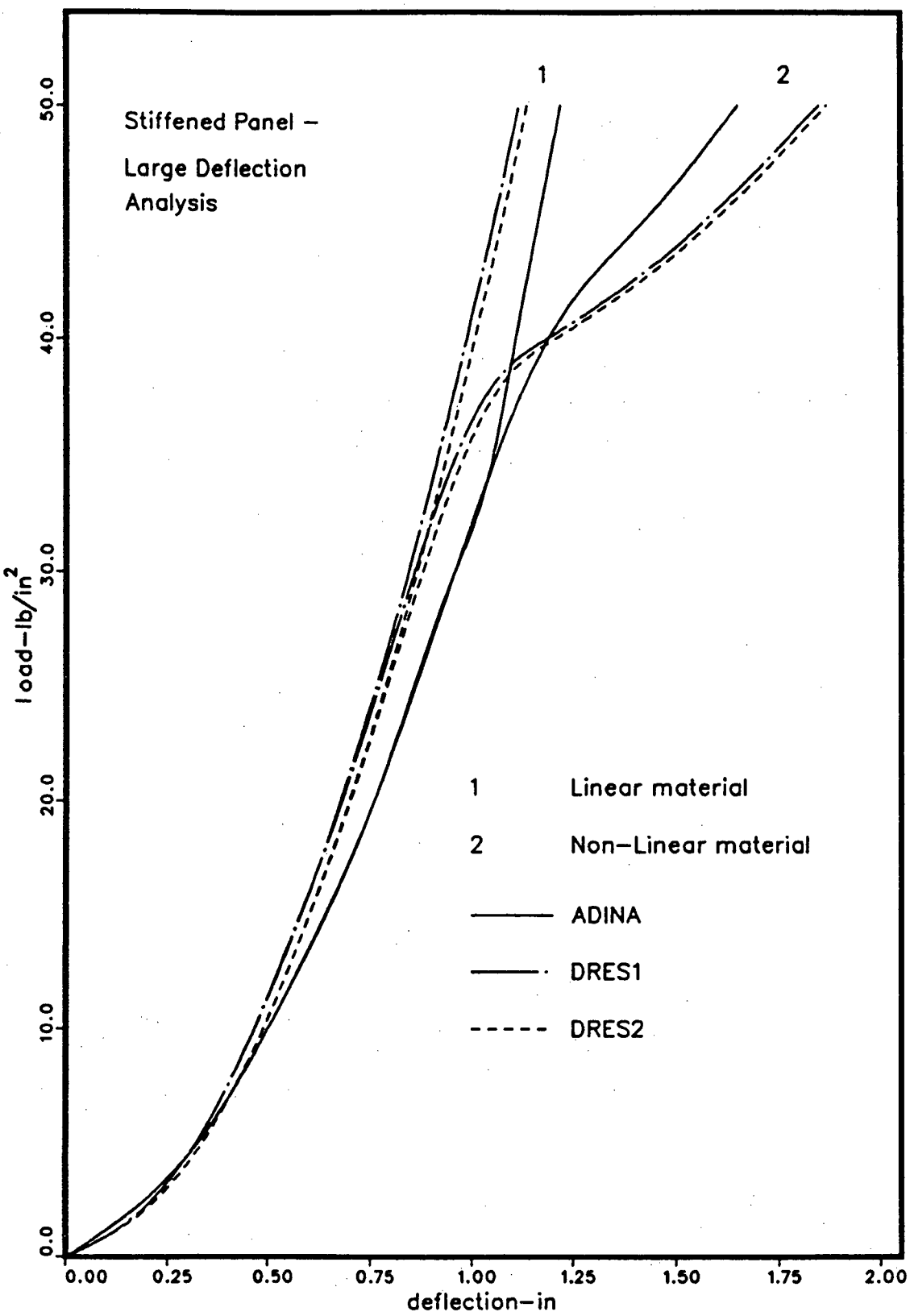

Figure 4.54 – Panel centre deflections with ADINA, DRES1 and DRES2 models

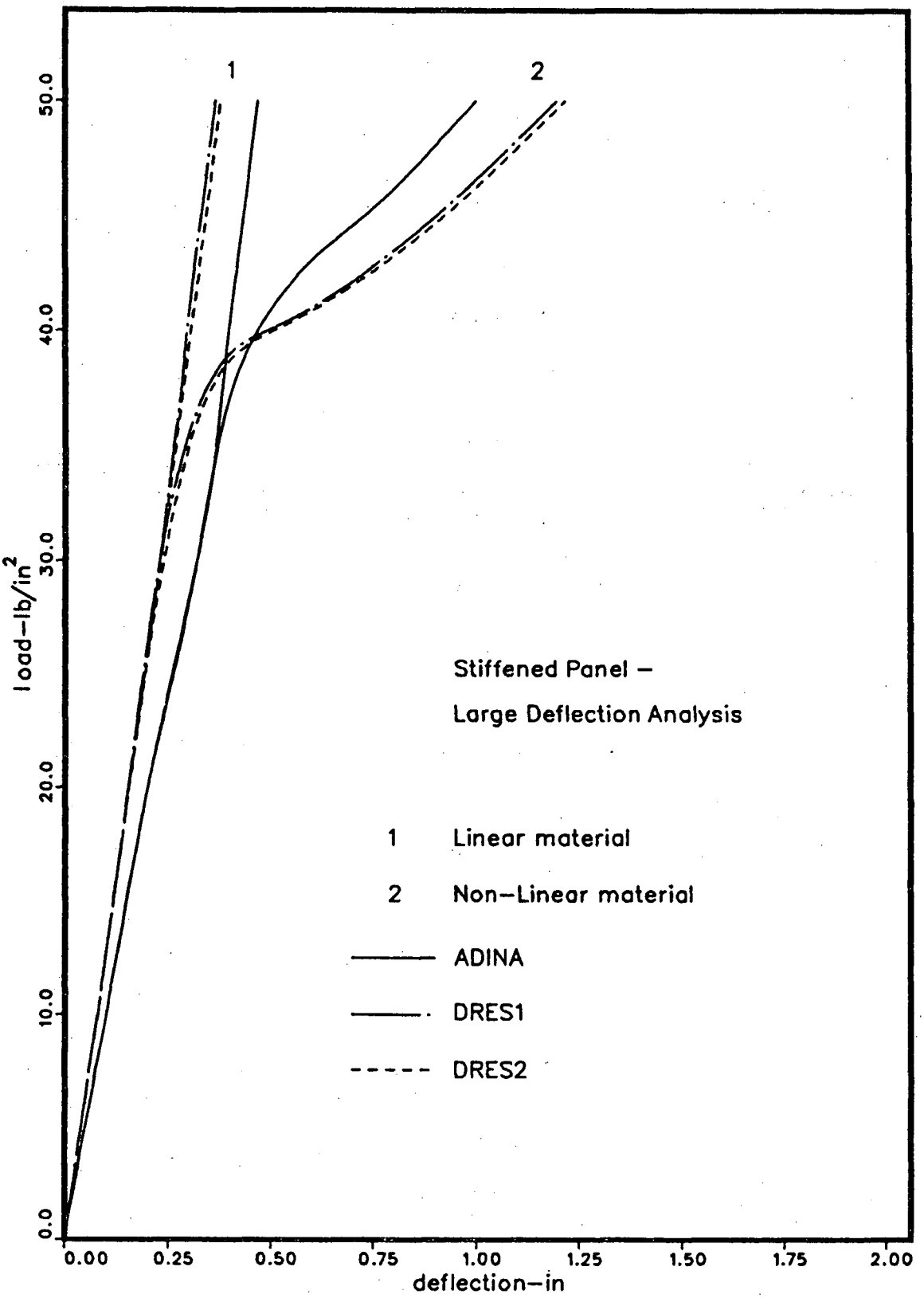

Figure 4.55 – Deflectons at mid span of the stiffener

To compare the displacement shape of the entire panel, three load levels were chosen; 0.5 psi, where the response is essentially linear, 20 psi, where there is a considerable stretching of the middle surface, and 33 psi, where membrane stresses are fully developed. The full ADINA results were not available for non-linear material response.

The deflected shapes of the panel are plotted in Figure 4.56 at the three load levels considered. Panel deflection along BF, EG and GF (Fig. 4.50) are presented in Figures 4.56(a),4.56(b) and 4.56(c) respectively.

It is seen in Figure 4.56(a) that finite strip results are stiffer than the ADINA results, except at the centre of panel at a load level of 0.5 psi. When only one w mode is employed, there is a considerable descrepancy between finite strip and ADINA results, especially between 10 and 25 in. away from the clamped boundary. This difference was substantially reduced by employing a second w mode in the analysis, though it reduced the central deflection.

The finite strip response is considerably stiff, as compared to ADINA, in the case of stiffener top deflections as shown in Figure 4.56(b). The addition of a second bending mode hardly changes the displacement pattern. The difference between ADINA and finite strip solutions seems to increase with increasing load. As the non-linearity increases with the load, this may be due to ADINA having more non-linear terms in its strain displacement relations than the finite strip analysis.

Comparison between ADINA and the finite strip results is quite good across the strip, as presented in Figure 4.56(c). This is expected as the lateral deflection is allowed to vary as a cubic polynomial within each strip, in this direction.

MARTEC report[54] also includes contour plots for the stresses on the top surface of the example panel. Normal stress components in two directions, one perpendicular and one parallel to the stiffeners, are considered. Stress contours are given at three load levels,

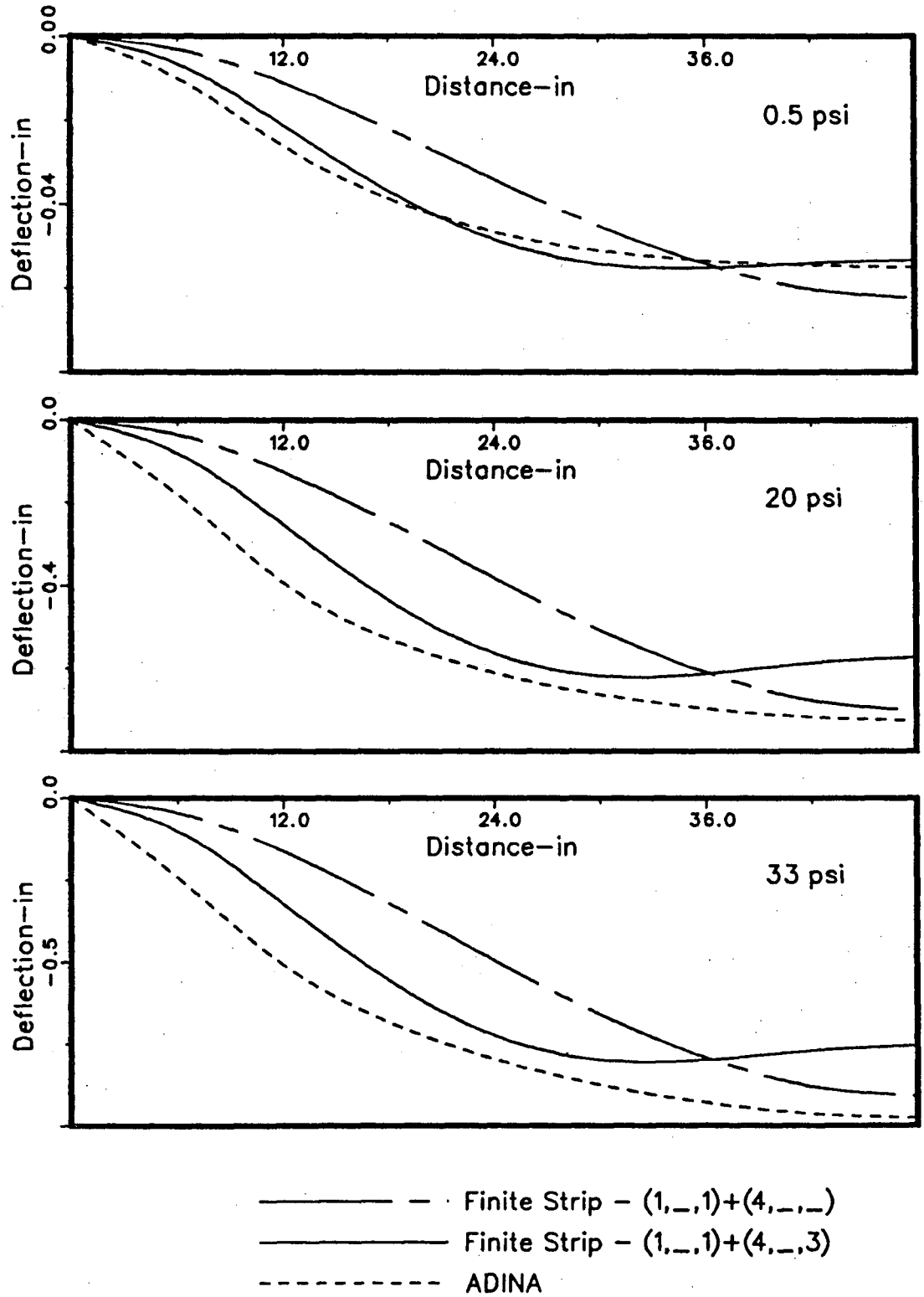

Figure 4.56(a) – Displacement shapes of DRES test panel along BF

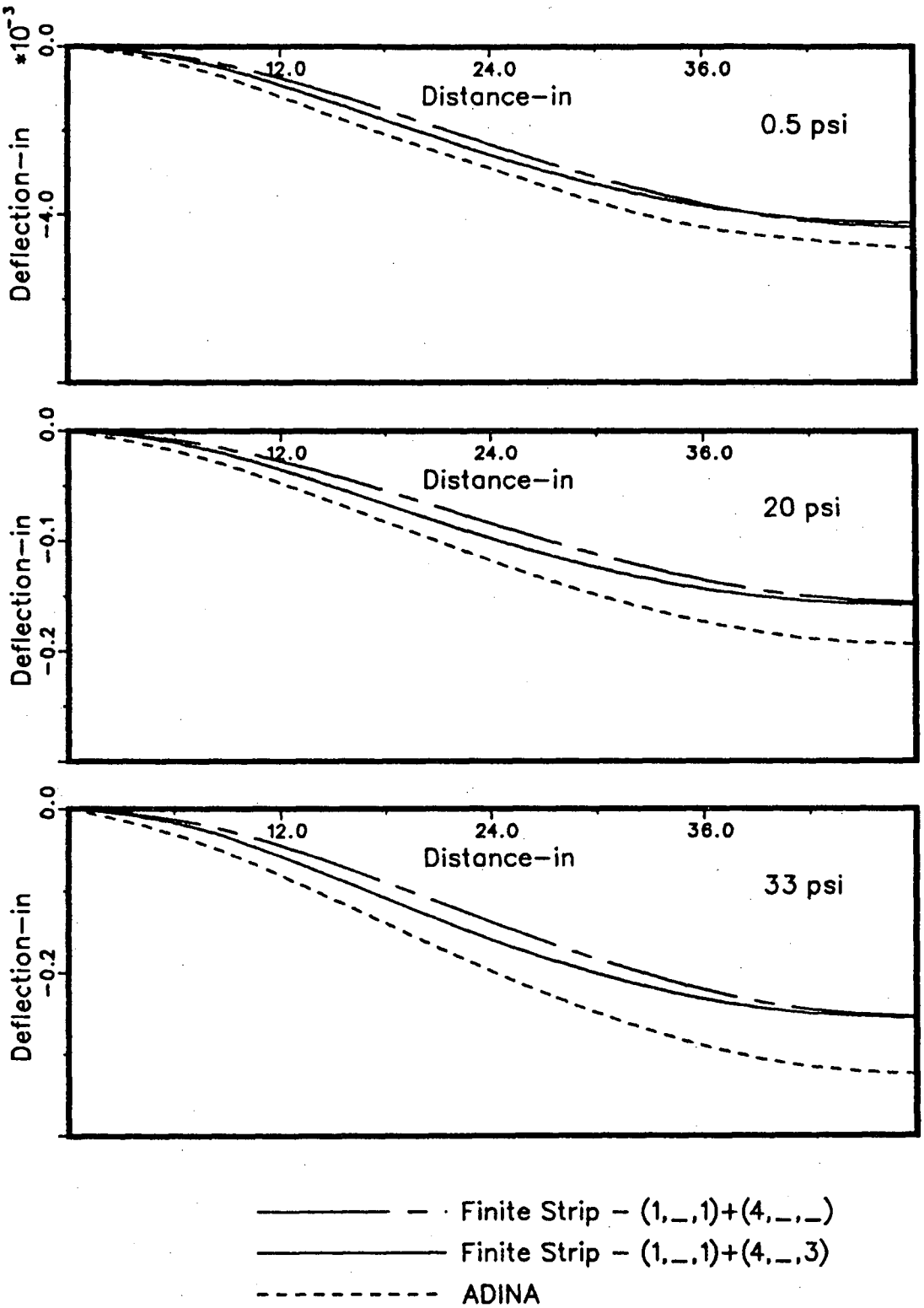

Figure 4.56(b) – Displacement shapes of DRES test panel along EG

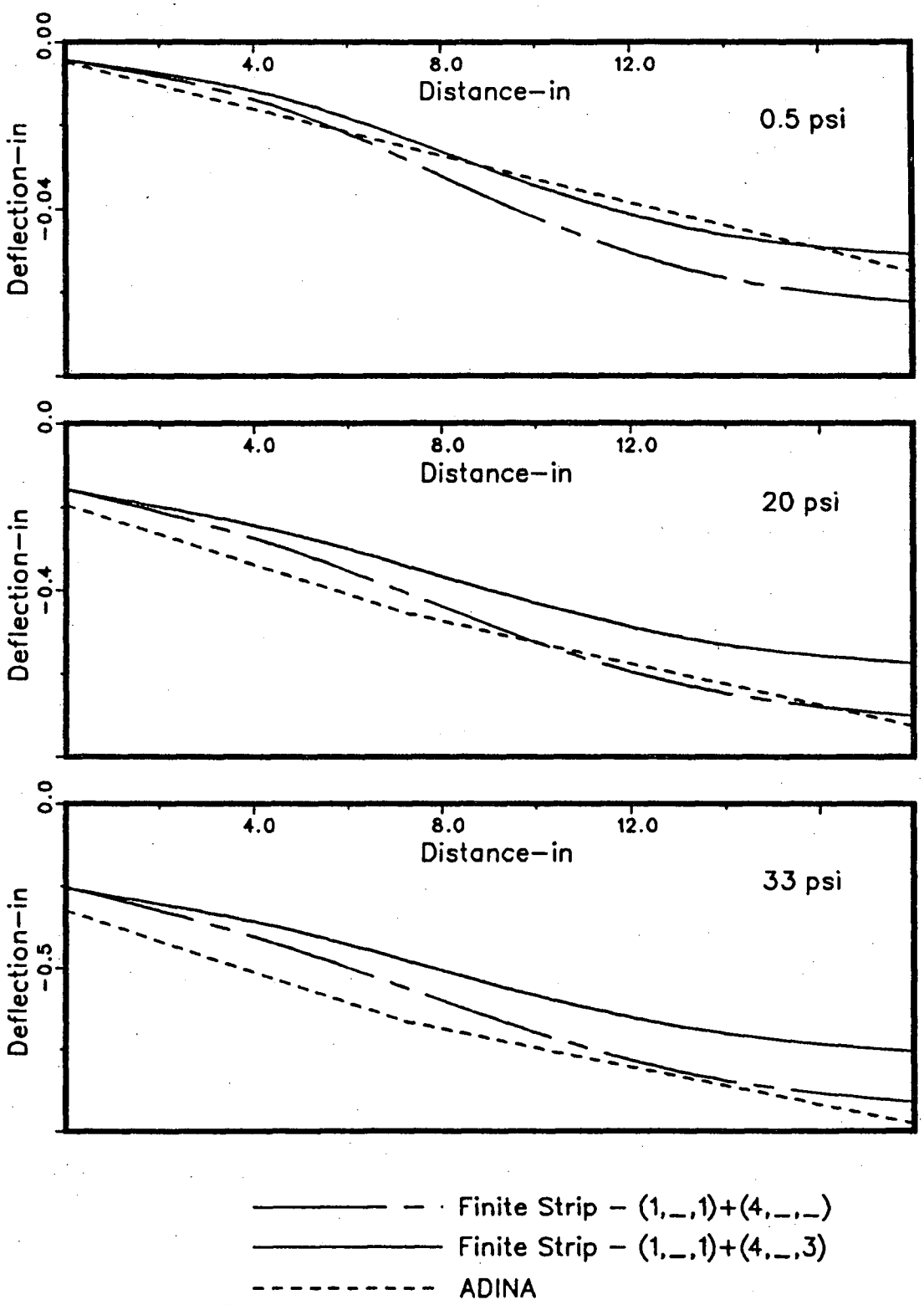

Figure 4.56(c) – Displacement shapes of DRES test panel along GF

0.5, 20 and 50 lb/in^2. The finite strip model DRES2 was used with a (1,1,1) + (4,-,-) mode combination to obtain stresses on a grid drawn on the top surface of the panel. A 3×17 grid was employed per strip on the top surface. On those grid points which are on a nodal line, stresses calculated from the two sides do not exactly match, except at the fixed boundary. For such points, the average values are taken. The stress contours obtained in a linear material, large deflection analysis are presented in Figures 4.57 and 4.58, in directions perpendicular and parallel to the stiffeners respectively, Parts (a), (b) and (c) of these Figures represent the three load levels, 0.5, 20 and 50 lb/in^2, respectively. Contours are given for a quarter of the middle bay, bounded by EBGF in the Figure 4.50. In all the contour plots, the bottom left hand corner denotes the center of the panel. The top line represents the centreline of the stiffener and the right line represents the clamped edge of the panel.

It was observed in the load - deflection plots that at a load level of 0.5 lb/in^2, the behaviour of the panel is essentially linear. In Figure 4.57(a), the similarity between the three models at this small load should be noted. The stress free contour lines agree very well. The area with a compressive stress larger than 2000 lb/in^2 is smaller in the finite strip plots than in the ADINA diagram. The maximum tensile stress predicted by the finite strip analyses is around 5000 lb/in^2, and that by the ADINA analysis is around 4000 lb/in^2. At a load of 20 lb/in^2, as shown in Figure 4.57(b), agreement among the stress contours obtained by the three methods is satisfactory. At this load, membrane stresses are comparable to those of bending. At a load level of 50 lb/in^2, the membrane stresses (perpendicular to the stiffeners) are fully developed and the ADINA results show a panel surface in complete tension in Figure 4.57(c). The finite strip results, however, show some small compressive zones. At all three load levels, the tensile stresses (perpendicular to the stiffeners) near the stiffener are very well predicted by the finite strip analyses.

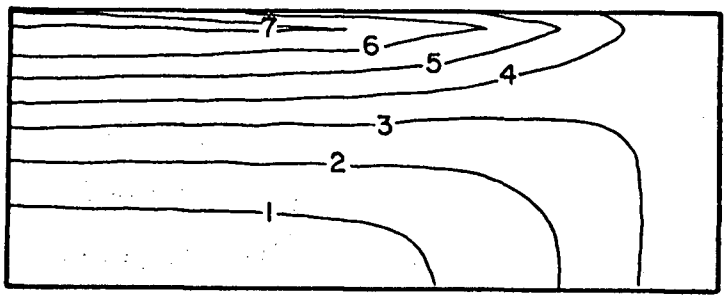

ADINA

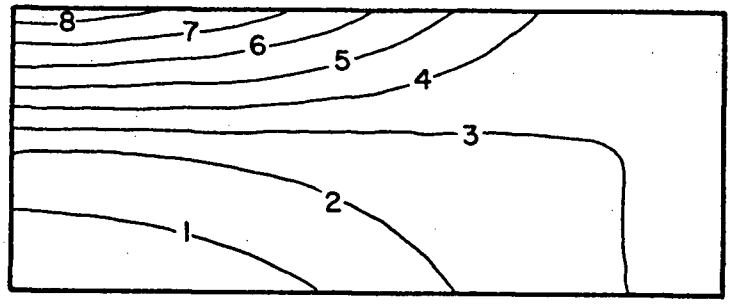

DRES1

CODE	STRESS
1	-2000
2	-1000
3	0
4	1000
5	2000
6	3000
7	4000
8	5000

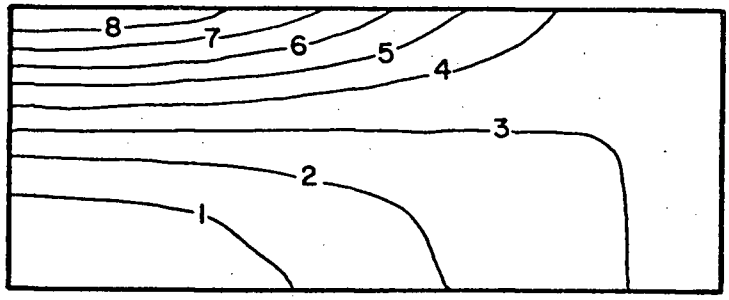

DRES2

Figure 4.57(a) – Normal stress perpendicular to the stiffener at 0.5 psi

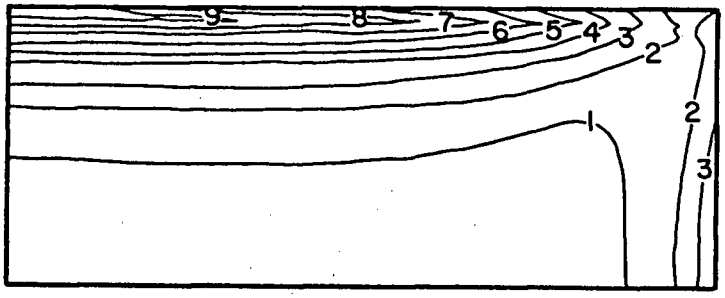

ADINA

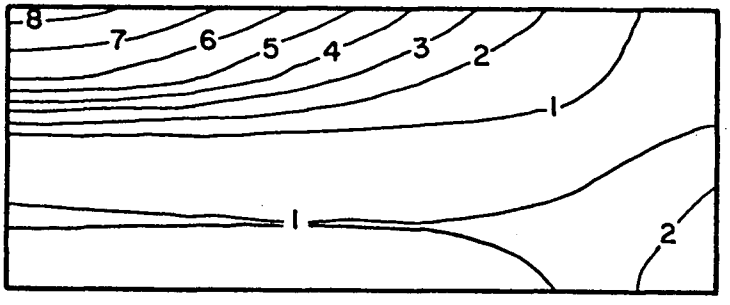

DRES1

CODE	STRESS
1	0
2	10000
3	20000
4	30000
5	40000
6	50000
7	60000
8	70000
9	80000

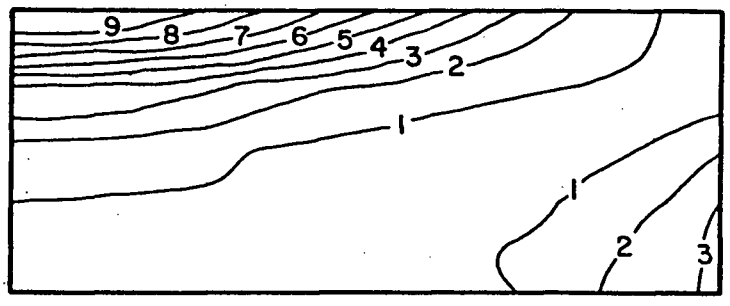

DRES2

Figure 4.57(b) – Normal stress perpendicular to the stiffener at 20 psi

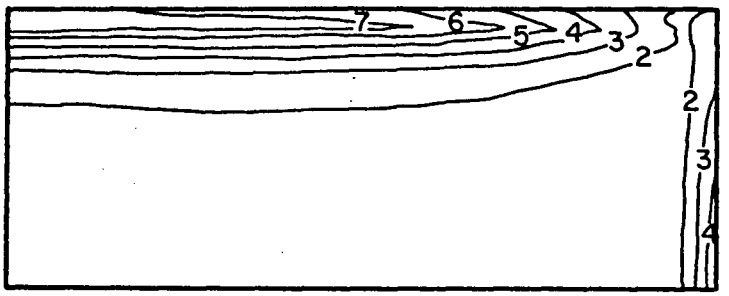

ADINA

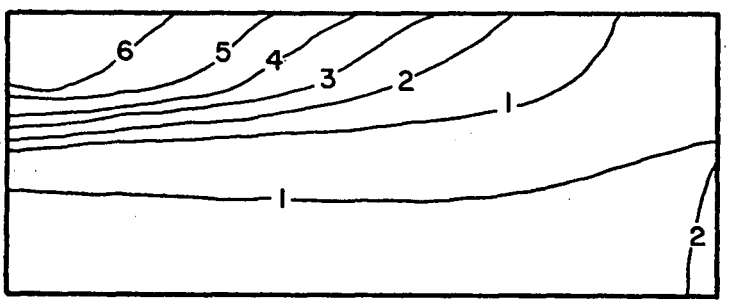

DRES1

CODE	STRESS
1	0
2	20000
3	40000
4	60000
5	80000
6	100000
7	120000
8	140000

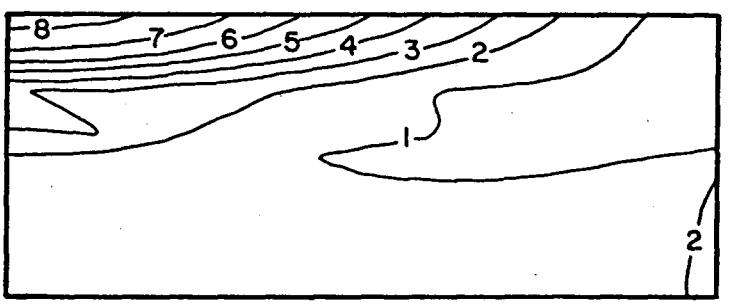

DRES2

Figure 4.57(c) – Normal stress perpendicular to the stiffener at 50 psi

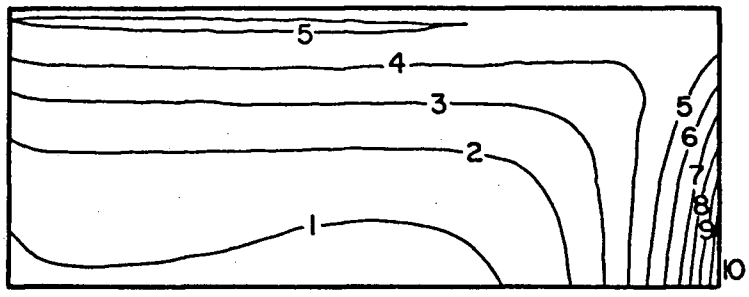

ADINA

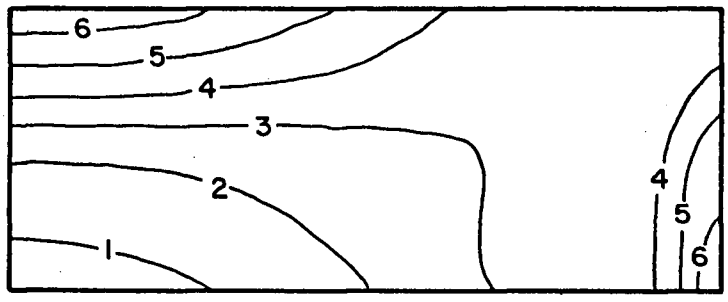

DRES1

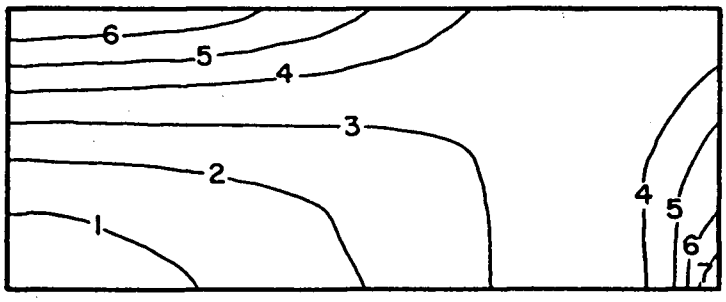

DRES2

CODE	STRESS
1	-1000
2	-500
3	0
4	500
5	1000
6	1500
7	2000
8	2500
9	3000
10	3500

Figure 4.58(a) – Normal stress parallel to the stiffener at 0.5 psi

ADINA

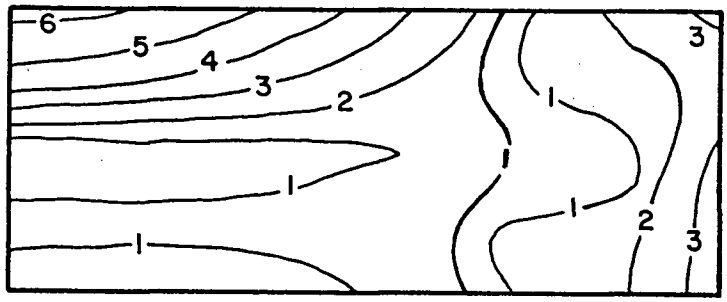

DRES1

CODE	STRESS
1	0
2	5000
3	10000
4	15000
5	20000
6	25000
7	30000
8	40000
9	60000
10	80000
11	100000

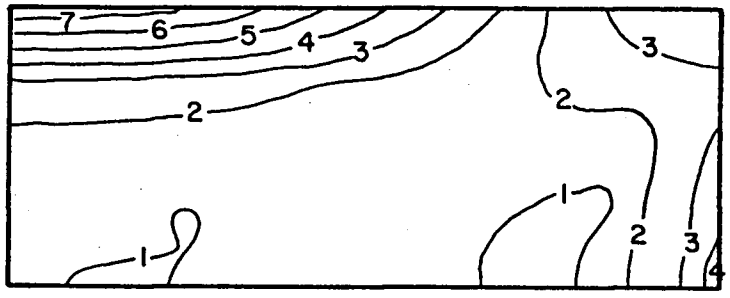

DRES2

Figure 4.58(b) – Normal stress parallel to the stiffener at 20 psi

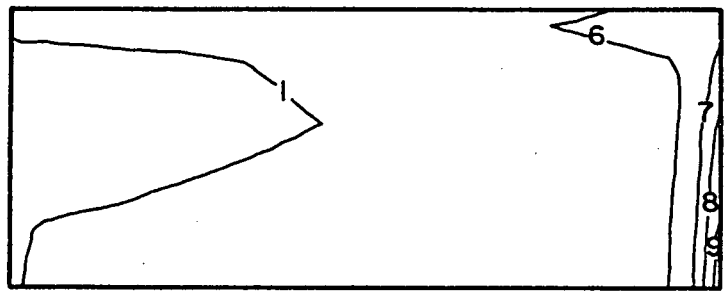

ADINA

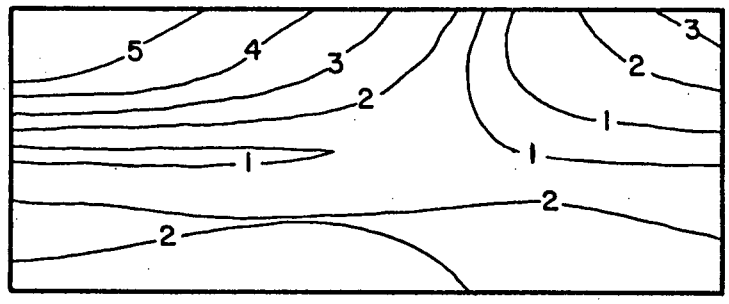

DRES1

CODE	STRESS
1	0
2	10000
3	20000
4	30000
5	40000
6	50000
7	100000
8	150000
9	200000

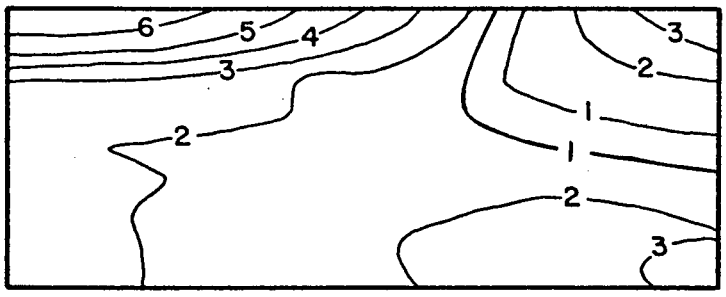

DRES2

Figure 4.58(c) – Normal stress parallel to the stiffener at 50 psi

Contour plots for the normal stress in the stiffener direction are given in Figure 4.58. At 0.5 lb/in^2, the zero stress contours are similar in all three diagrams. Stresses in the compressive zone and near the stiffener top are closely predicted by the finite strip models. However, agreement between finite strip and ADINA programmes is not as good near the fixed boundary. For example, at a load level of 0.5 lb/in^2, the maximum stress on the clamped edge obtained from the finite strip is around 2000 lb/in^2, as compared to 3500 lb/in^2 from ADINA. At loads of 20 lb/in^2 and 50 lb/in^2, the stress contour plots from ADINA are not complete and so comparison is more difficult. However, it is clear that agreement between ADINA and the present analysis is not good. At the fixed end, ADINA predicts high tensile stresses which are caused by sharp bending as the plate deforms more into a string mode than a bending mode. The finite strip analysis, with only one mode in the lateral direction, cannot model this sharp curvature and so predicts much smaller stresses. The stress near the mid span of the stiffener is difficult to compare with ADINA but the trends appear correct. High tension perpendicular to the stiffeners would cause tensile stresses in the longitudinal direction (by Poisson's effect) and coupled with the overall tension caused by the string effect, would lead one to expect high longitudinal tensions in this region. High stresses near the stiffeners may allow a reduction in the longitudinal stress in the plate near the centre and explain why there appear to be regions of low tension or even compression in some of these areas.

Stress contours were also drawn after including two bending modes in the analysis. The stress concentrations near the clamped boundary (bottom right hand corner of Fig. 4.58) were better predicted, but no significant changes were observed in other areas.

Comparisons between finite strip and ADINA stress patterns are very good for stresses perpendicular and in the vicinity of the stiffeners. On the other hand, for stresses parallel to the the stiffeners, a satisfactory agreement is seen only at a load level of 0.5 lb/in^2. In finite

strip analyses, displacement pattern in the strip direction is predetermined. However, in the direction perpendicular to the stiffeners, more flexibility is expected as a cubic displacement pattern is assumed. This is the reason for better comparisons in that direction.

4.7 Convergence of Newton-Raphson Iterative Scheme

In most of the examples discussed in the preceeding pages, 11 load increments were employed to apply the desired full load. Initially, two load increments, each equal to 5% of the full load, were used to avoid any starter problems that might occur. These were followed by nine increments with each increment representing 10% of the full load. In almost all the analyses, A TOLER value (chapter 3) of 0.001 was used and convergence was achieved in less than 6 iterations. However, it was necessary to apply the load in very small increments in some example problems to achieve convergence, especially when material softening occured. The size of these increments was determined by a trial and error procedure.

CHAPTER V

SUMMARY, CONCLUSIONS AND SUGGESTIONS FOR FUTURE RESEARCH

5.1 Summary

Observations of structures created by nature indicate that in most cases strength and rigidity depend not only on the material, but upon form. Realisation of this fact has resulted in the design of structural elements having a high load capacity, mainly due to their form, such as I beams and stiffened panels.

Analytical procedures of determining the response of these structures under non-linear conditions are not very practical because of their mathematical complexities. These difficulties have led to the development of several numerical methods for the analysis of stiffened structures. In the preceeding pages, a numerical procedure was presented following the finite strip method, to analyse large deflection, elastic plastic behaviour of beams, plates and stiffened panels.

In the finite strip method, the plate is divided into strips in which the ends are in coincidence with two opposite boundaries. Displacement variation along the strip is assumed depending on the boundary conditions at the ends of the strip. Equilibrium equations for a single finite strip were then written via a virtual work principle. Structure equilibrium

equations were subsequently obtained by summing up the individual strip equations. In the general case, the final set of equations are non linear in nodal variables and an iterative solution procedure is required. In the present formulation, this was done by incorporating the well known Newton-Raphson method. The numerical integration necessary for calculation of the tangent stiffness matrix was accomplished by adopting Gauss quadrature.

Numerical investigations were carried out to test the finite strip formulation discussed above. Several beam and plate examples and a stiffened panel example were presented. Finite strip solutions agree very well with analytical and/or other numerical solutions in most cases, even with only a single displacement mode in each of the three displacements considered. For some cases, however, it was necessary to use more than one mode to get satisfactory results. In the case of a clamped I beam or a clamped stiffened panel, finite strip solutions do not agree well with finite element solutions when material non linearities are included in the analyses. This was because of the crude mode used to simulate bending behaviour of such structures. Overall deflected shape of the stiffened panel was not too far away from ADINA predictions in a large deflection elastic analysis. Stress contours were drawn for the top surface of the stiffened panel example in two mutually perpendicular directions. The contours obtained by the finite strip method match very well with finite element results in the direction perpendicular to the stiffeners. In the stiffener direction, however, the agreement is not very good. This can be attributed to the predetemined displacement patterns in the stiffener direction.

5.2 Conclusions

5.2.1 Rectangular beam

When a rectangular beam was analysed with small deflections assuming a linear elastic material, excellent results were obtained for deflections with both simply supported and clamped boundary conditions by employing only a single bending mode. In examining bending moments and stresses, it was noted that the simply supported beam provided better comparisons with analytical solutions than the clamped beam, although errors in both cases were very small. When large deflections were included, it was found that the in-plane axial displacement had to vary along the beam so as to satisfy a constant strain requirement in the longitudinal direction to obtain accurate results. Therefore, it was concluded that the shape function for u has to be selected depending on the shape of the bending mode employed in the analysis. Plastic collapse load was overestimated by the finite strip method with the mode shapes used in the present analysis. If it is required to use the finite strip method in such an analysis, it is necessary to include a bending mode similar in shape to the corresponding collapse mechanism. Large deflection elastic-plastic response of rectangular beams agreed very well with finite element solutions in both simply supported and clamped examples.

5.2.2 I beam

Small deflection elastic analysis of an I beam by employing five finite strips produced displacement results that agree very well with theoretical calcuations, even with a single bending mode, in both simply supported and clamped cases. Errors in moments were also small and were comparable to the errors in rectangular beam problems. When large

deflections were included, it was necessary to incorporate an additional u mode to satisfy linear requirements. This additional u mode should vary as the slope of the bending(w) mode in the longitudinal direction. A combination of two u modes and one w mode produced results that agree very well with finite element solutions. This combination is also sufficient to yield accurate results in a large deflection, elastic-plastic analysis of a simply supported I beam. However, when the ends of the beam are clamped, it seemed that the present combination is unable to predict the deflected shape of the beam. Inclusion of more bending modes did help somewhat toward improving the solution, but convergence toward the finite element solution did not seem likely. A different bending mode, with zero slopes at the ends and a sharp curvature immediately away from the ends, is believed to perform better than the ϕ functions used in the present analysis.

5.2.3 Square plate

As in the beam examples, one mode linear elastic analysis of a square plate with small deflections produced very good results with both simply supported and clamped boundaries. It was revealed that 4 equal width finite strips were sufficient across the width to obtain accurate results. Even when large displacements are included, one u and one w mode analysis was sufficient to yield results comparable to finite element solutions. Plastic collapse loads were overestimated as in the case of rectangular beams. The pattern of plastification in a built-in plate can accurately be predicted by the finite strip analysis in a small deflection elastic plastic problem by employing only one u and one w mode.

5.2.4 Stiffened panel

Central deflection response in a small deflection elastic analysis of the DRES stiffened panel with clamped boundaries yielded a one mode solution which was 16% more flexible than the ADINA result. Inclusion of a second bending mode made the finite strip solution stiffer by 4.8% with respect to ADINA. The finite strip solution at the mid span of the stiffener was 11% more flexible than ADINA and did not change much with more modes. However, the finite strip solution was closer to an analytical solution calculated by using a wide flange I section, than the ADINA result. In large deflecton analysis, the one mode finite strip results were on the stiff side of ADINA solutions in terms of central as well as stiffener top deflections. Two mode results were even stiffer but they produced an overall deflection pattern of the plate closer to that of the finite element programme. It can also be concluded that present finite strip analysis can predict stress contours on the top surface of the panel fairly accurately.

5.2.5 Numerical integration

In the axial direction of a strip, 5 and 7 Gauss integration points are sufficient to obtain accurate results when employing one and two bending modes respectively. If more modes are used, 10 evaluation points will be sufficient in that direction. Across the width of the strip, 2 points are sufficient to integrate the expressions exactly if only a linear variation is allowed for the in-plane displacements in that direction. The number of Gauss points through the thickness of the plate has to be determined depending on the material behaviour. If an elastic material is assumed, 2 points will yield exact integration. However, at least 4 gauss points are required through the thickness for accurate results when material exhibits plastic behaviour.

5.3 Suggestions for Future Research

First and foremost preference should be given to solving the clamped I beam problem when the material behaves plastically. A viable solution may be to construct a new mode which is similar in shape to the classical collapse mechanism of a clamped beam.

Finite strip theory presented in this thesis has already been extended to carry out dynamic analyses via a central difference time integration scheme[56]. It is also being extended to include through-the-thickness shear effects which are important in analysing sandwich beams. Plastic analysis can be included in other more popular finite strip applications including folded, skew and sectoral plates.

REFERENCES

1 . BOOBNEV, I. G., "On the Stresses in a Ship's Bottom Plating due to Water Pressure", *Transactions of the Institute of Naval Architects,* Vol. 44, 1902.

2 . TIMOSHENKO, S. P. and WOINOWSKY KRIEGER, S., *Theory of Plates and Shells,* Second Edition, McGraw Hill Book Company, London, 1983.

3 . KARMEN, Th. VON, *Encyklopädie der Mathematischen Wissenschatten,* Vol. IV, 1910.

4 . HUBER, M. T., "Die Grundlagen einer Rationellen Berechnung der Kreuzweise Bewehrten Eisenbetonplattn", *Zeitschrift des Österreichischen Ingenieuru ,* Architekten-Vereines, Vol. 66, No. 30, 1914.

5 . BOOBNEV, I. G., *Theory of Structures of Ships,* Vol. 1 and 2, St. Petersburgh, 1912-1914.

6 . PFLÜGER, A., "Zum Beulproblem der anisotropen Rechteckplatte", *Ingenieur Archiv,* Vol. 16, 1947, pp 111-120.

7 . TROITSKY, M. S., *Stiffened Plates - Bending, Stability and Vibrations,* Elsevier Publishing Company, New York, 1976.

8 . TRENKS, K., "Beitrag zur Berechnung orthogonal anisotroper Rechteckplatten", *Der Bauingenieur,* Vol. 29, 1954, pp 372.

9 . GIENKE, E., "Die Berechnung von Hohlrippenplatten", *Der Stahlbau,* Vol. 29, 1960, pp 1-11 and 47-59.

10. WILDE, P., "An Orthotropic Plate with Thin-walled assymetric Ribs " (in Polish), *Rozprawy Inzynierskie,* Vol. 7, 1959, pp 275-310.

11. GANOWICZ, R., "A Plate Strip Having Ribs on One Side" (in Polish), *Rozprawy Inzynierskie,* Vol. 8, 1960, pp 325-342.

12. CLIFTON, R. J., CHANG, J. C. L. and AU, T., "Analysis of Orthotropic Plate Bridges", *Journal of the Structural Division, ASCE,* Vol. 89, No. ST4, Aug. 1963, pp 133-171.

13. VOGEL, U., *Approximate Determination of Bending and Membrane Stresses of the Rectangular Orthotropic Plate with Large Deflections Under Uniformly Distributed Load of Navier's Boundary Conditions,* Dissertation, Technische Hochschnle Stuttgart (in German), 1961.

14. STEINHARDT, O. and ABDEL SAYED, G., "Zur Tragfähigkeit von versteifen Flachblechtafeln im Metallbau", *Berichte der Versuchsanstalt für Stahl, 8. Folge-Heft 1,* Karlsruhe, 1963.

15. BAKER, J. F., "A Review of Recent Investigations into the Behaviour of Steel Frames in the Plastic Range", *Journal of The Institution of Civil Engineers,* No. 1, 1948-49,

Nov. 1948, pp 188-224.

16. SZILARD, R., *Theory and Analysis of Plates,* Prentice Hall, 1974.
17. SAVE, M. A. and MASSONNET, C. E., *Plastic Analysis and Design of Plates, Shells and Disks,* North Holland Publishing Company, Amsterdam, 1972.
18. COOK, R. D., *Concepts and Applications of Finite Element Analysis,* Second Edition, John Wiley and Sons, New York, 1981.
19. ZIENKIEWICZ, O.,C., *The Finite Element Method,* Third Edition, McGraw Hill Book Company, 1973.
20. CHEUNG, Y. K., *Finite Strip Method in Structural Analysis,* Pergamon Press, 1976.
21. CHEUNG, Y. K., "The Finite Strip Method in the Analysis of Elastic Plates with two Opposite Simply Supported Ends", *Proceedings, The Institution of Civil Engineers, London,* Vol. 40, May/Aug 1968, pp 1-7.
22. CHEUNG, Y. K., "Finite Strip Method in the Analysis of Elastic Slabs", *Journal of the Engineering Mechanics Division, ASCE,* Dec.1968, pp 1365-1378.
23. CHEUNG, Y. K., "Folded Plate Structures by the Finite Strip Method ", *Journal of the Structural Division, ASCE,* Dec.1969, pp 2963-2978.
24. CHEUNG, Y. K. and CHEUNG, M. S., "Flexural Vibrations of Rectangular and Other Polygonal Plates", *Journal of the Engineering Mechanics Division, ASCE,* Apr. 1971, pp 391-411.
25. DAWE, D. J., "Finite Strip Models for Vibration of Mindlin Plates", *Journal of Sound and Vibration,* Vol. 59, No. 3, 1978, pp 441-452.
26. CHEUNG, M. S. and CHAN, M. Y. T., " Static and Dynamic Analysis of Thin and Thick Sectoral Plates by the Finite Strip Method ", *Computers and Structures,* Vol. 14, No. 2, 1981, pp 79-88.
27. GRAVES SMITH, T. R. and SRIDHARAN, S., "Interactive Buckling Analysis with Finite Strips", *International Journal for Numerical Methods in Engineering,* Vol. 21, 1985, pp 145-161.
28. MAWENYA, A. S. and DAVIS, J. D., "Finite Strip Analysis of Plate Bending including Transverse Shear Effects", *Building Scince,* Vol. 9, 1974, pp 175-180.
29. HANCOCK, G. J., "Non-Linear Analysis of Thin Sections in Compression", *Journal of the Structural Division, ASCE,* Vol. 107, 1981, pp 455-471.
30. GIERLINSKI, J. T. and GRAVES-SMITH, T. R., "The Geometric Non-Linear Analysis of Thin Walled Structures by Finite Strips", *Thin Walled Structures,* Vol. 2, 1984, pp 27-50.
31. LANGYEL, P. and CUSENS, A. R., "A Finite Strip Method for the Geometrically Non-Linear Analysis of Plate Structures", *International Journal for Numerical Methods in Engineering,* Vol. 19, 1983, pp 331-340.
32. AZIZAN, Z. G. and DAWE, D. J., "Geometrically Non-Linear Analysis of Rectangular Mindlin Plates Using the Finite Strip Method ", *Computers and Structures,* Vol. 21, No. 3, 1985, pp 423-436.
33. CHEUNG, Y. K., FAN, S. C. and WU, C. Q., "Spline Finite Strip in Structural Analysis", *Proceedings, The International Conference on Finite Element Method ,* Shanghai, 1982, pp 704-709.

34. LI, W. Y., CHEUNG, Y. K. and THAM, L. G., "Spline Finite Strip Analysis of General Plates", *Journal of the Engineering Mechanics Division, ASCE*, Vol. 112, No. 1, 1986, pp 43-54.

35. PUCKETT J. A. and GUTKOWSKY, R. M., "Compound Strip Method for Analysis of Plate Systems", *Journal of the Structural Division, ASCE*, Vol. 112, No. 1, 1986, pp 121-138.

36. PUCKETT J. A. and LANG, G. J., "Compound Strip Method for Continuous Sector Plates", *Journal of the Engineering Mechanics Division, ASCE*, Vol. 112, No. 5, 1986, pp 498-514.

37. PUCKETT J. A. and LANG, G. J., "Compound Strip Method for Free Vibration Analysis of Continuous Plates", *Journal of the Engineering Mechanics Division, ASCE*, Vol. 112, No. 12, 1986, pp 1375-1389.

38. MOFFLIN, D. S., "A Finite Strip Method for the Collapse Analysis of Compressed Plates and Plate Assemblages", *Report CUED/D-Struct/TR101,* University of Cambridge, Department of Engineering, 1983.

39. MOFFLIN, D. S., OLSON, M. D. and ANDERSON, D. L., "Finite Strip Analysis of Blast Loaded Plates", *Proceedings, Europe-US Symposium on Finite Element Method s for Non-Linear Problems*, The Norwegian Institute of Technology, Norway, 1985, pp I.12-1 - I.12-15.

40. MENDELSON, A., *Plasticity, Theory and Application*, The MacMillan Company, New York, 1968.

41. WU, R. W. H. and WITMER, E. A., "Non-linear Transient Responses of Structures by the Spatial Finite Element Method", *AIAA Journal,* Vol. 11, No. 8, 1973, pp 1110-1117.

42. SOREIDE, T. A., MOAN, T. and NORDSVE, N. T., "On The Behaviour and Design of Stiffened Plates in Ultimate Limit State", *Journal of Ship Research,* Vol. 22, No. 4, 1978, pp 238-244.

43. BÄCKLUND, J., "Finite Element Analysis of Non-Linear Structures", *Chalmers Tekniska Högskola*, Goteburg, Sweden, 1973.

44. JONES, N., "Plastic Behaviour of Ship Structures", *Transactions, SNAME*, Vol. 84, 1976, pp 115-145.

45. FOLZ, B. R., *FENTAB - Finite Element Non-Linear Transient Analysis of Beams - Version 1.0*, Department of Civil Engineering, The University of British Columbia, Vancouver, Canada, 1986.

46. ROARK, R. J. and YOUNG, C., *Formulas for Stress and Strain - Fifth Edition,* McGraw Hill Book Company, 1976.

47. FÖPPL, A., *Drang and Zwang* , pp 345.

48. BATHE, K. J. and BOLOURCHI, S., "A Geometric and Material Non-Linear Plate and Shell Element", *Computers and Structures*, Vol. 11, 1980, pp 23-48.

49. LEVY, S., "Bending of Rectangular Plates with Large Deflections", *NACA,* Report No. 737, 1942.

50. COWPER, G. R., KOSKO, E., LINDBERG, G. M. and OLSON, M. D., "A High Precision Triangular Plate Bending Element", *Aeronautical Report LR-514*, National Research Council Canada, Ottawa, 1968.

51. SOUTHWELL, R. V., "On the Analogues Relating Flexture and Displacements of Flat Plates", *Quarterly Journal of Mechanics and Applied Mathematics,* Vol. 3, 1950, pp 257-270.

52. OWEN, D. R. J. and FIGUEIRAS, J. A., "Elasto-Plastic Analysis of Anisotropic Plates and Shells by The Semiloof Element", *International Journal for Numerical Methods in Engineering,* Vol. 19, 1983, pp 521-539.

53. BATHE, K. J., "ADINA - A Finite Element Program for Automatic Dynamic Incremental Non-Linear Analysis", *Report 82448-1, Acoustics and Vibration Laboratory, Department of Mechanical Engineering,* Massachusetts Institute of Technology, Cambridge, Massachusetts, 1975.

54. DESROCHERS, C and NORWOOD, M., "Finite Element Analysis of Stiffened Planel Structure Subjected to Three Air Blast Loadings", A Report Prepared for the Defence Research Establishment Suffield, Alberta, 1986.

55. TIMOSHENKO, S. P. and GOODIER, J. N., *Theory of Elasticity* , Third Edition, McGraw Hill Book Company, 1983.

56. KHALIL, M. R., OLSON, M. D. and ANDERSON, D. L., "Large Deflection Elastic-Plastic Dynamic Response of Air-Blast Loaded Plate Structures by the Finite Strip Method", *Structural Research Series, Report No. 33,* The University of British Columbia, Vancouver, Canada, 1987.

APPENDIX A

Strain-Displacement Relations for Stiffener Strips

Equation 3.42 will be modified for the stiffener strips with the addition of non-linear terms in v. Corresponding strain-displacement relations are given below in matrix form.

$$\{\epsilon\} = \begin{Bmatrix} \epsilon_x \\ \epsilon_y \\ \gamma_{xy} \end{Bmatrix}$$

$$= \begin{bmatrix} \frac{\partial N_1^u}{\partial x} & 0 & -z\frac{\partial^2 N_1^w}{\partial x^2} & -z\frac{\partial^2 N_2^w}{\partial x^2} & \frac{\partial N_2^u}{\partial x} & 0 & -z\frac{\partial^2 N_3^w}{\partial x^2} & -z\frac{\partial^2 N_4^w}{\partial x^2} \\ 0 & \frac{\partial N_1^v}{\partial y} & -z\frac{\partial^2 N_1^w}{\partial y^2} & -z\frac{\partial^2 N_2^w}{\partial y^2} & 0 & \frac{\partial N_2^v}{\partial y} & -z\frac{\partial^2 N_3^w}{\partial y^2} & -z\frac{\partial^2 N_4^w}{\partial y^2} \\ \frac{\partial N_1^u}{\partial y} & \frac{\partial N_1^v}{\partial x} & -z\frac{\partial^2 N_1^w}{\partial x \partial y} & -z\frac{\partial^2 N_2^w}{\partial x \partial y} & \frac{\partial N_2^u}{\partial y} & \frac{\partial N_2^v}{\partial x} & -z\frac{\partial^2 N_3^w}{\partial x \partial y} & -z\frac{\partial^2 N_4^w}{\partial x \partial y} \end{bmatrix} \{\delta_e\} +$$

$$\begin{bmatrix} \frac{1}{2}\frac{\partial N_i^w}{\partial x}\frac{\partial N_j^w}{\partial x} w_i w_j \\ \frac{1}{2}\frac{\partial N_i^w}{\partial y}\frac{\partial N_j^w}{\partial y} w_i w_j \\ \frac{1}{2}\left(\frac{\partial N_i^w}{\partial x}\frac{\partial N_j^w}{\partial y} + \frac{\partial N_i^w}{\partial x}\frac{\partial N_j^w}{\partial y}\right) w_i w_j \end{bmatrix} + \begin{bmatrix} \frac{1}{2}\frac{\partial N_k^v}{\partial x}\frac{\partial N_l^v}{\partial x} v_k v_l \\ \frac{1}{2}\frac{\partial N_k^v}{\partial y}\frac{\partial N_l^v}{\partial y} v_k v_l \\ \frac{1}{2}\left(\frac{\partial N_k^v}{\partial x}\frac{\partial N_l^v}{\partial y} + \frac{\partial N_k^v}{\partial x}\frac{\partial N_l^v}{\partial y}\right) v_l v_k \end{bmatrix}$$

where $i, j = 1, 2, 3, 4$ and $k, l = 1, 2$.

APPENDIX B

Elements of the $'U'$ matrix

In Chapter 3, U matrix was defined as

$$\left(\frac{\partial}{\partial\{\delta\}}[C]^T\right)\{\sigma\} = [U] \tag{3.58}$$

Considering only one mode for simplicity, it is clear that $[C]$ matrix is of size 3×8 and the array of nodal displacements, $\{\delta\}$ consists of 8 elements. Therefore, $\partial[C]^T/\partial\{\delta\}$ results in a three dimensional array W of size $8 \times 8 \times 3$. The elements of W are given by,

$$W_{ikj} = \frac{\partial C_{ik}^T}{\partial \delta_j}$$

with $i, j = 1, 2, ..., 8$ and $k = 1, 2, 3$. Now, as the stress array $\{\sigma\}$ is of size 3×1, the product matrix U can be given by,

$$[U] = [W]\{\sigma\}$$

where,

$$U_{ij} = \sum_{k=1}^{3} \frac{\partial \left(C^T\right)_{ik}}{\partial \left(\delta\right)_j}\sigma_k \tag{3.59}$$

The U matrix can also be written as,

$$[U] = \begin{bmatrix} 0 & 0 & 0 & 0 & 0 & 0 & 0 & 0 \\ 0 & 0 & 0 & 0 & 0 & 0 & 0 & 0 \\ 0 & 0 & Q_{11} & Q_{12} & 0 & 0 & Q_{13} & Q_{14} \\ 0 & 0 & Q_{21} & Q_{22} & 0 & 0 & Q_{23} & Q_{24} \\ 0 & 0 & 0 & 0 & 0 & 0 & 0 & 0 \\ 0 & 0 & 0 & 0 & 0 & 0 & 0 & 0 \\ 0 & 0 & Q_{31} & Q_{32} & 0 & 0 & Q_{33} & Q_{34} \\ 0 & 0 & Q_{41} & Q_{42} & 0 & 0 & Q_{43} & Q_{44} \end{bmatrix},$$

where,

$$Q_{ij} = N^w_{i,x} N^w_{j,x} \sigma_x + N^w_{i,y} N^w_{j,y} \sigma_y + \left(N^w_{i,x} N^w_{j,y} + N^w_{i,y} N^w_{j,x} \right) \tau_{xy}, \qquad i,j = 1,2,3,4,$$

and

$$N^w_{i,x} = \partial N^w_i / \partial x,$$

$$N^w_{i,y} = \partial N^w_i / \partial y,$$

$$N^w_{j,x} = \partial N^w_j / \partial x,$$

$$N^w_{j,y} = \partial N^w_j / \partial y.$$

APPENDIX C

Bending moments at the ends of a simply supported plate

Bending moment distribution in the strip direction along the centreline of the example square plate in a large deflection, elastic-plastic analysis is presented here, at a load $Q = 5.0$. Bending moments are obtained by calculating the stresses at Gauss evaluation points and then integrating these stresses through the thickness of the plate. A smooth curve is then drawn through those points as shown below. Note that, the end moment is only 3% of the moment in the middle.